(12) LEVEL

DNA 5687F

THEORY OF EMP COUPLING IN THE SOURCE REGION

Conrad L. Longmire
James L. Gilbert
Mission Research Corporation
P.O. Drawer 719
Santa Barbara, California 93102

28 February 1980

Final Report for Period 1 February 1979—28 February 1980

CONTRACT No. DNA 001-79-C-0186

THIS WORK SPONSORED BY THE DEFENSE NUCLEAR AGENCY
UNDER RDT&E RMSS CODE B323079464 R99QAXEB08896 H2590D.

Prepared for
Director
DEFENSE NUCLEAR AGENCY
Washington, D. C. 20305

Destroy this report when it is no longer needed. Do not return to sender.

PLEASE NOTIFY THE DEFENSE NUCLEAR AGENCY, ATTN: STTI, WASHINGTON, D.C. 20305, IF YOUR ADDRESS IS INCORRECT, IF YOU WISH TO BE DELETED FROM THE DISTRIBUTION LIST, OR IF THE ADDRESSEE IS NO LONGER EMPLOYED BY YOUR ORGANIZATION.

UNCLASSIFIED

SECURITY CLASSIFICATION OF THIS PAGE *(When Data Entered)*

REPORT DOCUMENTATION PAGE	READ INSTRUCTIONS BEFORE COMPLETING FORM
1 REPORT NUMBER DNA 5687F	3. RECIPIENT'S CATALOG NUMBER 751
4. TITLE *(and Subtitle)* THEORY OF EMP COUPLING IN THE SOURCE REGION	TYPE OF REPORT & PERIOD COVERED Final Report for Period 1 Feb 79—28 Feb 80 PERFORMING ORG. REPORT NUMBER MRC-R-546
7 AUTHOR(s) Conrad L. Longmire James L. Gilbert	8. CONTRACT OR GRANT NUMBER(s) DNA 001-79-C-0186
9 PERFORMING ORGANIZATION NAME AND ADDRESS Mission Research Corporation P. O. Drawer 719 Santa Barbara, California 93102	10 PROGRAM ELEMENT, PROJECT, TASK AREA & WORK UNIT NUMBERS Subtask R99QAXEB088-96
11 CONTROLLING OFFICE NAME AND ADDRESS Director Defense Nuclear Agency Washington, D.C. 20305	12 REPORT DATE 28 February 1980 13. NUMBER OF PAGES 216
14 MONITORING AGENCY NAME & ADDRESS *(if different from Controlling Office)*	15 SECURITY CLASS *(of this report)* UNCLASSIFIED 15a. DECLASSIFICATION DOWNGRADING SCHEDULE N/A

16. DISTRIBUTION STATEMENT *(of this Report)*

Approved for public release; distribution unlimited.

17 DISTRIBUTION STATEMENT *(of the abstract entered in Block 20, if different from Report)*

18 SUPPLEMENTARY NOTES

This work sponsored by the Defense Nuclear Agency under RDT&E RMSS Code B323079464 R99QAXEB08896 H2590D.

19 KEY WORDS *(Continue on reverse side if necessary and identify by block number)*

Electromagnetic Pulse
Nuclear Explosions
System Interactions of EMP
Coupling of EMP

20 ABSTRACT *(Continue on reverse side if necessary and identify by block number)*

This report presents methods, primarily analytical, for calculating the coupling of EMP to systems in the source region. The first chapter discusses Maxwell's equations and units. The second chapter presents an adequate model for the impedance of soils, and discusses causality and reality conditions on solutions in the domain of complex variables. The third chapter is a survey of EMP sources and fields for surface bursts. The remaining chapters →

DD FORM 1 JAN 73 1473 EDITION OF 1 NOV 65 IS OBSOLETE

UNCLASSIFIED

SECURITY CLASSIFICATION OF THIS PAGE *(When Data Entered)*

20. continued

discuss coupling to short buried conductors, long buried conductors, short vertical conductors in the air, and long elevated conductors.

PREFACE

This report is the first draft of what we hope will eventually be a comprehensive treatise on the theory and calculation of EMP coupling to systems located in the source region.

There has been a strong tendency for many years to rely on computer codes for EMP coupling calculations. We have noticed that computer codes built in the absence of theoretical understanding almost always give the wrong answer for the right problem, even though they may give the right answer for the wrong problem. Source-region coupling, being only a little more difficult subject than EMP environments, is quite amenable to theoretical analysis, and the present report shows how such analysis can be carried out for some important examples.

We hope to add to this report over the next few years. More examples are needed. A problem not discussed in the present report is the effect of breakdown in air (e.g., nuclear lightning) and in the soil on coupled currents. There are reasonable prospects that sufficient progress will be made on these problems in the next year or so that they can be included. Further, experience with real systems such as MX and LoADS may show us other problems that need analysis. We therefore hope that the copies of this report will not be bound so tightly that they cannot be supplemented by revisions and further chapters.

TABLE OF CONTENTS

TABLE OF CONTENTS (cont'd)

TABLE OF CONTENTS (cont'd)

LIST OF ILLUSTRATIONS

LIST OF ILLUSTRATIONS (cont'd)

LIST OF ILLUSTRATIONS (cont'd)

LIST OF TABLES

CHAPTER 1
INTRODUCTION AND BASIC EQUATIONS

1.1 INTRODUCTION

A nuclear explosion on or near the air-ground interface produces a large electromagnetic pulse (EMP). The principal source of the EMP is the current of Compton recoil electrons resulting from collisions of gamma rays with the electrons in air molecules. The Compton current is significant out to distances of several kilometers from megaton explosions. Within this source region, the air conductivity, associated with secondary ionization produced by the Compton electrons, has a strong influence on the fields generated. The presence of a conducting ground also has a strong influence.

Calculations of the coupling of electromagnetic energy into systems located within the source region must take into account the existence of the gamma rays, the Compton current, and the air conductivity, as well as the EMP fields. Thus source region coupling is more complicated than free-field coupling, where only the fields need to be considered. Nevertheless, a useful approximate theory of source region coupling can be constructed, and this report presents the theory for coupling to some simple but practically relevant system geometries. The theory will hopefully be extended to other geometries as needs arise.

The coupling theory presented here closely parallels the theory of source-region EMP environments developed previously by this author

(References 1-2 to 1-4). The latter theory was important in that it:

- gave the first predictions of general EMP environments;
- showed what parameters EMP depends on;
- showed how to build competent computer codes for more detailed predictions;
- provided accuracy tests for the codes.

The goals and uses of the theory of source-region coupling are similar:

- to make approximate predictions of coupled currents and voltages, especially in regimes where present computer codes are not valid;
- to test computer codes and show how to improve them;
- to provide understanding of coupling and how it depends on parameters;
- to allow other scientists to judge the correctness of coupling predictions.

It is thus hoped that this report will be useful to a variety of readers, from engineers faced with the task of making predictions for actual systems to scientists who need or wish to judge the adequacy of our understanding of the phenomena and of methods for making predictions. In this connection, a particular reader may be more interested in some sections of this report and less interested in others. We have tried, however, to make all of the report readable for the entire spectrum of likely readers.

1.2 MAXWELL'S EQUATIONS

The material media that we shall be dealing with most commonly, air and soil, are essentially non-magnetic; that is, the magnetic permeability has the value μ_0 appropriate to free space. Both media are generally

conductive, and the soil has a dielectric permittivity substantially different from ε_0, the free space value.

The two time-dependent Maxwell equations are then

$$\frac{\partial \vec{B}}{\partial t} = - \nabla \times \vec{E} \ , \tag{1-1}$$

$$\varepsilon \frac{\partial \vec{E}}{\partial t} = - \vec{J} + \frac{1}{\mu_0} \nabla \times \vec{B} \ , \tag{1-2}$$

where $\vec{B}$ is the magnetic field (webers/m^2), $\vec{E}$ is the electric field (volts/m), and $\vec{J}$ is the current density (amps/m^2). It is clear that these equations are sufficient to carry the fields forward in time if initial values are given and if $\vec{J}$ is specified. From these initial values we can evaluate the right-hand sides of Equations 1-1 and 1-2, which then tell us how $\vec{E}$ and $\vec{B}$ will change in the next infinitesimal time interval δt. From the new values of $\vec{E}$ and $\vec{B}$ we can re-evaluate the right-hand sides and advance the fields another δt, and so on. This, in fact, is precisely how numerical solutions of Maxwell's equations are obtained (the spatial derivatives in the curl operations are also evaluated in finite difference form).

Note that the relation of cause and effect in this way of looking at Maxwell's equations is different from what most of us were taught, particularly for Equation 1-1. The picture just given is that the value of $\nabla \times E$ determines how $\vec{B}$ will change in the next infinitesimal time interval, whereas the traditional picture is that a changing $\vec{B}$ generates (inductively) a solenoidal $\vec{E}$, i.e., an $\vec{E}$ with finite curl. Either picture gives the same result, namely that the right- and left-hand sides are equal, and we do not actually need to decide which side causes the other. However, the new picture, which is the one generally used by physicists, makes it easier to understand how time-dependent solutions evolve.

There are two other Maxwell equations,

$$\nabla \cdot B = 0 \ , \tag{1-3}$$

$$\nabla \cdot (\varepsilon \vec{E}) = \rho \ , \tag{1-4}$$

where ρ is the charge density. It would appear from the foregoing discussion that these equations are not needed in advancing the fields in time. Such is indeed the case, for taking the divergence of Equation 1-1 gives

$$\frac{\partial}{\partial t} (\nabla \cdot \vec{B}) = - \nabla \cdot (\nabla \times \vec{E}) = 0 \ . \tag{1-5}$$

(The divergence of the curl of any field vanishes.) This equation says that, if Equation 1-1 is satisfied, $\nabla \cdot \vec{B}$ will be independent of time at all points in space. Thus if $\nabla \cdot \vec{B}$ vanishes everywhere initially, then the solution of Equation 1-1 will have $\nabla \cdot \vec{B} = 0$ everywhere at all times. Therefore Equation 1-3 needs only to be imposed as a condition on the initial magnetic field. If the initial magnetic field vanishes, Equation 1-3 is satisfied.

To understand the role of Equation 1-4, take the divergence of Equation 1-2, and obtain

$$\frac{\partial}{\partial t} (\nabla \cdot \varepsilon \vec{E}) = - \nabla \cdot \vec{J} \ . \tag{1-6}$$

Now the conservation of charge, which is a well verified law of nature, states that

$$\frac{\partial \rho}{\partial t} = - \nabla \cdot \vec{J} \ . \tag{1-7}$$

Subtracting Equation 1-7 from Equation 1-6 gives

$$\frac{\partial}{\partial t} (\nabla \cdot \varepsilon \vec{E} - \rho) = 0 \ . \tag{1-8}$$

Thus it follows from Equation 1-2 that, if the quantity in parentheses vanishes everywhere initially, it will vanish everywhere at all times.

Therefore Equation 1-4 also needs only to be imposed as a condition on the initial $\vec{E}$ and ρ. If $\vec{E}$ and ρ both vanish initially, Equation 1-4 is satisfied.

If $\vec{B}$, $\vec{E}$ and ρ all vanish initially, we need only concern ourselves with Equations 1-1 and 1-2. Note that these equations do not contain ρ at all; ρ need not be calculated. If ρ is desired, it can be found by time integration of Equation 1-7.

Note that Maxwell's equations and the conservation of charge, Equation 1-7, are linear in the variables $\vec{J}$, ρ, $\vec{E}$ and $\vec{B}$. Thus if current density $\vec{J}_1$ produces ρ_1, $\vec{E}_1$ and $\vec{B}_1$, and $\vec{J}_2$ produces ρ_2, $\vec{E}_2$, and $\vec{B}_2$, then current density $\vec{J}_1 + \vec{J}_2$ will produce $\rho_1 + \rho_2$, $\vec{E}_1 + \vec{E}_2$ and $\vec{B}_1 + \vec{B}_2$. We have assumed here that ε (and μ_0 of course) is the same in all cases. This linearity is somewhat restricted in practice when $\vec{J}$ depends on $\vec{E}$, as we shall see.

1.3 SOURCE AND CONDUCTION CURRENTS

In EMP problems the current density is made up of two parts. First, there is the source current $\vec{J}_s$ of Compton recoil electrons produced by the flux of gamma rays, which is the source of the EMP. Second, there is the conduction current J_c associated with the flow of low-energy electrons and ions induced by the electric field. The total current is the sum

$$\vec{J} = \vec{J}_s + \vec{J}_c \ . \qquad (1\text{-}9)$$

The Compton current is formed by recoil electrons that have starting energies of the order of 1 MeV. These electrons are stopped, in material media, by inelastic collisions with the media atoms. In air, the stopping range of the recoil electrons is a few meters. Therefore, if the electric field E is less than about 10^5 V/m, the effect of this field on

range will be small and may be neglected. If the field were 10^6 V/m, the range would be substantially affected by the field. The magnetic field B deflects the recoil electrons. The deflection will be small if the Larmor radius is long compared with the stopping range. The Larmor radius is a few meters when B is about 20 gauss = 2×10^{-3} webers/m^2. Thus for magnetic fields of this size or larger the deflection will be substantial.

In many applications the fields are less than the critical values just given. In these cases we may assume that J_s depends only on the gamma flux and is independent of the fields. In cases where the fields are higher, we shall estimate corrections to J_s due to the fields.

In soil, the recoil electron range is only a few millimeters (soil is about 10^3 times more dense than air). Here the fields are never large enough to affect the Compton current. Gamma rays are attenuated by a factor e in 15 to 20 cm of soil. Hence the Compton current is appreciable only in the top meter or two of the ground.

The conduction current is generally well approximated, in both air and soil, by Ohm's law,

$$\vec{J}_c = \sigma E \ , \qquad (1\text{-}10)$$

where σ(mhos/m) is the conductivity. In air, σ depends somewhat on E, making Maxwell's equations nonlinear. We can usually choose an E-independent value of σ which over-estimates coupling effects. Since the air conductivity results from ionization produced by the Compton recoil electrons, σ depends on time and position. In the ground, σ is independent of E, except at very high fields where breakdown occurs. It is also little affected by ionization, except at very high dose rates. It may be assumed independent of time and position, but it does depend on the frequency of the driving E-field (as does also ϵ). These points will be discussed in detail in later sections.

1.4 A STANDARD FORM FOR MAXWELL'S EQUATIONS

We shall write the dielectric permittivity in terms of the value ε_0 for free space,

$$\varepsilon = \varepsilon_r \varepsilon_0 \ , \tag{1-11}$$

where ε_r is the relative permittivity. If we also make use of Equations 1-9 and 1-10, the Maxwell Equation 1-2 becomes

$$\varepsilon_r \varepsilon_0 \frac{\partial \vec{E}}{\partial t} = - \vec{J}_s - \sigma \vec{E} + \frac{1}{\mu_0} \nabla \times \vec{B} \ . \tag{1-12}$$

It is convenient to replace ε_0 and μ_0 by two other parameters, namely the speed of light in vacuum,

$$c = \frac{1}{\sqrt{\mu_0 \varepsilon_0}} \approx 3 \times 10^8 \text{ m/sec} \ , \tag{1-13}$$

and the impedance of free space,

$$Z_0 = \sqrt{\frac{\mu_0}{\varepsilon_0}} \approx 120\pi \approx 377 \text{ ohms} \ . \tag{1-14}$$

These equations can be solved for μ_0 and ε_0,

$$\mu_0 = Z_0/c \quad , \quad \varepsilon_0 = 1/cZ_0 \ . \tag{1-15}$$

Inserting these expressions in Equation 12 gives

$$\frac{\varepsilon_r}{c} \frac{\partial \vec{E}}{\partial t} = - Z_0 \vec{J}_s - Z_0 \sigma \vec{E} + cV \times \vec{B} \ . \tag{1-16}$$

Every term in this equation now has the dimensions volt/m^2; note that cB is the electric field of a wave in vacuum, as follows from Equation 1-1.

In the remainder of this report we shall drop the subscript r on ε_r; ε will always mean the relative permittivity. Thus our standard form for Maxwell's equations is

$$\frac{\partial \vec{B}}{\partial t} = - \nabla \times \vec{E} \ , \tag{1-17}$$

$$\frac{\varepsilon}{c} \frac{\partial \vec{E}}{\partial t} = - Z_0 \vec{J}_s - Z_0 \sigma \vec{E} + c \nabla \times \vec{B} \ . \tag{1-18}$$

We note here also the relation between the current I(amps) in a wire and the static magnetic field B_θ encircling it at radius r,

$$2\pi r B_\theta = \mu_0 I = Z_0 I / c \quad \text{or} \quad I = 2\pi r c B_\theta / Z_0 \ . \tag{1-19}$$

Finally, note that

$$Z_0 / 2\pi \approx 120\pi / 2\pi = 60 \text{ ohms} \ . \tag{1-20}$$

REFERENCES FOR CHAPTER 1

1-1. For general background in electromagnetic theory, see Stratton, J.A., "Electromagnetic Theory," McGraw-Hill Book Company, New York, 1941.

1-2. Longmire, C. L., "Close-in EM Effects Lectures," LAMS-3072 and 3073, Los Alamos Scientific Laboratory, Los Alamos, New Mexico, 1964 (Unpublished).

1-3. Longmire, C. L., "Theory of the EMP From Nuclear Surface Bursts," LANC-R-8, Los Alamos Nuclear Corporation, Los Alamos, New Mexico, 1970.

1-4. Longmire, C. L., "On the Electromagnetic Pulse Produced by Nuclear Explosions," IEEE Trans. on Ant. and Prop., Vol. AP-26, No. 1, p. 3 (January 1978).

CHAPTER 2
THE IMPEDANCE OF SOILS

2.1 THE RC MODEL

Scott[2-1] measured the conductivity and permittivity of many samples of soil over the frequency range 10^2 to 10^6 Hz. He noticed that the results correlated quite well with the water content of the soil. He made mathematical fits to his σ and ε results as functions of frequency and water content. In making these fits, he made no attempt to ensure that $\sigma(\omega)$ and $\varepsilon(\omega)$ bear the relation to each other required by causality.

Longmire and Longley[2-2] noticed that Scott's fits could be refitted very well by assuming that between opposite faces of the soil sample there is an RC network of the type shown in Figure 2-1. In this network, $1/R_0$ represents the zero-frequency conductivity, C_∞ represents the infinite-frequency dielectric constant, and the other branches account for the change in σ and ε with frequency. A good fit was obtained with one such branch for each decade in frequency covered, with the time constant R_iC_i of the relevant branch chosen equal to the reciprocal of the median ω in that

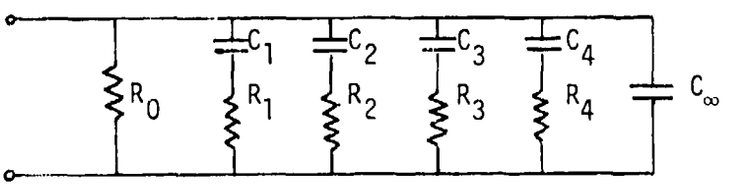

Figure 2-1. Network representing soil impedance.

decade, i.e., $(R_i C_i)^{-1} = \sqrt{10}\, 2\pi f_i$, where f_i is the frequency at the lower end of the decade in question. Thus the products $R_i C_i$ were chosen arbitrarily, to cover the frequency range uniformly. The ratios R_i/C_i and C_ω were then chosen to fit Scott's ε curve. Only one parameter, R_0, was then left to fit the σ curve, but it was found that a good fit to σ was obtained. Furthermore, it was noticed that changing the fit for a soil of different water content was accomplished by scaling all of the resistors, except R_0, by the same factor and leaving the capacitors unchanged. Longmire and Smith[2-3] used these results, and data at higher frequencies, to make a "universal impedence function" of soils over the frequency range 10^2 to 10^8 Hz.

2.2 THE SOIL ADMITTANCE

The Maxwell Equation 1-18 for fields varying as $e^{j\omega t}$ $(j^2 = -1)$ takes the form

$$\eta \vec{E} = -Z_0 \vec{J}_s + c\nabla \times \vec{B} \ , \tag{2-1}$$

where

$$\eta = Z_0 \sigma + j \frac{\omega \varepsilon}{c} \quad (\text{meters})^{-1} \ . \tag{2-2}$$

In Equation 2-1 the conduction and displacement currents have been combined into the term on the left. If we define the admittance $Y(\omega)$ of unit volume of soil by the relation between total E-driven current $\vec{J}_E$ and $\vec{E}$

$$\vec{J}_E = Y\vec{E} \ , \tag{2-3}$$

then obviously

$$\eta = Z_0 Y \ , \ Y = \frac{\eta}{Z_0} = \sigma + j\omega\varepsilon\varepsilon_0 \ . \tag{2-4}$$

The dimensions of Y are mhos/meter, while those of η are $(\text{meters})^{-1}$. We shall call η the relative admittance.

The admittance of the RC network is

$$Y = \frac{1}{R_0} + j\omega C_\infty + \sum_n \frac{j\omega C_n}{1 + j\omega R_n C_n} , \qquad (2\text{-}5)$$

The real and imaginary parts of Y are related to σ and ε by Equation 2-4. Defining RC rates β_n by

$$\beta_n \equiv (R_n C_n)^{-1} , \qquad (2\text{-}6)$$

Reference 3 fits Scott's data by the formula

$$Y = \sigma_0 + j\omega\varepsilon_\infty\varepsilon_0 + \sum_{n=1}^{13} a_n \frac{j\omega\varepsilon_0}{1 + j\omega/\beta_n} . \qquad (2\text{-}7)$$

Here σ_0 is the zero-frequency conductivity, ε_∞ is the infinite-frequency relative permittivity, ε_0 is the permittivity of free space in MKS units, the β_n are a fixed set of rates,

$$\beta_n = 2\pi(10)^{n-1} \ \text{sec}^{-1} , \qquad (2\text{-}8)$$

and the a_n are a set of dimensionless fit coefficients. For soil containing 10 percent water by volume the fit parameters are given in Table 2-1.

For this fit the relative permittivity and conductivity are

$$\varepsilon = \varepsilon_\infty + \sum_{n=1}^{13} \frac{a_n}{1 + (\omega/\beta_n)^2} , \qquad (2\text{-}9)$$

$$\sigma = \sigma_0 + \sum_{n=1}^{13} \frac{a_n \omega^2/\beta_n}{1 + (\omega/\beta_n)^2} . \qquad (2\text{-}10)$$

It can be seen that ε decreases while σ increases with increasing frequency. Graphs of ε and $\sigma-\sigma_0$ as functions of frequency are given in Figures 2-2 and 2-3. Figure 2-4 shows how σ_0 varies with water content, and also gives the scale factor F by which the rates β_n must be multiplied for different water content.

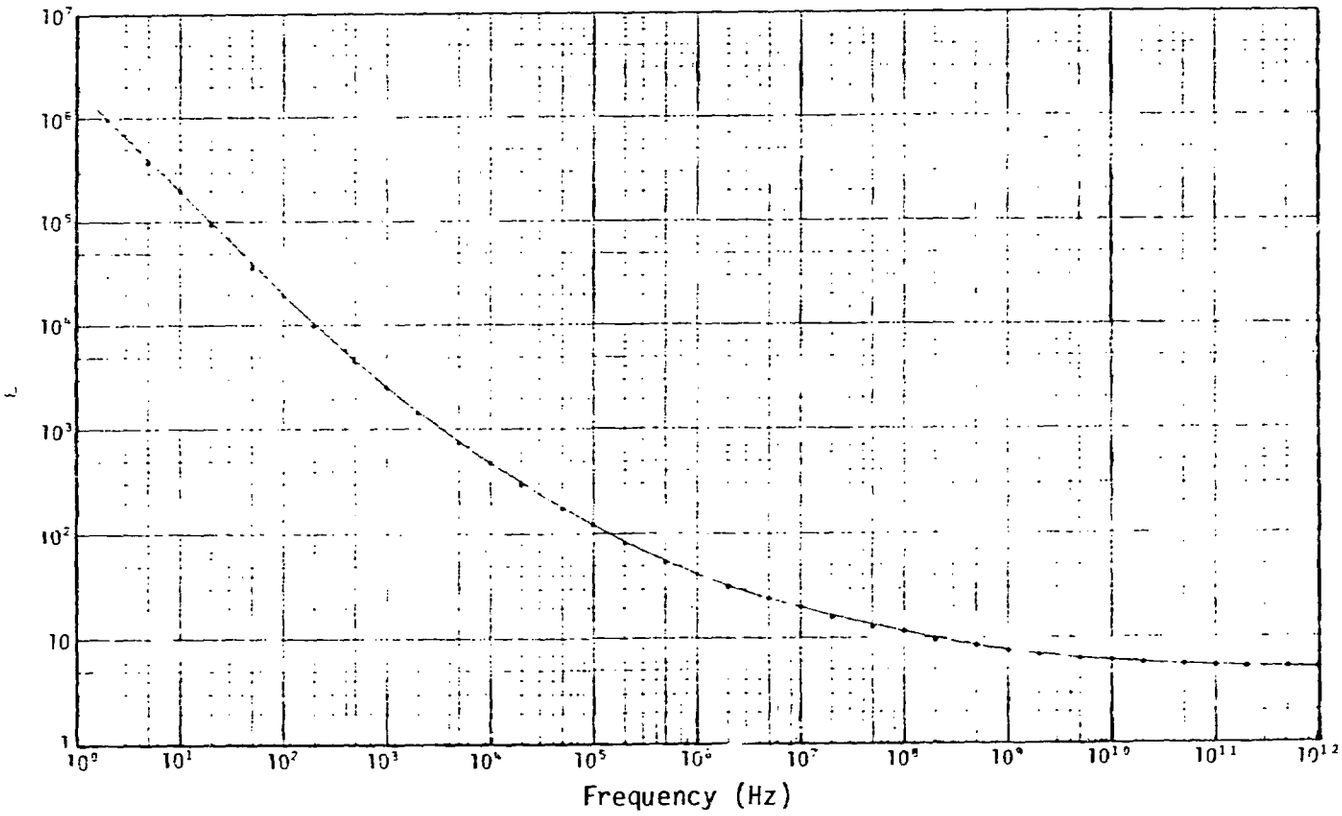

Figure 2-2. Universal curve for relative dielectric constant ε. Points are calculated from Equation 2-9, with Equation 2-8 and Table 2-1. Smooth curve is drawn through decade points.

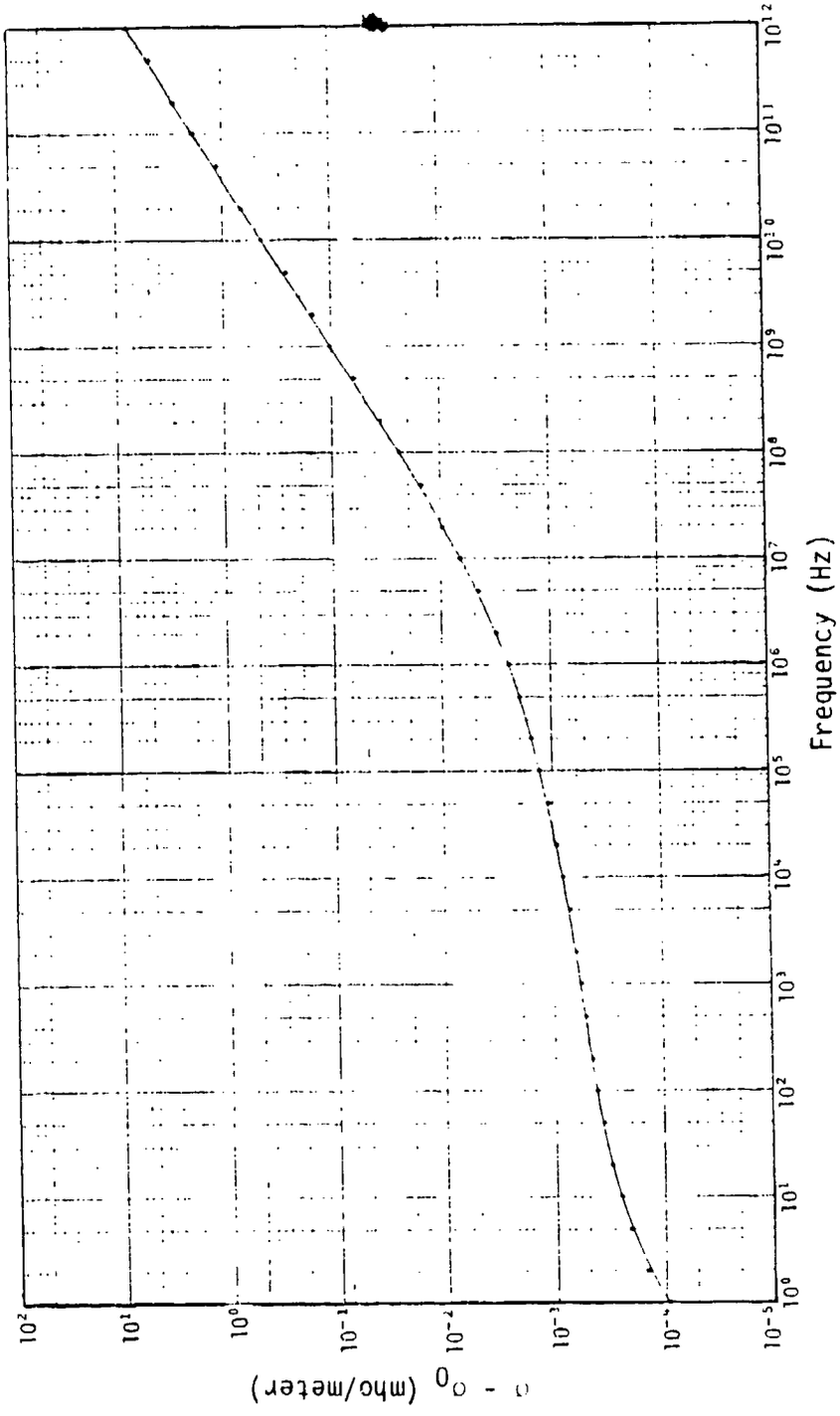

Figure 2-3. Universal curve for conductivity $\sigma - \sigma_0$. Points are calculated from Equation 2-10, with Equation 2-8 and Table 2-1. Smooth curve is drawn through decade points.

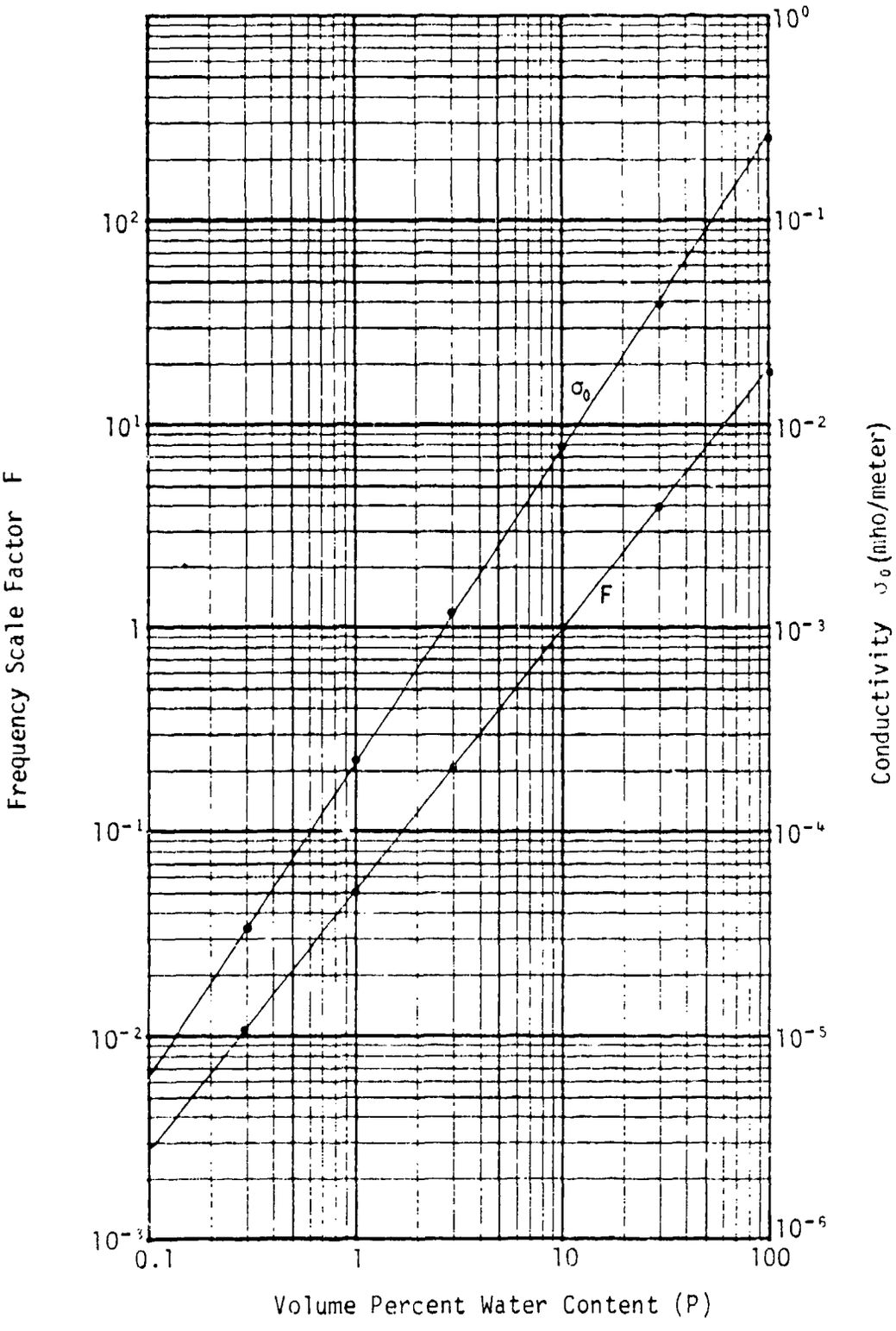

Figure 2-4. Frequency scale factor F and zero frequency conductivity σ_0 from Scott's results.

Table 2-1. Fit parameters for soil containing 10 percent water by volume.

$\sigma_0 = 8 \times 10^{-3}$ mho/m		$\varepsilon_\infty = 5$ (relative)			
n	a_n	n	a_n	n	a_n
1	3.40(6)	6	1.33(2)	11	9.80(-1)
2	2.74(5)	7	2.72(1)	12	3.92(-1)
3	2.58(4)	8	1.25(1)	13	1 73(-1)
4	3.38(3)	9	4.80(0)		
5	5.26(2)	10	2.17(0)		

This fit is expected to be good for frequencies between 10^2 and 10^8 Hz for a wide range of water contents. The author has never seen any data that cannot be fitted reasonably well by this model by adjusting only the assumed water content and the value of σ_0 (to a value that may be different from that indicated by Figure 2-4).

The fit for the relative admittance is, according to Equations 2-4 and 2-7,

$$\eta = Z_0\sigma_0 + j\frac{\omega}{c}\varepsilon_\infty + \sum_{n=1}^{13} a_n \frac{j\omega/c}{1 + j\omega/\beta_n} \quad , \tag{2-11}$$

2.3 CAUSALITY AND REALITY

The requirement of causality is that the current must vanish until a field is applied. For example, let $E(t)$ be

$$E(t) = 0 \quad , \quad t < 0 \ ,$$
$$E(t) = E_0 e^{-\gamma t} \quad , \quad t \geq 0 \ . \quad (\gamma = \text{real, positive}) \tag{2-12}$$

The Fourier transform of E is

$$E(\omega) = \int_{-\infty}^{\infty} E(t)e^{-j\omega t}dt = \frac{E_0}{\gamma + j\omega} . \qquad (2\text{-}13)$$

The current density in the frequency domain is then

$$J(\omega) = Y(\omega) \frac{E_0}{\gamma + j\omega} , \qquad (2\text{-}14)$$

and in the time domain

$$J(t) = \frac{1}{2\pi} \int_{-\infty}^{\infty} Y(\omega) \frac{E_0}{\gamma + j\omega} e^{j\omega t}d\omega . \qquad (2\text{-}15)$$

For $t < 0$, the integration contour can be extended to enclose the negative imaginary half plane. The factor $1/(\gamma+j\omega)$ has a pole at $\omega = j\gamma$. If $Y(\omega)$ has no poles in the negative imaginary half plane, the integral will vanish as required, for $t < 0$. Inspection of Equation 2-7 shows that the poles of Y are at $\omega = j\beta_n$, in the positive imaginary half plane. Thus causality is satisfied. The generally required relation between a physical σ and $\varepsilon_0(\omega$ is that they must form the real and imaginary parts of a complex function which, when analytically continued from the real ω axis into the negative imaginary half plane, has no poles there. Any RC network provides this property. Resonances in σ and ε could be accommodated by adding inductances, but it appears that none are needed.

The fact that the electric field $E(t)$ and the current density $J(t)$ are real functions of time places another condition on the admittance $Y(\omega)$ and the relative admittance $\eta(\omega)$. For general real $E(t)$, Equation 2-13 shows that the complex conjugate $E^*(\omega)$ is related to $E(\omega)$ by

$$E^*(\omega) = E(-\omega) . \qquad (2\text{-}16)$$

The same relation holds between $J^*(\omega)$ and $J(\omega)$. Since

$$Y(\omega) = J(\omega)/E(\omega) , \qquad (2\text{-}17)$$

it follows that Y and η also obey the reality condition

$$Y^*(\omega) = Y(-\omega) \ ,$$
$$\eta^*(\omega) = \eta(-\omega) \ . \tag{2-18}$$

From Equations 2-2 and 2-4, it then follow that

$$\sigma(-\omega) = \sigma(\omega) \quad , \quad \varepsilon(-\omega) = \varepsilon(\omega) \ . \tag{2-19}$$

2.4 EXPONENTIALLY RISING FIELD

In the early part of the LMP the electric field rises approximately exponentially to a level fairly near the peak field,

$$E(t) \approx E_0 e^{\alpha t} \ . \tag{2-20}$$

Hence it is useful to evaluate η for the case in which $j\omega$ is replaced by α. One obtains the real expression,

$$\eta = Z_0\sigma_0 + \frac{\alpha}{c}\varepsilon_\infty + \sum_{n=1}^{13} a_n \frac{\alpha/c}{1 + \alpha/\beta_n} \ . \tag{2-21}$$

A graph of η as a function of α for the 10 percent water soil is shown in Figure 2-5. The same figure shows the real and imaginary parts of η as a function of ω for the oscillatory case. Note that while there is no simple relation between $\eta(\alpha)$ and $\eta_r(\omega)$ and $\eta_i(\omega)$, except that contained in Equation 2-11, $\eta(\alpha)$ is not far from the sum of $\eta_r(\omega)$ and $\eta_i(\omega)$ for $\omega = \alpha$. (Actually, $\eta(\alpha)$ is a little less than the sum.)

We shall call the case graphed in Figure 2-5 our standard soil.

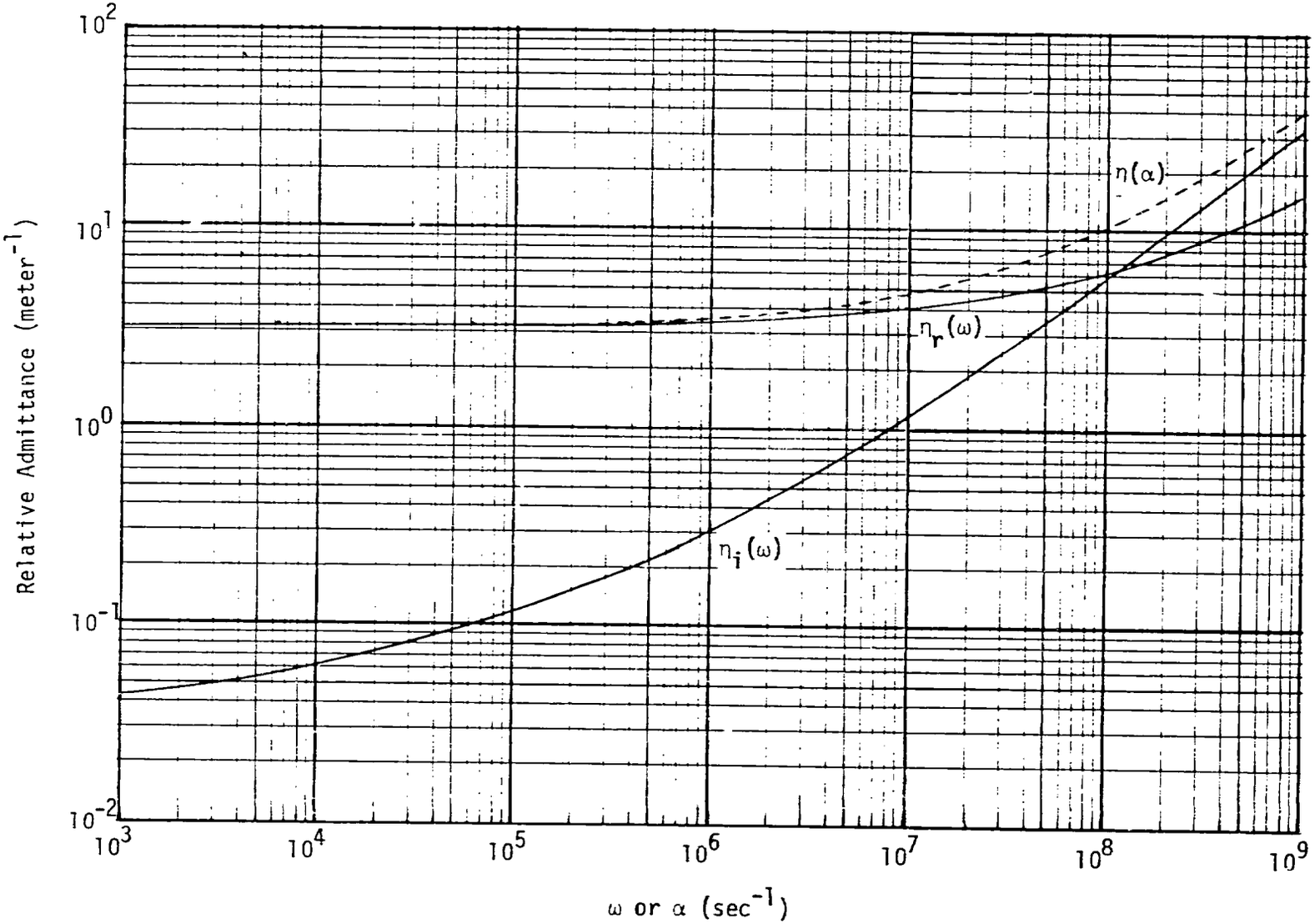

Figure 2-5. Relative admittance $\eta = \eta_r + j\eta_i$ of standard soil (10 percent water) for oscillatory ($e^{j\omega t}$) and exponential ($e^{\alpha t}$) fields.

2.5 TIME DOMAIN TREATMENT

Reference 2 showed how to treat frequency-dependent media in the time domain. Write the total E-driven current that flows into the network as the sum of the currents in its branches,

$$\vec{J}_E = C_\infty \frac{\partial \vec{E}}{\partial t} + \frac{\vec{E}}{R_0} + \sum_n \vec{J}_n \ , \tag{2-22}$$

where

$$J_n = (\vec{E} - \frac{1}{C_n}\int_{-\infty}^{t} \vec{J}_n dt)/R_n$$

$$= \beta_n (C_n \vec{E} - \int_{-\infty}^{t} \vec{J}_n dt) \ . \tag{2-23}$$

Comparison of Equation 2-5 with the fit formula (2-7) establishes the relations

$$C_\infty = \epsilon_\infty \epsilon_0 \quad , \quad \frac{1}{R_0} = \sigma_0 \quad , \quad C_n = a_n \epsilon_0 = \frac{a_n}{cZ_0} \ . \tag{2-24}$$

Thus Equations 2-22 and 2-23 can be written as

$$Z_0 \vec{J}_E = \frac{C_\infty}{c} \frac{\partial \vec{E}}{\partial t} + Z_0 \sigma_0 \vec{E} + Z_0 \sum_n \vec{J}_n \ , \tag{2-25}$$

$$\vec{J}_n = \beta_n \left(\frac{a_n}{cZ_0} \vec{E} - \int_{-\infty}^{t} \vec{J}_n dt \right) \ . \tag{2-26}$$

Inserting $Z_0 \vec{J}_E$ for $\eta \vec{E}$ in Equation 2-1), we can take that equation back to the time domain, with the result

$$\frac{C_\infty}{c} \frac{\partial \vec{E}}{\partial t} = - Z_0 (\vec{J}_s + \sigma_0 E + \sum_n \vec{J}_n) + cV \times \vec{B} \ . \tag{2-27}$$

This is the time-domain form of the Maxwell equation (1-18) for the frequency-dependent medium. The $\vec{J}_n$ are to be obtained from Equation 2-26, which can

be converted into a differential equation, if desired, by differentiating it with respect to t.

The fact that $\vec{J}_n$ is a vector means that Equation 2-26 must be solved for each non-vanishing component of $\vec{E}$. In a stratified medium, the parameters σ_0, ε_∞, and the a_n could have different values for different directions.

REFERENCES FOR CHAPTER 2

2-1. Scott, J. H., "Electrical and Magnetic Properties of Rock and Soil," Note 18 in AFWL EMP 2-1, Electromagnetic Pulse Theoretical Notes, April 1971.

2-2. Longmire, C. L., and H. J. Longley, "Time Domain Treatment of Media With Frequency Dependent Electrical Parameters," MRC-N-1, DNA 3167F, Mission Research Corporation, Santa Barbara, California, March 1971.

2-3. Longmire, C. L., and K. S. Smith, "A Universal Impedance for Soils," MRC-N-214, DNA 3788T, Mission Research Corporation, Santa Barbara, California, October 1975.

CHAPTER 3
SOURCE REGION ENVIRONMENTS

3.1 INTRODUCTION

A complete discussion of EMP environments is beyond the scope of this report. Theoretical discussions are given in References 1-2 to 1-4, and many detailed computer-based calculations have been made. Access to much of the available information is controlled by such U.S. Government agencies as the Defense Nuclear Agency and the Air Force Weapons Laboratory. The Government normally provides EMP environment specifications for systems it sponsors.

For the purposes of this report, it will be necessary to know only the general features of the EMP environment, such as the order of magnitude of rise times, amplitudes, and decay times, and approximate relations between Compton current, air conductivity, and the fields. These will be presented in this chapter. Predictions of coupling to actual systems should use environments supplied by the sponsoring agency.

While it should not be assumed that the environments hypothesized in this chapter are precisely correct for any particular real case, they are representative, in crude approximation, of those that might be observed at a point on or near the ground surface at a distance of 500 meters from a 1 megaton explosion at the ground surface or within a few tens of meters above the surface.

3.2 THE GAMMA FLUX

Figure 3-1 shows a gamma flux as a function of time, which will be used as an example in later sections of this report. The quantity graphed is actually the dose rate delivered to air, and the relation between dose rate and the actual flux F_γ of gamma energy is

$$F_\gamma \left(\frac{\gamma\text{-MeV}}{m^2 \text{sec}}\right) \approx 2 \times 10^{13} \dot{D} \left(\frac{\text{rads}}{\text{sec}}\right) . \qquad (3\text{-}1)$$

The average energy of the gammas is about 2 MeV per photon, although the total spectrum covers the range from a fraction of 1 MeV to many MeV.

The time indicated in Figure 3-1 is actually retarded time, i.e., the time origin is set when gammas first begin to arrive at the observer's position. The time for gammas to travel 500 meters is 1.67 microseconds, since the speed of light is 300 m/μs.

In a crude approximation, the gamma flux is collimated in the radial direction from the burst point (the point of the nuclear explosion). In the case assumed here, the flux is approximately horizontal. Due to scattering and finite source size, the actual angular distribution of the gammas covers several tens of degrees around the radial direction.

Figure 3-1 indicates what sources are responsible for various parts of the gamma flux. The prompt gammas are emitted by the nuclear device itself. Air inelastic gammas are made in inelastic collisions of energetic neutrons, emitted by the device, with the nuclei of air atoms. Ground capture gammas are produced when neutrons are captured in the ground near the burst point. Air capture gammas are produced later when neutrons are captured in the air. Fission product gammas are emitted over long times by the nuclear fragments resulting from fission of uranium or plutonium. Of these sources, only the prompt gammas have effectively a point source; the others originate in volumes with dimensions of the order of a few

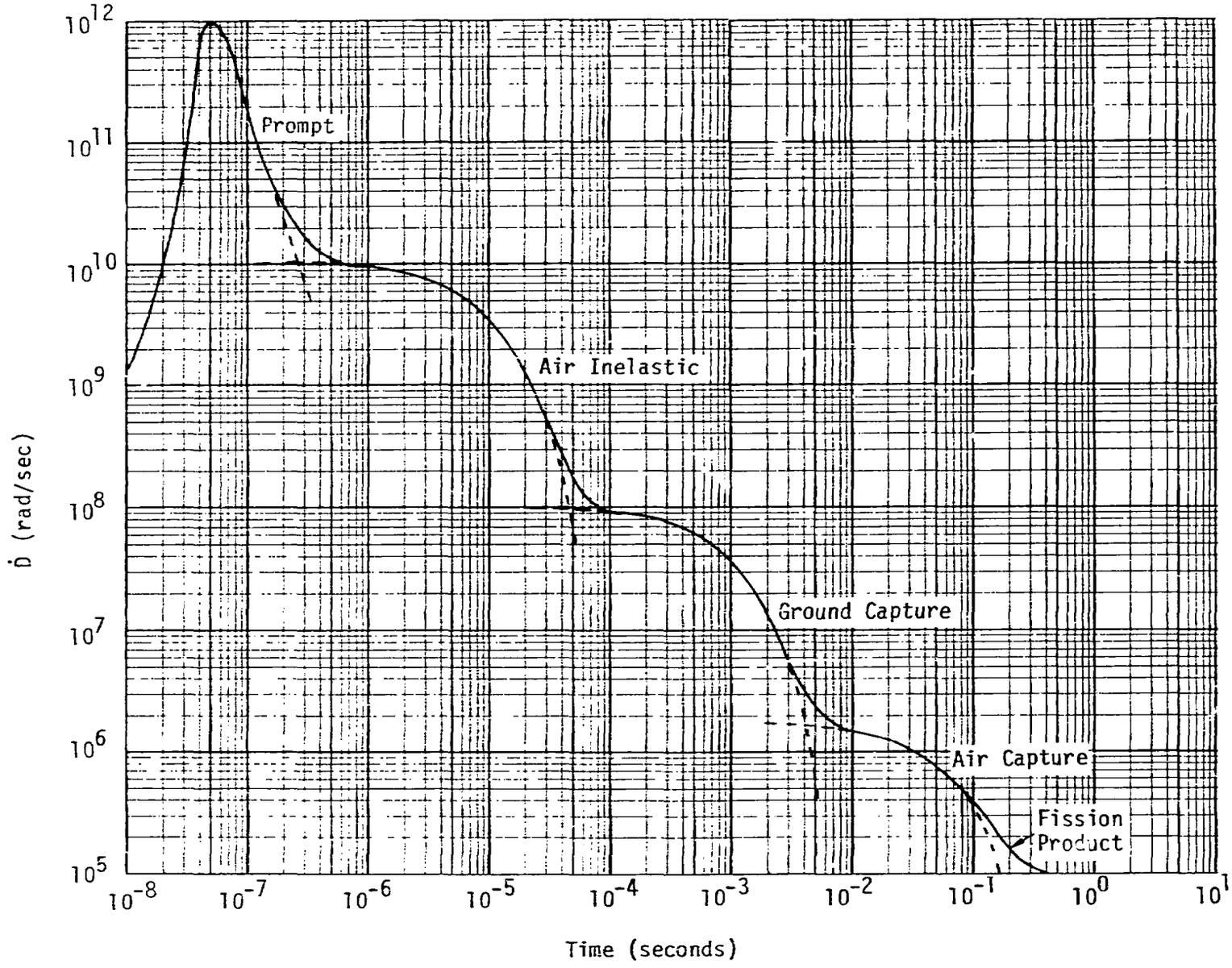

Figure 3-1. Sample gamma flux, given as dose rate in air. Sources of the various parts of the gamma flux are indicated.

hundred meters. Figure 3-1 has been drawn as if each of the sources, except the prompt and fission product gammas, were a decaying exponential. Note that the doses from each of the sources are about equal, since the sources with lower dose rates last longer in time.

The rise of the prompt gamma flux has been chosen exponential in time, i.e.,

$$\dot{D} = \Lambda e^{\alpha t} , \tag{3-2}$$

where Λ is a constant and α has been taken as

$$\alpha = 2 \times 10^{8} \text{ sec}^{-1} . \tag{3-3}$$

The exponential form is crudely representative, and is convenient for calculations. The value of α chosen is in the correct range, but should not be taken as either an upper or a lower bound on actual values.

3.3 THE COMPTON CURRENT

Gamma rays traveling through matter collide occasionally with atomic electrons, knocking the electron generally forward and scattering the photon. The mean free path of the gammas in air for these Compton scattering collisions is a few hundred meters. The recoil electrons, which have initial energies of about 1 MeV, move forward an average of a few meters before stopping. Thus a steady flux of gammas will produce a steady flux F_e of recoil electrons, in the same direction, of about 1 percent of the gamma flux. The relation

$$F_e\left(\frac{\text{electrons}}{\text{m}^2\text{sec}}\right) \approx 0.006 F_\gamma\left(\frac{\gamma\text{-MeV}}{\text{m}^2\text{sec}}\right) , \tag{3-4}$$

holds approximately in air (and in other media of low atomic number, such as soil) over the gamma energy range of interest here. From Equations 3-4 and 3-1, and the charge of an electron, one can deduce an approximate relation for the Compton current density J_s (the source of EMP),

$$J_s\left(\frac{\text{amps}}{\text{m}^2}\right) \approx 2 \times 10^{-8}\ \dot{D}\left(\frac{\text{rads}}{\text{sec}}\right) . \qquad (3\text{-}5)$$

The lifetime of a recoil electron (before stopping) is about 10^{-8} second in real time, and about 10^{-9} second in retarded time (the electron moves forward at about 0.9 of the speed of light). Thus the steady-state relation (3-5) is valid when the changes in $\dot{D}$ in periods of 10^{-9} second are small compared with $\dot{D}$. This condition is fairly well satisfied by the dose rate in Figure 3-1. The Compton current density graphed in Figure 3-2 is obtained from Equation 3-5.

3.4 THE AIR CONDUCTIVITY

Each Compton recoil electron, in slowing down, produces about 3×10^4 pairs of secondary electrons and positive ions, which make the air electrically conducting. The rate of production of ionization is directly proportional to the dose rate,

$$S\left(\frac{\text{ion pairs}}{\text{m}^3\text{sec}}\right) \approx 2 \times 10^{15}\ \dot{D}\left(\frac{\text{rads}}{\text{sec}}\right) . \qquad (3\text{-}6)$$

The free electrons, because of their small mass, respond more quickly than ions to applied electric fields, and are the dominant contributors to the air conductivity at early times. However, the electrons gradually attach themselves to O_2 molecules, forming the negative ion O_2^-. The rate a of attachment per electron is about

$$a \approx 1 \times 10^8 \text{sec}^{-1} , \qquad (3\text{-}7)$$

in sea-level air. Thus the density N_e of free electrons satisfies the equation

$$\frac{\partial N_e}{\partial t} = S - aN_e . \qquad (3\text{-}8)$$

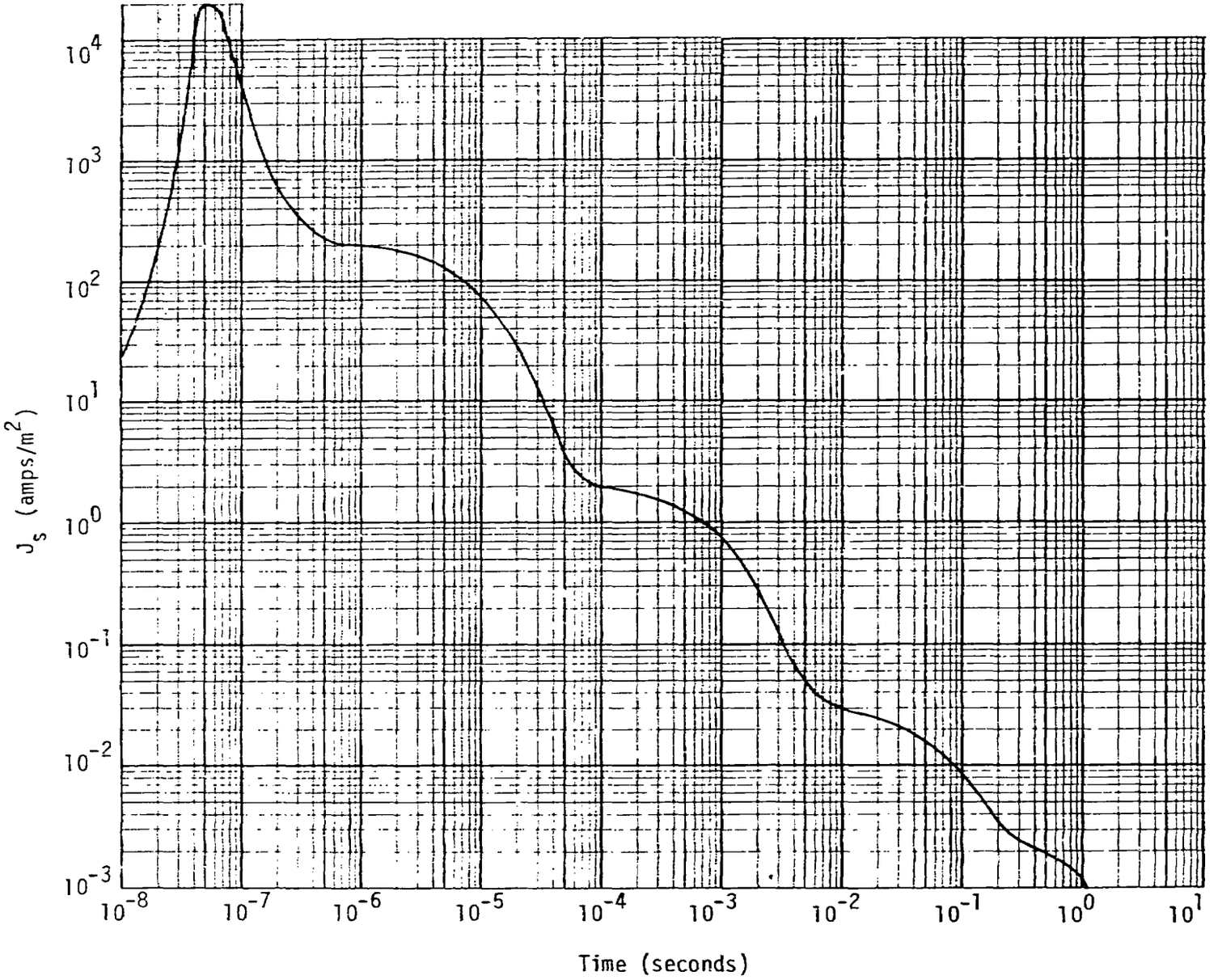

Figure 3-2. Compton current density J_s, for the gamma flux of Figure 3-1.

If the dose rate rises exponentially, as in Equation 3-2, the solution is

$$N_e\left(\frac{\text{electrons}}{m^3}\right) = \frac{S}{a+\alpha} \approx 2 \times 10^{15} \frac{\dot{D}}{a+\alpha} \quad . \tag{3-9}$$

On the other hand, if the dose rate changes little in periods of 10^{-8} second,

$$N_e \approx \frac{S}{a} \approx 2 \times 10^{7} \dot{D} \quad . \tag{3-10}$$

This equation is obtained from (3-9) by setting $\alpha = 0$.

In the presence of an electric field E, the free electrons drift through the air at an average speed v which is roughly proportional to E,

$$\vec{v} = \mu_e \vec{E} \quad . \tag{3-11}$$

The electron <u>mobility</u> μ_e is of the order of magnitude

$$\mu_e \approx 0.3 \ \frac{m}{sec}/\frac{volt}{m} \quad , \tag{3-12}$$

in sea-level air. Actually, μ_e depends significantly on E, because of Joule heating of the electrons, and a better expression, over the range $3 \times 10^3 \lesssim E \lesssim 3 \times 10^5$, is

$$\mu_e \approx 0.25\sqrt{\frac{E^*}{E}} \quad , \quad E^* = 3 \times 10^4 \text{ V/m} \quad . \tag{3-13}$$

The electrical conductivity σ is the ratio of the conduction current density J_c to E. From the equations above and the electron charge e, the electronic conductivity can be deduced as

$$\sigma_e = N_e e \mu_e \approx 0.8 \times 10^{-4} \frac{\dot{D}}{a+\alpha}\sqrt{\frac{E^*}{E}} \text{ mho/m} \quad . \tag{3-14}$$

After the peak of the dose rate, α should be set equal to zero here.

At late times, the air conductivity is dominated by positive and negative ions, because they disappear more slowly than electrons. The equation governing the positive ion density N_+ is

$$\frac{\partial N_+}{\partial t} = S - bN_+N_- \quad . \tag{3-15}$$

Here N_- is the density of negative ions (O_2^- etc.), and b is the mutual neutralization coefficient for positive and negative ions. The value of b is

$$b \approx 2 \times 10^{-12} \ m^3/sec \quad . \tag{3-16}$$

At late times, most of the electrons that have been produced are attached to O_2, so that $N_- \approx N_+$. The solution of Equation 3-15 is such that the two terms on the right-hand side nearly balance, and $\partial N_+/\partial t$ is small compared with either of these terms, so that

$$N_- \approx N_+ \approx \sqrt{S/b} \quad . \tag{3-17}$$

The mobility of the ions is about

$$\mu_i \approx 2.5 \times 10^{-4} \ \frac{m}{sec}/\frac{V}{m} \quad . \tag{3-18}$$

The ion conductivity can then be deduced as

$$\sigma_i \approx 2N_+e\mu_i \approx 2.5 \times 10^{-9}\sqrt{\dot{D}} \quad mho/m \quad . \tag{3-19}$$

Comparison of this result with Equation 3-14 with $\alpha = 0$, $E = E^*$, shows that σ_i and σ_e are equal when $\dot{D} \approx 10^7$ rads/sec.

The electronic and ionic conductivities and the total conductivity are graphed in Figure 3-3. For the electronic conductivity, E has been set equal to E^*, so that the result is indicative rather than precise, especially at early times when E will be larger than E^*.

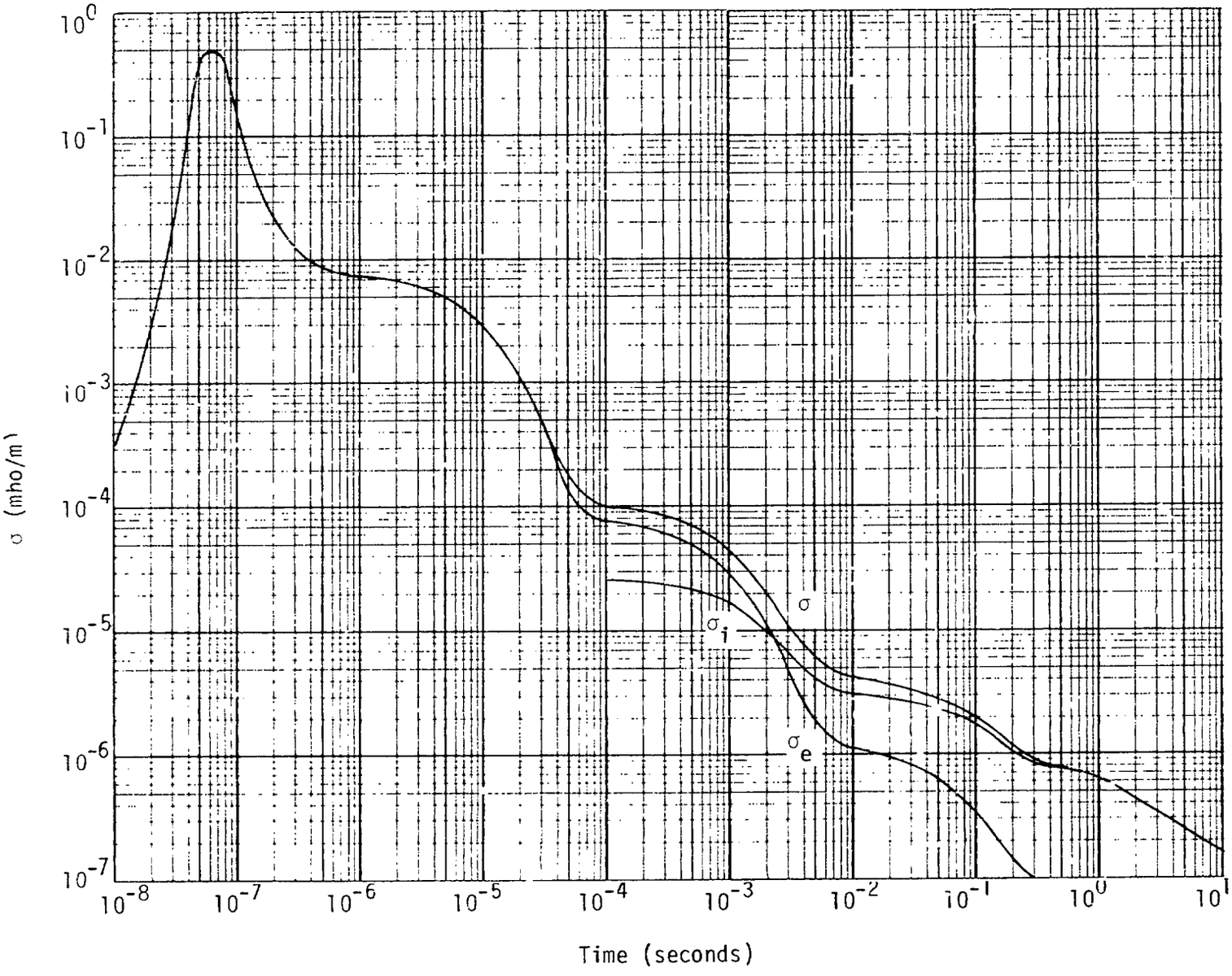

Figure 3-3. Air conductivity for the dose rate of Figure 3-1. The electronic and ionic conductivities σ_e and σ_i are shown separately, along with the total σ.

3.5 SCALING WITH DISTANCE

The gamma flux of Figure 3-1 is crudely representative for an observer at 500 meters from a 1 megaton burst near the ground surface. For other yields $\mathcal{Y}$ and distances r, the gamma flux scales roughly as

$$\dot{D} \sim \mathcal{Y} \frac{e^{-r/\lambda}}{r^2} . \tag{3-20}$$

Here λ is the effective mean free path of the gammas in air; a representative value in sea-level air is

$$\lambda \approx 300 \text{ meters} . \tag{3-21}$$

According to Section 3.3, the Compton current density has the same scaling as $\dot{D}$. The scaling of the air conductivity is less simple; σ_e scales as $\dot{D}$, while σ_i scales as $\sqrt{\dot{D}}$. At early times, σ_e is dominant at most distances of interest in this report.

3.6 THE RADIAL E FOR SPHERICAL SYMMETRY

The Compton current J_s and the air conductivity σ are approximately independent of angle about the burst point. The presence of the ground destroys complete spherical symmetry, of course. However, for observers above the ground, e.g., at power line heights, the effect of the ground on the fields will not occur immediately, but will be delayed by the finite speed of light and, more importantly, by the diffusion time of fields through the conducting air between ground and elevated observer. It is therefore useful to examine the solution of Maxwell's Equations 1-17 and 1-18 for the case of radial $\vec{J}_s$ and spherical symmetry in J_s and σ. Note that $\epsilon = 1$ in the air.

The fields $\vec{E}$ and $\vec{B}$ start from zero. Integrating Equation 1-18 over a small time interval will give, by integration of $\vec{J}_s$, a radial and

spherically symmetric $\vec{E}$. The curl of such an $\vec{E}$ vanishes, so that integration of Equation 1-17 leaves $\vec{B} = 0$. Thus the $\nabla \times \vec{B}$ term in Equation 1-18 remains equal to zero, and $\vec{E}$ remains radial and spherically symmetrical. The vector signs may be dropped and Equation 1-18 becomes

$$\frac{1}{c}\frac{\partial E}{\partial t} = - Z_0 J_s - Z_0 \sigma E \ . \qquad (3\text{-}22)$$

Note that this equation contains no spatial derivatives: E is determined at each point by the local J_s and σ.

At sufficiently early times J_s and σ are small and E will be small, and σE will be negligible compared with J_s. In this time frame

$$E \approx cZ_0 \int J_s dt \ . \qquad (3\text{-}23)$$

If J_s rises as $\exp(\alpha t)$, E will also, and

$$E \approx - \frac{cZ_0}{\alpha} J_s \ . \qquad (3\text{-}24)$$

In this time frame, it can be said that J_s is charging up the capacitance of space ($cZ_0 = 1/\varepsilon_0$).

Eventually σE will become comparable with J_s, if the dose rate is large enough. In this case the $\partial E/\partial t$ term can be neglected in Equation 3-22, giving the approximate solution

$$E = - \frac{J_s}{\sigma} \equiv E_s \ . \qquad (3\text{-}25)$$

This equation defines the <u>saturated field</u> E_s, which is such that conduction current cancels Compton current. Since J_s and σ are both proportional to $\dot{D}$ (at early times), they tend to rise and fall together, so that E is almost constant after saturation is reached. Thus $\partial E/\partial t$ is indeed small.

The value of E_s can be determined from Equations 3-5, 3-14, and 3-25. The result comes out directly as

$$E_s \approx 2.5 \times 10^4 \left(\frac{a + \alpha}{10^8}\right) \sqrt{\frac{E_s}{E^*}} \quad .$$

With the value of E^* given in Equation 3-13, this result becomes

$$E_s\left(\frac{V}{m}\right) \approx 2 \times 10^4 \left(\frac{a + \alpha}{10^8}\right)^2 \quad . \tag{3-26}$$

Thus, if saturation occurs during the exponential rise in the sample gamma flux with $\alpha = 2 \times 10^8$, the peak E will be

$$E_s \approx 1.8 \times 10^5 \text{ V/m} \quad . \tag{3-27}$$

However, after the peak in the gamma flux $\alpha \approx 0$, and

$$E_s \approx 2 \times 10^4 \text{ V/m} \quad . \tag{3-28}$$

At late times, when the ion conductivity is dominant, E_s falls roughly as $\sqrt{D}$. However, by this time the effect of the ground asymmetry will usually be felt. Figure 3-4 shows $E(t)$ for the sample case, neglecting the ground effect altogether. Note that the peak E occurs before the peaks in $\dot{D}$ and J_s.

The question as to whether or when E reaches the saturated value can be answered by comparing the capacitively-limited field of Equation 3-23 or 3-24 with E_s. Thus saturation will occur during the exponential rise if

$$\left|\frac{cZ_0}{\alpha} J_s\right| \geq E_s = \left|\frac{J_s}{\sigma}\right| \quad ,$$

or if

$$\sigma \leq \alpha/cZ_0 \approx 2 \times 10^{-3} \text{ mho/m} \quad , \tag{3-29}$$

in the example. Figure 3-3 shows that this occurs well before the peak σ. Saturation is much easier to reach after the peak of the gamma flux.

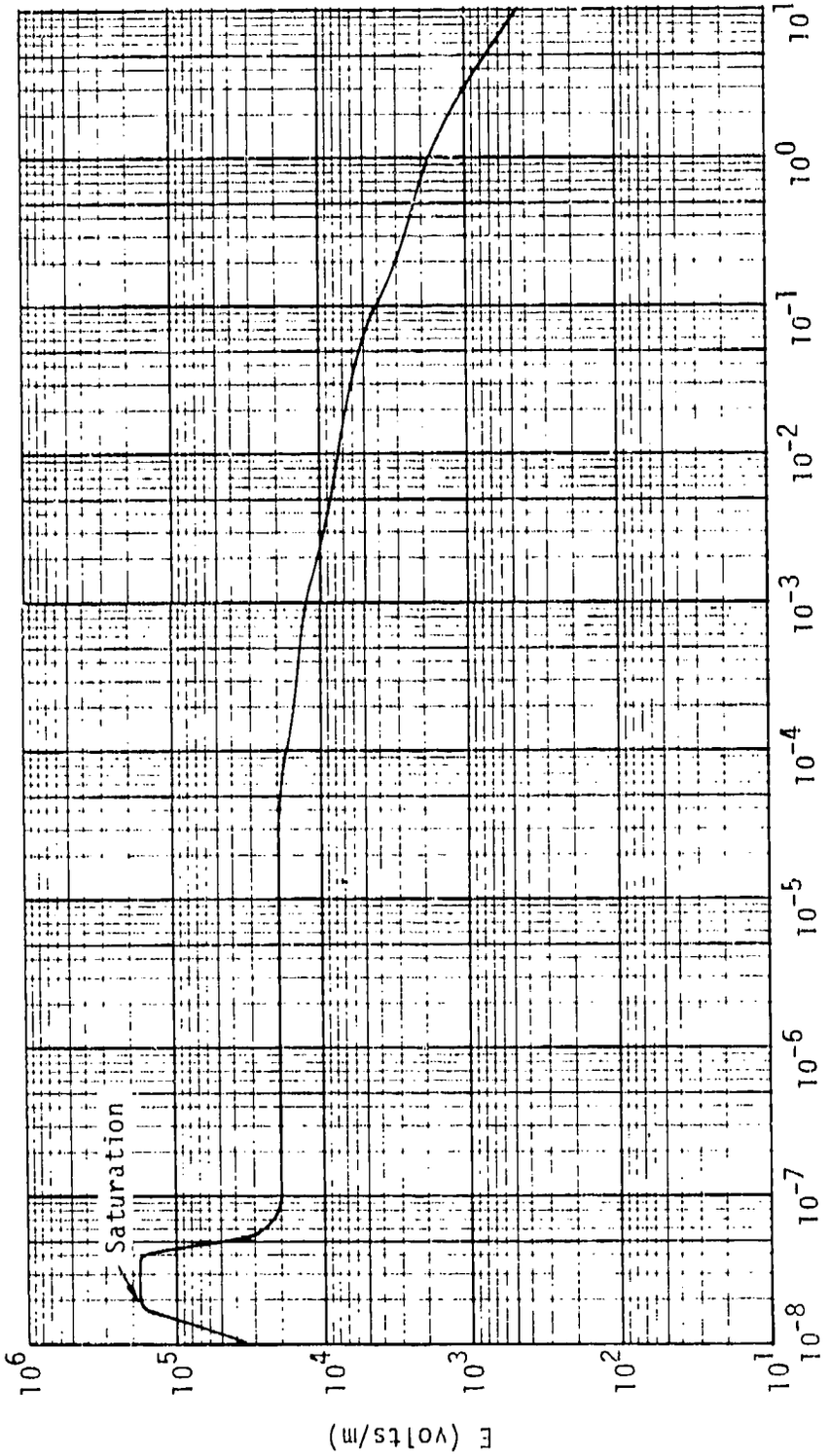

Figure 3-4. Radial electric field E for assumed spherical symmetry and sample gamma flux.

The diffusion time of ground-induced fields to elevated observers will be discussed in Section 3.9.

3.7 FIELDS GENERATED BY AIR-GROUND ASYMMETRY

The radial E of Section 3.6 is generated everywhere in the air in the beginning. However, the ground, being usually (but not always) a better conductor than the air, shorts out the radial E applied to it. A current flows in the ground, and this current induces a horizontal magnetic field, in the direction perpendicular to the applied radial E (i.e., in the azimuthal direction around the burst point), and horizontal and vertical electric fields. The induced horizontal E-field approximately cancels the applied radial E at the ground surface. In the usual system of spherical polar coordinates with r measured from the burst point, θ measured from the vertical, and ϕ the azimuthal angle, the field components present are E_r, E_θ, and B_ϕ. The induced fields propagate away from their point of generation, through the conducting air and soil.

A detailed exposition of the ground-induced fields is possible (see References 1-2 to 1-4) but lengthy, and will not be given here. Qualitative understanding can be had by recognizing three phases. The wave phase occurs at early times when the air conductivity is negligible or small. In this phase the ground-induced fields propagate through the air rather freely, but with some attenuation due to the small conductivity. Because the radial E applied to the ground appears to move outward with the speed of light (the speed of the gamma flux), the ground induced fields radiate chiefly outward in a small angular zone (in θ) just above the ground. The fields are predominantly E_θ and B_ϕ, and they have the relation $E_\theta \approx cB_\phi$ appropriate for a vertically polarized transverse wave propagating along the ground. E_r is small at the ground, but rises to the radial E of Section 3.6 at the upper edge of the small angular zone. For a gamma flux rising as $\exp(\alpha t)$, E_θ and B_ϕ rise first as $\exp(\alpha t)$, then as $\exp(\alpha' t)$ where

α' is a small fraction of α, and then as $\exp(\alpha t/2)$, the differences being due to the effects of air conductivity between the burst point and the observer. The last time dependence is the most important, since it goes with the largest field amplitudes.

The wave phase ends and the diffusion phase begins when σ reaches the value indicated in Equation 3-29. This is the time when the radial E saturates (without ground effects) and also the time when the conduction current exceeds the displacement current. In the diffusion phase the term $\partial E/c\partial t$ can be dropped from the Maxwell Equation 1-18. The two Equations 1-17 and 1-18 then define a diffusion problem like that in the well-known skin effect, as will be discussed in Section 3.9. True wave propagation ceases, due to conductivity. E_ϕ continues to increase as $\exp(\alpha t/2)$ and E_θ decreases as $\exp(-\alpha t/2)$. E_r is limited, at the ground surface, by the finite ground conductivity, and is nowhere greater than E_s. The ground-induced fields diffuse up into the air until they can go no further, i.e., until the skin depth in the air is comparable with the radius r from the burst.

When the diffusion is complete, the quasistatic phase begins. In this phase, the deposition of charge by the Compton current is balanced by removal of charge by the conduction current driven by the static electric field. The electric field is thus derivable from a potential Φ,

$$\vec{E} = -\nabla\Phi \quad (\nabla \times \vec{E} = 0) \ , \tag{3-30}$$

and the conservation of charge, Equation 1-7, becomes

$$\nabla \cdot (\vec{J}_s - \sigma\nabla\Phi) = 0 \ . \tag{3-31}$$

With $\vec{J}_s$ and σ given, this equation determines Φ, from which $\vec{E}$ can be computed. The magnetic field is then determined by the static form of Equation 1-18,

$$\nabla \times \vec{B} = \frac{Z_0}{c} (\vec{J}_s + \sigma \vec{E}) \quad . \tag{3-32}$$

The fields in the quasistatic phase are not exactly static, of course, but the changes are so slow that the time derivative terms in Maxwell's equations are small compared with other terms. The correct fields at each time are near the static solution for the instantaneous $\vec{J}_s$ and σ. The approximate solution of Equations 3-31 and 3-32 will be discussed in Section 3.12.

One additional point must be made regarding the diffusion phase. At positions sufficiently close to the burst, the peak air conductivity σ_a exceeds the ground conductivity σ_g. Since soil conductivities are usually not much greater than about 10^{-2} mho/m, this is true in the case of Figure 3-3. This condition modifies the diffusion problem to some extent. When $\sigma_a >> \sigma_g$, $E_r \ll E_s$ right down to the ground surface. In addition, the Compton current in the top layer of the ground (the top half meter or so) becomes an important source of fields, as will be discussed in Section 3-11.

Figure 3-5 shows the fields in the air just above the ground as functions of time. These fields are consistent with the sources in the example discussed in this chapter. Although they have not been obtained in detailed calculations, they will suffice for our development of source-region coupling theory.

In the remaining sections of this chapter, somewhat more detailed discussions of the phases are given. In reading these sections, it will be useful to refer to Figure 3-5 for illustration of the features deduced or stated.

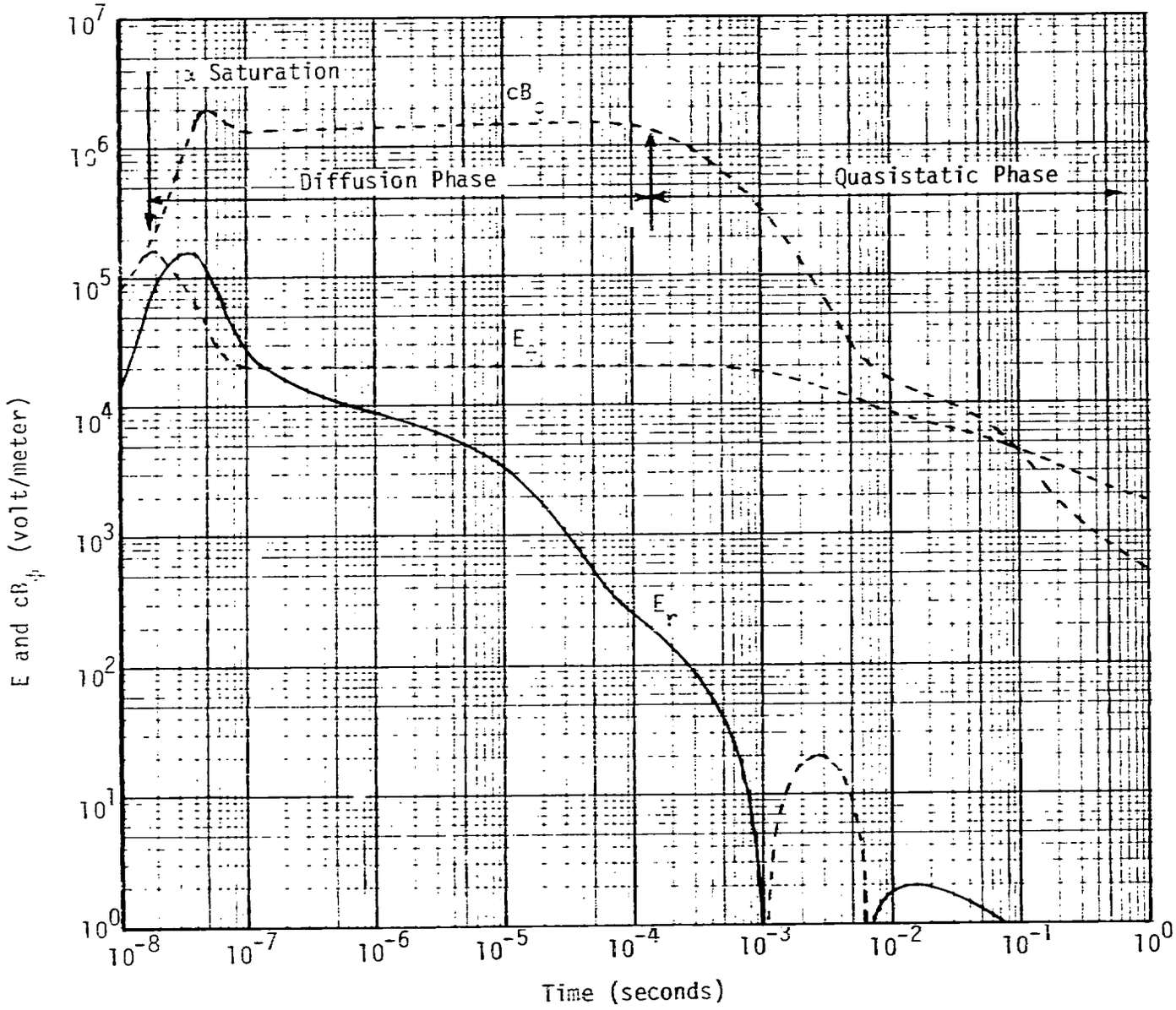

Figure 3-5. Electric fields E_r and E_z and magnetic field B_ϕ as functions of retarded time for example sources. For comparison with E_r and E_z, cB_ϕ is graphed instead of B_ϕ. Solid curves indicate positive fields, dashed curves negative.

3.8 THE WAVE PHASE

At early times the effect of the air conductivity is either negligible or small. At these times the ground-induced fields are well represented by outgoing spherical waves. While both outgoing and ingoing waves are generated by the Compton current (in the presence of the ground asymmetry), the fact that the Compton current moves outward with the speed of light, maintaining approximate phase with outgoing EM waves, causes the outgoing waves to be built up to amplitudes much larger than those of the ingoing waves. The effect of the air conductivity is to attenuate the outgoing waves to some degree. In the wave phase, the air conductivity is generally small compared with the ground conductivity, and in first order the ground may be regarded as a perfect conductor. The finiteness of the ground conductivity leads to some additional attenuation of the outgoing waves.

The relation between $\vec{E}$ and $\vec{B}$ and the attenuation of the outgoing waves can be understood by considering plane waves in a conducting medium. On the assumption that $\vec{E}$ and $\vec{B}$ have the forms

$$\vec{E},\vec{B} = (\vec{E}_0,\vec{B}_0)e^{j(\omega t-\vec{k}\cdot\vec{r})} , \tag{3-33}$$

where $\vec{E}_0,\vec{B}_0$ are constants denoting amplitude and polarization, Equations 1-17 and 1-18 become, for freely propagating waves (J_s=0),

$$\omega\vec{B}_0 = \vec{k} \times \vec{E}_0 , \tag{3-34}$$

$$(\frac{\epsilon\omega}{c} - jZ_0\sigma)\vec{E}_0 = - c\vec{k} \times \vec{B}_0 . \tag{3-35}$$

Crossing $\vec{k}$ into (3-35) and using (3-34) to eliminate $\vec{k} \times \vec{E}_0$ leads to:

$$\begin{aligned}\frac{\omega}{c}(\frac{\epsilon\omega}{c} - jZ_0\sigma)\vec{B}_0 &= - \vec{k} \times (\vec{k}\times\vec{B}_0) \\ &= - \vec{k}(\vec{k}\cdot\vec{B}_0) + (\vec{k}\cdot\vec{k})\vec{B}_0 .\end{aligned} \tag{3-36}$$

The initial condition (1-3) becomes, for the present case,

$$\vec{k} \cdot \vec{B}_0 = 0 \ .$$

(It is necessary here to use the initial condition since the assumed fields are oscillatory at all times, rather than starting from zero.) Therefore

$$\vec{k} \cdot \vec{k} = k_0^2 (1 - j \frac{Z_0 \sigma}{\sqrt{\varepsilon} k_0}) \ , \tag{3-37}$$

where k_0 is defined as the propagation constant in the absence of conductivity,

$$k_0 \equiv \sqrt{\varepsilon} \frac{\omega}{c} \ . \tag{3-38}$$

Equation 3-37 indicates that for non-vanishing σ, $\vec{k}$ will be complex, with real and imaginary parts $\vec{k}_r$ and $\vec{k}_i$,

$$\vec{k} = \vec{k}_r + j\vec{k}_i \ . \tag{3-39}$$

As will be seen in Section 3.10, Equation 3-37 does not require that the <u>directions</u> of $\vec{k}_r$ and $\vec{k}_i$ be the same. If they are arbitrarily chosen to be the same, so that

$$\vec{k} = \vec{n} k \ , \tag{3-40}$$

where $\vec{n}$ is a real unit vector and k is a complex number, then Equation 3-37 allows $\vec{n}$ to be arbitrary but determines k,

$$k = k_0 \sqrt{1 - j \frac{Z_0 \sigma}{\sqrt{\varepsilon} k_0}} \ . \tag{3-41}$$

When the magnitude of the imaginary term in the radical is small compared with unity, this solution is approximately

$$k \approx k_0 - j \frac{Z_0 \sigma}{2\sqrt{\varepsilon}} \ . \tag{3-42}$$

In the air, $\varepsilon = 1$, and the <u>attenuation length</u> ℓ is independent of frequency,

$$\ell = 2/Z_0\sigma \ . \qquad \text{(air)} \tag{3-43}$$

The directions of $\vec{E}_0, \vec{B}_0$ and $\vec{n}$ are mutually orthogonal, with $\vec{E}_0 \times \vec{B}_0$ in the direction of $\vec{n}$. From Equation 3-34 it follows that the complex amplitudes of $\vec{E}_0$ and $\vec{B}_0$ are related by

$$cB_0 \approx \sqrt{\epsilon} \left(1 - j \frac{Z_0\sigma}{2\sqrt{\epsilon}k_0}\right) E_0 \ . \tag{3-44}$$

Since the imaginary term here has been assumed to be small compared with unity, the magnitudes of E_0 and B_0 are related approximately by

$$\left.\begin{aligned} |E_0| &\approx \frac{c}{\sqrt{\epsilon}} |B_0| \ , \\ &\approx c|B_0| \quad \text{in air} \ . \end{aligned}\right\} \tag{3-45}$$

In the earliest part of the wave phase, σ is negligible everywhere. In this case, the fields will rise as $e^{\alpha t}$ if the Compton current J_s does; hence the name <u>α wave phase</u> for this regime. The ground-induced fields are E_0 and B_ϕ in the spherical coordinates indicated in Figure 3-6, and these fields are produced by the shorting out of E_r at the ground surface.

The exponential rise of the fields ceases when the attenuation becomes important anywhere. Since σ is largest very near the nuclear device, attenuation first becomes important at $r = r_0$, the radius of the device itself. The transition occurs when the attenuation length ℓ becomes less than r_0, i.e., when

$$\sigma(r_0) \simeq \frac{2}{Z_0 r_0} \ . \tag{3-46}$$

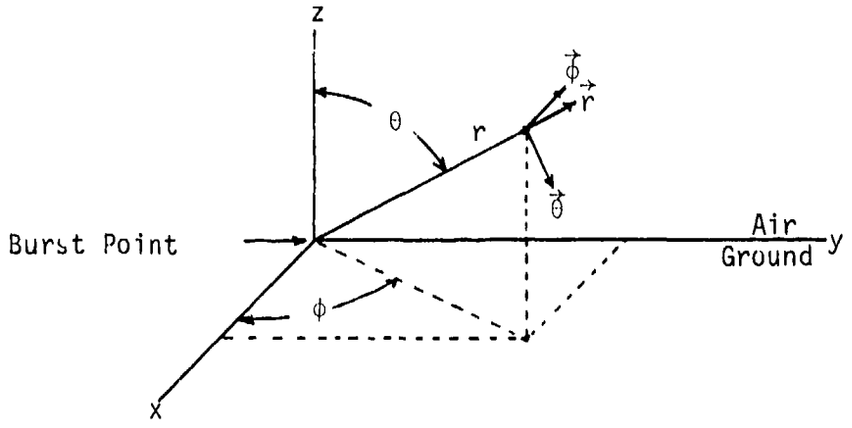

Figure 3-6. Cartesian and spherical coordinates. The x,y plane is the air-ground interface.

This condition is reached very early in the rise, and it is difficult to detect the α wave phase at appreciable distances from the explosion.

Let an observer be located at radius $r >> r_0$. If r is not too large, attenuation will eventually become important at this distance. At most distances of interest, the dominant variation of σ with distance (at constant retarded time) comes from the factor $e^{-r/\lambda}$ in Equation 3-20. The time of λ-saturation at the observer is defined as that when ℓ becomes less than λ, i.e., when

$$\sigma(r) \geq \frac{2}{Z_0 \lambda} \approx 2 \times 10^{-5} \text{ mho/m} \quad \text{at} \quad r \,. \tag{3-47}$$

The condition (3-46) is also called λ-saturation at r_0. Between the retarded times at which the conditions (3-46) and (3-47) are reached, the fields at r rise roughly as $e^{\alpha' t}$, where α' is a small fraction of α.

After λ-saturation at the observer, the fields E_0 and B_ϕ rise as $e^{\alpha t/2}$, provided J_s is still rising as $e^{\alpha t}$. This dependence continues until σ reaches the value indicated by Equation 3-29, which is called α-saturation, and is the condition that conduction current exceed displacement current.

The end of the wave phase occurs, for a given observer, at the time of α-saturation at his location. During the entire wave phase, the relation (3-45) holds between E_θ and B_ϕ. These fields are confined chiefly to a layer of air just above the ground, with thickness δ of the order of a few meters. At the onset of α-saturation

$$\delta \approx c/\cdot \tag{3-48}$$

and the fields are

$$cB_\phi \approx E_\theta \approx - E_s \ . \tag{3-49}$$

Here E_s is the saturated field defined in Section 3.6.

3.9 THE DIFFUSION PHASE

The diffusion phase begins when the air conductivity reaches the value given by Equation 3-29, and in it the displacement current is negligible in the air. The dominant fields are E_r and B_ϕ. E_r is near the saturated field E_s except in a layer just above the ground, and B_ϕ is appreciable only in this layer. In this thin layer it is convenient to use the Cartesian coordinates indicated in Figure 3-6. For an observer located on or near the y axis, the y-direction is approximately the same as the r-direction and the x-direction is approximately the same as the -ϕ-direction. The distance above the ground is z. Maxwell's Equations 1-17 and 1-18 become, for this case

$$- \frac{\partial B_\phi}{\partial t} = \frac{\partial E_r}{\partial z} \ , \tag{3-50}$$

$$Z_0 \sigma E_r = - Z_0 J_r - c \frac{\partial B_\phi}{\partial z} \ . \tag{3-51}$$

Substituting E_r from the second equation into the first gives

$$\frac{\partial B_\phi}{\partial t} = \frac{\partial}{\partial z}\left(\frac{J_r}{\sigma}\right) + \frac{c}{Z_0} \frac{\partial}{\partial z} \frac{1}{\sigma} \frac{\partial B_\phi}{\partial z} \ . \tag{3-52}$$

This is a type of diffusion equation for the magnetic field. The first term on the right-hand side is the source, for without it $B_\phi = 0$ would be a solution. Both J_r and σ are approximately independent of z in the air, so the source exists only at the ground surface, where σ changes from air to ground, and in the top 10 to 30 cm of the ground, where J_r falls rapidly due to attenuation of the gamma flux in the ground. If the ground conductivity is large compared with the air conductivity, most of the source occurs at the ground surface.

The total magnetic flux $\mathscr{F}$ per radial meter,

$$\mathscr{F} = \int B_\phi dz \ , \tag{3-53}$$

produced by the source can be found by integrating Equation 3-52 over z. Since B_ϕ and $\partial B_\phi/\partial z$ vanish deep in the air and ground and J_r/σ vanishes deep in the ground,

$$\frac{\partial \mathscr{F}}{\partial t} = \left(\frac{J_r}{\sigma}\right)_{air} = - E_s \ . \tag{3-54}$$

Thus

$$\mathscr{F}(t) = \mathscr{F}_s - \int_{t_s}^{t} E_s dt \ , \tag{3-55}$$

where $\mathscr{F}_s$ is the flux at the time t_s of the beginning of the diffusion phase (α-saturation). (Note that B_ϕ and $\mathscr{F}$ are negative, i.e., B_ϕ runs clockwise around the burst point.)

In the air the source term vanishes and σ is (roughly) independent of z. Thus Equation 3-52 becomes

$$\frac{\partial B_\phi}{\partial t} = \frac{c}{\varepsilon_0 \sigma} \frac{\partial^2 B_\phi}{\partial z^2} \ . \tag{3-56}$$

This equation governs the diffusion of B_ϕ up into the air. The solution is qualitatively different during the exponential rise and after the peak of the gamma flux. During the rise, let us try the assumption that

$$B_\phi \sim e^{\beta t} , \tag{3-57}$$

where β is a constant to be determined. Equation 3-56 then determines the z-dependence,

$$B_\phi \sim e^{-z/\delta} , \tag{3-58}$$

where the skin depth δ is

$$\delta = \sqrt{\frac{c}{z_0 \sigma \beta}} = \sqrt{\frac{1}{\mu_0 \sigma \beta}} . \tag{3-59}$$

Since σ increases as $e^{\alpha t}$, δ decreases during the rise as $e^{-\alpha t/2}$. The amplitude of B_ϕ can be estimated from δ and the total flux

$$B_\phi \delta \approx \mathcal{F} , \quad \text{or} \quad B_\phi \approx \mathcal{F}/\delta . \tag{3-60}$$

Since E_s is constant during the exponential rise of the gamma flux, Equation 3-55 indicates that $(-)\mathcal{F}$ increases only linearly with time, or slowly compared with the exponential increase of $1/\delta$. Thus approximately

$$B_\phi \sim e^{\alpha t/2} . \tag{3-61}$$

Comparison with Equation 3-57 shows that

$$\beta \approx \frac{\alpha}{2} , \quad \delta \approx \sqrt{\frac{2c}{z_0 \sigma \alpha}} = \sqrt{\frac{2}{\mu_0 \sigma \alpha}} . \tag{3-62}$$

Note that in writing Equation 3-60, we neglected the flux in the ground. This is permissible if the skin depth in the ground is small compared with that in the air (so that the ground contains little flux), or if the ground conductivity is large compared with the air conductivity. The case in which this condition does not hold will be discussed in Section 3.11.

After the peak in the gamma flux, σ falls and the skin depth increases. Note that Equation 3-56 can be brought to simpler appearance by changing the time variable to T defined by

$$dT = \frac{c\,dt}{Z_0\sigma} \quad , \quad T = \int_{t_p}^{t} \frac{c\,dt}{Z_0\sigma} \quad , \tag{3-63}$$

where t_p is the time of the peak. Equation 3-56 then becomes

$$\frac{\partial B_\phi}{\partial T} = \frac{\partial^2 B_\phi}{\partial z^2} \quad . \tag{3-64}$$

Solutions of this equation can be found as functions of the similarity variable $z/\sqrt{T}$. Thus the skin depth is

$$\delta \approx \sqrt{T} = \left(\int_{t_p}^{t} \frac{c\,dt}{Z_0\sigma} \right)^{1/2} \quad . \tag{3-65}$$

The amplitude of B_ϕ can again be estimated from Equations 3-55 and 3-60.

Figure 3-4 shows that E_s, after falling about one decade from its peak, is then almost constant for several decades in time. During most of this interval, Equation 3-55 becomes

$$\mathcal{E}(t) \approx - E_s t \quad . \tag{3-66}$$

Figure 3-3 shows that, to a crude approximation, σ can be written over the same time interval as

$$\sigma(t) \approx \sigma_p \frac{t_p}{t} \quad , \tag{3-67}$$

where the subscript p indicates peak values. With this approximation, the skin depth becomes

$$\delta = \left(\frac{ct^2}{2Z_0 \sigma_p t_p} \right)^{1/2} . \qquad (3\text{-}68)$$

From Equation 3-60, the estimate of B_ϕ is

$$B_\phi \approx E_s \left(\frac{2Z_0 \sigma_p t_p}{c} \right)^{1/2} . \qquad (3\text{-}69)$$

Thus B_ϕ is roughly constant in time in the diffusion phase after the peak of the gamma flux.

As stated before, E_r tends to be small at the ground surface and rises to E_s at heights of a few skin depths. If the ground conductivity σ_g is not very large compared with the air conductivity σ_a, then E_r at the surface is given approximately by

$$E_r \approx \frac{\sqrt{\sigma_a}}{\sqrt{\sigma_a} + \sqrt{\sigma_g}} E_s . \qquad (3\text{-}70)$$

This formulae comes from considering the impedances of air and soil within one skin depth from the surface. The return conduction current that would flow in one skin depth in the air, if the ground were not present, is shared with one skin depth in the ground.

The field E_θ would be small in the diffusion phase if it were not for the effect of the magnetic field B_ϕ on the Compton current. The Compton electrons are turned upwards, away from the ground by the magnetic force on them. For B_ϕ greater than about 10^{-3} Weber/m^2 = 10 gauss, the resulting J_θ is comparable with J_r. A roughly static field E_θ then arises, of sufficient magnitude to drive a conduction current cancelling J_θ. Thus E_θ is comparable with E_s, provided B_ϕ is as large as indicated above.

3.10 FIELDS IN THE GROUND AT EARLY TIMES

Cables and other components of systems are often buried at depths of one to a few meters in the ground. It is therefore important to see how fields propagate in the ground. The assumption of oscillatory fields of the form (3-33) leads to Equation 3-37, which can also be written as

$$\vec{k} \cdot \vec{k} = \frac{\omega}{c}\left(\frac{\varepsilon\omega}{c} - jZ_0\sigma\right) . \qquad (3\text{-}71)$$

The factor in parentheses here is $-j\eta$, where η is the relative admittance of the soil defined in Chapter 2. Figure 2-5 shows that at the higher frequencies of interest, neither the real or imaginary part of η is negligible.

The fields in the ground can be related to the magnetic field B_ϕ at the surface, discussed in previous sections. Over distances of only several meters, B_ϕ at the surface can be regarded as a function only of $t - \frac{r}{c}$; i.e., except for time delay, B_ϕ is the same at different r. Thus the radial phase velocity of all Fourier components of B_ϕ is c, so that the component with frequency ω has radial wave number

$$k_r = \omega/c . \qquad (3\text{-}72)$$

Since $\vec{k}$ has the two components k_r and k_z, and since k_r in the ground must match that of B_ϕ at the surface, Equation 3-71 determines k_z as

$$\pm k_z = \frac{\omega}{c}\sqrt{(\varepsilon-1) - j\frac{Z_0\sigma c}{\omega}} . \qquad (3\text{-}73)$$

Thus k_z is complex, so that the waves attenuate as they propagate downward in the ground.

The fact that k_z is complex while k_r is real means that the real and imaginary parts of $\vec{k}$ do not have the same direction. The dispersion relation (3-71) does not force real and imaginary parts to be

parallel, i.e., phase planes and amplitude planes need not be parallel. Equation 3-71 determines one Cartesian component of $\vec{k}$ if the other components are specified.

The real and imaginary parts of k_z are plotted as the points in Figure 3-7 as a function of ω for our standard soil, for which the relative admittance was graphed in Figure 2-5. Messier (Reference 3-1) noticed that a remarkably good fit to soil propagation constants is obtained by the simple formula

$$\pm k_z = \sqrt{\varepsilon_\infty - 1}\,\frac{\omega}{c} + \sqrt{-jZ_0\sigma_0\,\frac{\omega}{c}}\,, \tag{3-74}$$

The curves in Figure 3-6 represent the real and imaginary parts of this formula, which obviously has the same limits for low and high ω as Equation 3-73. The values of ε_∞ and σ_0 used in the fit are

$$\varepsilon_\infty = 6.5 \quad , \quad \sigma_0 = 8 \times 10^{-3} \text{ mho/m} \,. \tag{3-75}$$

Note that σ_0 has the same value as in Table 2-1, whereas ε_∞ has been adjusted slightly to give a better fit over the range $10^3 \leq \omega \leq 10^9$ sec^{-1}.

If the magnetic field $B_\phi(t)$ at the ground surface is represented by its Fourier transform $B_a(\omega)$, then B_ϕ in the ground at depth z (taken positive) is obtained by propagating each frequency component with its k_z,

$$B_\phi(z,t) = \frac{1}{2\pi}\int_{-\infty}^{\infty} B_a(\omega)\exp\left[j(\omega t - k_z z)\right]d\omega \,. \tag{3-76}$$

If Messier's approximation for k_z is used, this equation can be written as

$$B_\phi(z,t) = \frac{1}{2\pi}\int_{-\infty}^{\infty} B_a(\omega)\exp\left[j\omega t' - \sqrt{j\omega T_2}\right]d\omega \,, \tag{3-77}$$

where

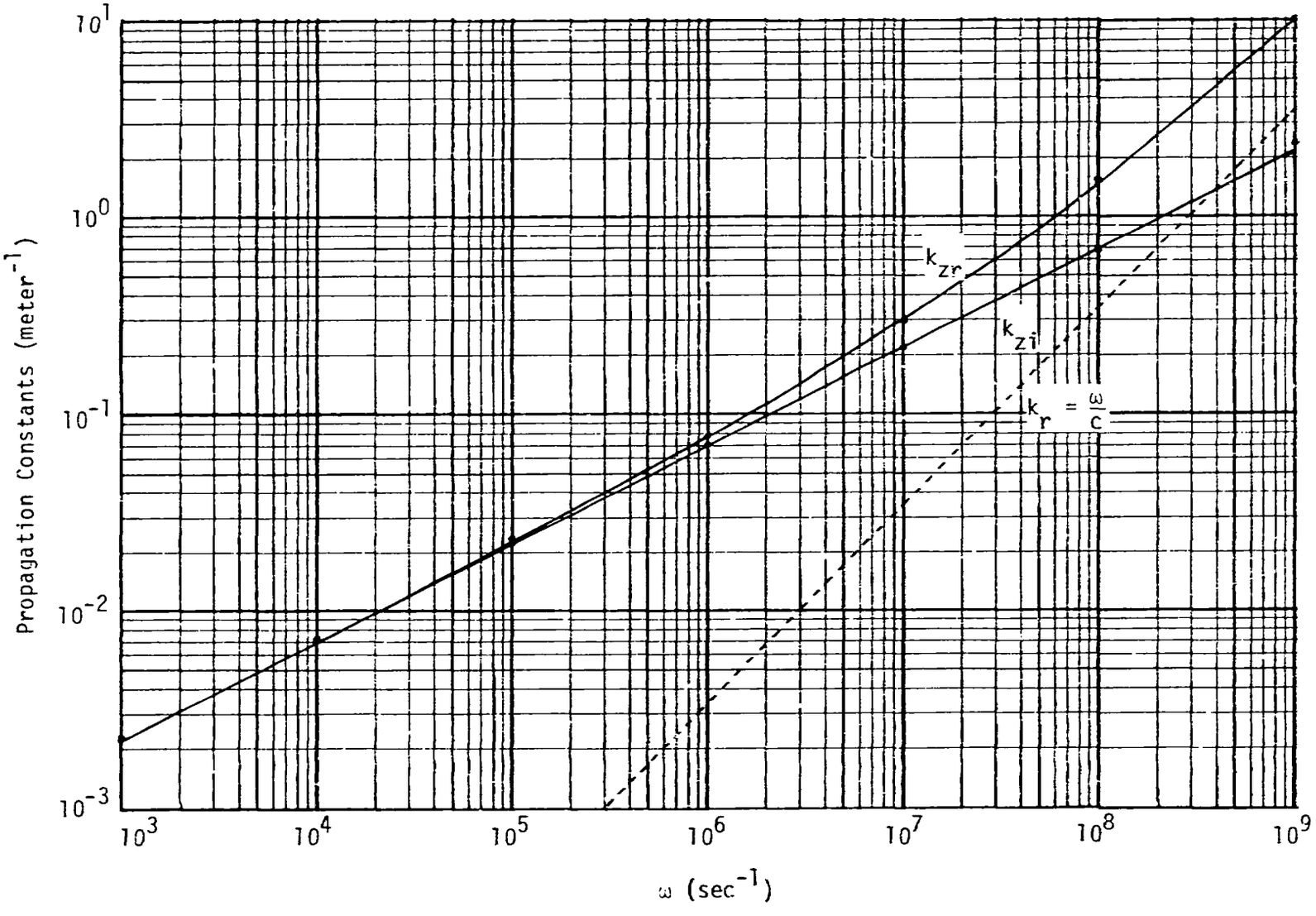

Figure 3-7. Propagation constants in standard soil. Points: real and imaginary parts computed from exact Equation 3-73. Solid curves: Messier's approximation, Equation 3-74. Dashed line: assumed $k_r = \omega/c$.

$$t' = t - T_1 \quad , \quad T_1 \equiv \sqrt{\varepsilon_\infty - 1}\ z/c \ , \tag{3-78}$$

and

$$T_2 \equiv Z_0 \sigma_0 z^2/c \ . \tag{3-79}$$

The appearance of t' in the integral has the result that the onset of the field at depth z is delayed by the time T_1 after onset at $z = 0$. T_1 is the time for the highest frequencies to propagate a distance z in the vertical direction. (The actual phase propagation direction is not vertical, but is in the direction corresponding to the components k_r, k_{zr}.)

The radical in the exponential in Equation 3-77 gives a diffusive spreading in time, in addition to the delay. This can be seen if $B_a(t)$ is taken as an impulse function at $t = 0$, for which $B_a(\omega) = 1$. Evaluation of the integral then gives

$$B_\phi(z,t) = \frac{4}{\sqrt{\pi} T_2} \left(\frac{T_2}{4t'}\right)^{3/2} \exp(-T_2/4t') \ . \tag{3-80}$$

It can be seen that the time integral of this function is unity, independent of T_2. A graph of $T_2 B_\phi$ is presented in Figure 3-8. Since $T_2 \sim z^2$, the impulse function at $z = 0$ is broadened into a longer and lower pulse with increasing z. For our standard soil

$$T_2 = 1.01 \times 10^{-8}\ z^2 \text{sec} \ . \tag{3-81}$$

Thus at 1 meter depth, the impulse response is a pulse of approximately 10^{-8} second duration. For arbitrary $B_0(t)$, the response at depth z can be obtained by folding $B_0(t)$ with the impulse response.

It is also instructive to examine the z-dependence of the impulse response (3-80) for fixed t. For this purpose it is convenient to define a skin depth

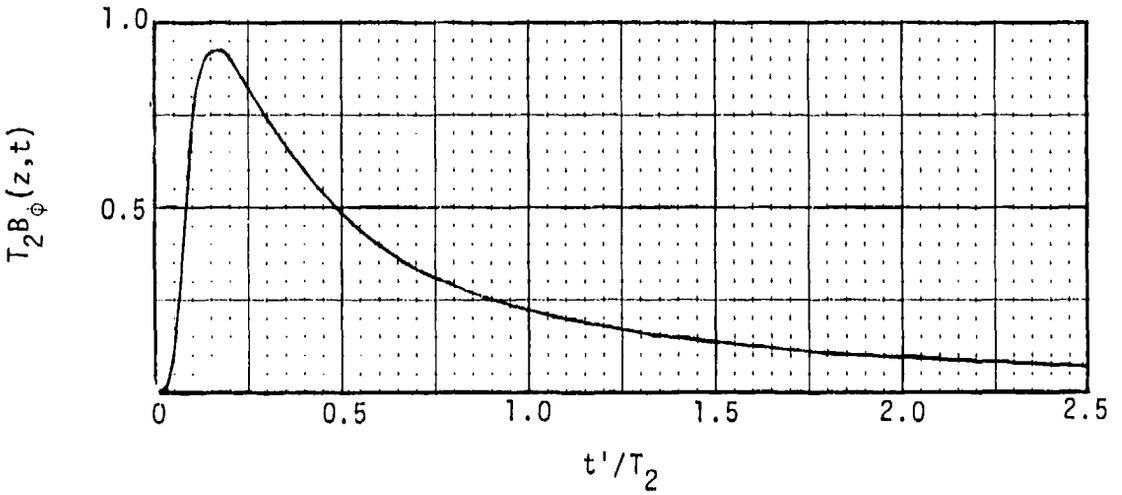

Figure 3-8. Magnetic field as a function of time for impulse field at ground surface.

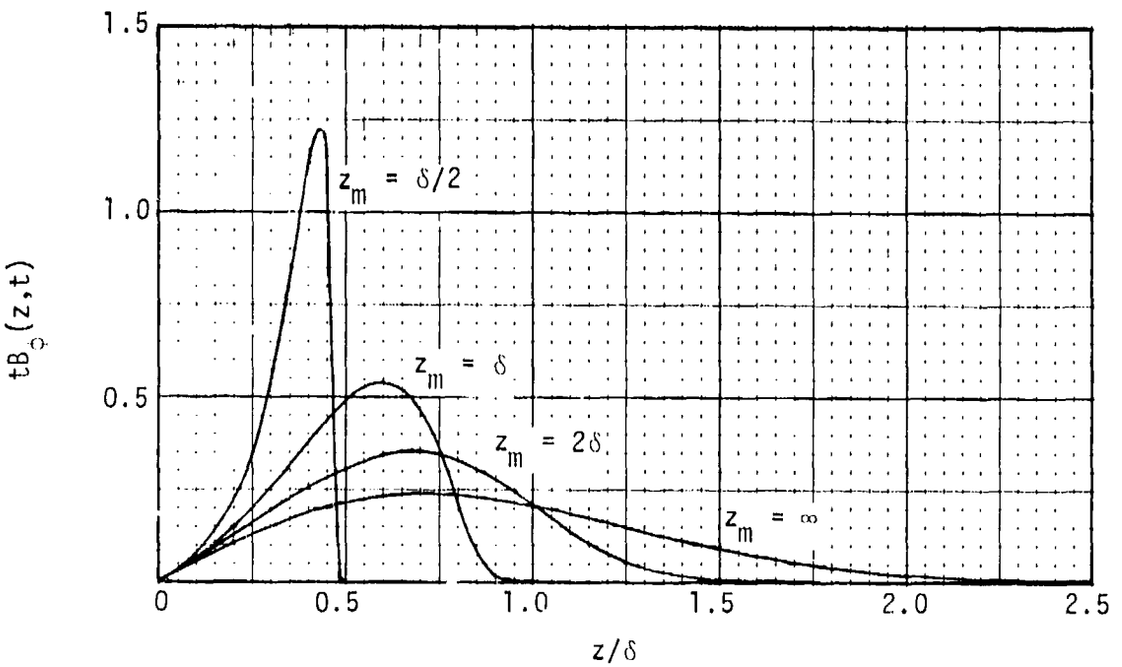

Figure 3-9. Magnetic field as a function of depth for impulse field at ground surface, at various times. z_m is maximum depth reached by speed of light in medium, δ is skin depth.

$$\delta(t) = \sqrt{\frac{4ct}{z_0\sigma_0}} \quad , \tag{3-82}$$

and the maximum depth reachable by waves in the ground in time t

$$z_m(t) = ct/\sqrt{\varepsilon_\infty - 1} \, . \tag{3-83}$$

With these definitions, Equation 3-80 can be written as

$$B_\phi(z,t) = \frac{1}{\sqrt{\pi}t} \frac{z/\delta}{(1 - \frac{z}{z_m})^{3/2}} \exp\left[-\frac{(z/\delta)^2}{(1 - \frac{z}{z_m})}\right] . \tag{3-84}$$

This formula contains two characteristic lengths, and so is not graphable as a single curve. The two lengths δ and z_m are equal when

$$ct = \frac{4(\varepsilon_\infty - 1)}{z_0\sigma_0} \approx 7.3 \text{ m} \quad , \quad \text{or} \quad t \approx 2.43 \times 10^{-8} \text{ sec} \, . \tag{3-85}$$

For smaller t, $z_m < \delta$, and for larger t, $z_m > \delta$. The numerical values here are from Equation 3-75 for Messier's fit. Figure 3-9 shows $tB_\phi(z,t)$ for $z_m = \frac{1}{2}\delta$, δ, and 2δ, corresponding to $t = 0.61$, 2.43, and 9.72×10^{-8} second. Also shown is the limiting case for $z_m >> \delta$. In this presentation evidence of propagation, as contrasted with diffusion, practically disappears by the time $z_m > 2\delta$.

If instead of $B\phi$, E_r at the surface (or E_z) is specified as $E_{ra}(t)$ or $E_{ra}(\omega)$ the same formulae can be used to obtain E_r (or E_z) at depth. Thus these fields are also broadened in time and decreased in amplitude with increasing depth.

The determination of B_ϕ, E_r and E_z at the surface must be accomplished by solving Maxwell's equations in the air and ground simultaneously. The analysis of this section does not avoid that work, but only explains the relation of the fields in the ground to those at the surface. The analytical method developed here could be used to determine

the ground fields if the ground conductivity were always large compared with the air conductivity. In this case, $B_a(t)$ could be determined by solving Maxwell's equations in the air over perfectly conducting ground. Next, B_ϕ could be found in the ground by the methods of this section, and E_r and E_z determined from B_ϕ. It is more convenient to obtain the fields by use of the finite-difference codes LEMP-SUBL.

3.11 EFFECT OF COMPTON CURRENT IN THE GROUND

The attenuation length of the gamma rays in soil is about

$$\lambda_g \approx 0.2 \text{ m} . \tag{3-86}$$

The relation of this length to that in air, Equation 3-21, is determined by the density of soil, about 2 gm/cm^3, as compared with that of air, about 1.23×10^{-3} gm/cm^3. It is clear that any gammas observed in the ground at appreciable distances from the burst must have traveled mostly through the air and entered the ground only near the point of observation. If the burst were on a flat surface and there were no air scattering, the prompt gamma flux would drop to zero at the air-ground interface. Gammas scattered in the air can enter the ground, but arrive with a time delay corresponding to their longer path. Since the prompt pulse is only a few times 10^{-8} second in width, scattered paths that are longer by more than about 10 meters than the direct path do not contribute to the prompt pulse at distance. Only gammas scattered through small angles can contribute, and the number of these is only about 5 percent of the unscattered gammas during the prompt pulse. Thus for a burst on a flat surface, the gamma flux drops by a factor of about 20 at the air-ground interface and decays further to negligible values in depths of the order of 10 cm. Since the ratio of Compton current density to gamma flux is approximately independent of material and density (see Equation 3-4), the total Compton current in the ground is equal to that in only about 10/20 = 0.5 cm of air above the surface. The Compton current in the ground is negligible during the prompt pulse for a burst on a flat surface.

If the burst is above the surface, or if the surface is curved and is exposed to line of sight from the burst at the observer, unscattered gammas can enter the ground. If the angle between the line of sight and the surface tangent is ψ, as in Figure 3-10, then the Compton current density in the ground attenuates with depth approximately as

$$\vec{J}_s = \vec{J}_{s0} e^{-|z|/d} , \tag{3-87}$$

where

$$d = \lambda_g \sin\psi = 0.2 \sin\psi \text{ m} . \tag{3-88}$$

Here $\vec{J}_{s0}$ is the Compton current density in the air-ground interface. The current density is (approximately) continuous across the interface, but decays in the ground in a depth d.

The Compton current in the ground is important when the air conductivity exceeds the grou d conductivity. At distances of interest, this happens only during the prompt pulse. In this case, the electric field in the air is limited by

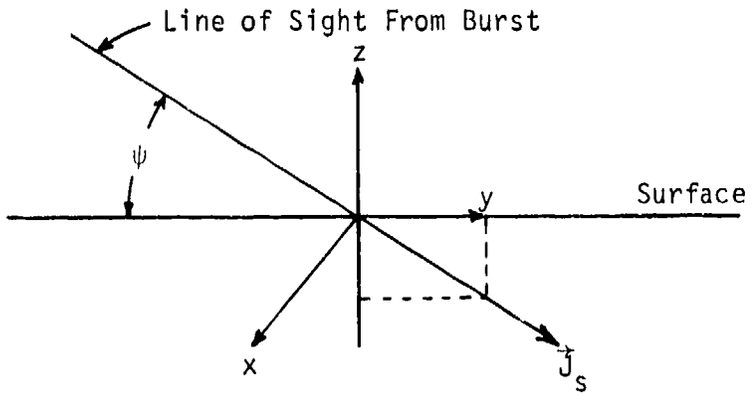

Figure 3-10. Geometry and coordinates for ground field analysis.

$$E \leq E_s = -\frac{J_s}{\sigma_a} ,$$
$$\approx 2 \times 10^5 \text{ V/m} . \qquad (3\text{-}89)$$

In the ground, if E reached the value J_s/σ_g, it would be larger than that in the air. The field in the ground does not generally reach this value, because the return conduction current flows over a thickness of one skin depth δ of soil, and δ is usually larger than d.

The fields produced in the ground can be calculated exactly for a gamma flux rising as $\exp(\alpha t)$, as is done in Reference 3-2, under the assumption that $\sigma_a >> \sigma_g$ so that the air can be regarded as a perfect conductor. The results of that calculation are summarized briefly here.

The relative admittance $\eta(\alpha)(m^{-1})$ has been defined in Section 2.2, and Figure 2-5 shows $\eta(\alpha)$ for our standard soil. The a ual admittance $Y = \eta/Z_0$ (mho/m). The skin depth in the soil is

$$\delta = \sqrt{\frac{c}{\alpha\eta}} \approx 0.4 \text{ m} . \qquad (3\text{-}90)$$

The numerical value here is for the example presented in this chapter.

If the conduction current returned on the same paths followed by the Compton current, the electric field in the ground would be

$$\vec{E} \Leftarrow -\frac{Z_0}{\eta} \vec{J}_s . \qquad (3\text{-}91)$$

Instead of this relation, Reference 3-2 shows that the maximum horizontal component E_y in the ground is

$$E_{ym} \approx -\frac{Z_0}{\eta} J_{s0y} \frac{d^2}{\delta^2} , \qquad (3\text{-}92)$$

where J_{s0y} is the y component of the Compton current density at the surface. This value is reached at depth $\approx d$ in the ground; $E_y = 0$ at the surface in

this model (large air conductivity) because the field produced in the air was neglected. (One could add $E_s(air)$.) The factor d^2/δ^2 in Equation 3-92 comes from two sources. One factor d/δ comes from the fact that the return current flows over depth δ while the Compton current flows over depth $d < \delta$. The other factor comes from the proximity of the Compton current to the highly conducting air. By using Equation 3-89 to relate E_y to the saturated field E_s in the air and Equations 3-88 and 3-90, Equation 3-92 can be written

$$\left.\begin{aligned} E_{ym} &\approx E_s \sigma_a Z_0 \frac{\alpha}{c} \lambda_g^2 \sin^2\psi\cos\psi \ , \\ &\approx 5\sin^2\psi\cos\psi E_s \quad \text{(example)} \ . \end{aligned}\right\} \qquad (3\text{-}93)$$

In the example, the peak σ_a was used from Figure 3-3. The maximum value of $\sin^2\psi\cos\psi$ is about 0.36, at $\psi = 63°$.

The maximum value of E_z in the ground occurs just below the surface, and is

$$\left.\begin{aligned} E_{zm} &\approx \frac{Z_0}{\eta} J_{s0z} \approx E_s \frac{Z_0 \sigma_a}{\eta} \sin\psi \ , \\ &\approx 19\sin\psi E_s \quad \text{(example)} \ . \end{aligned}\right\} \qquad (3\text{-}94)$$

Skin depth spreading does not reduce the vertical conduction current density or E_z. This large E_z decays in the depth d.

The magnetic field $B_x(=-B_\phi)$ is reversed from the usual direction near the surface, because most of the Compton current in the ground returns as conduction current in the air. The value of B_x at the surface is

$$\left.\begin{aligned} B_{x0} &\approx \frac{Z_0}{c} dJ_{sy0} = \mu_0 \lambda_g J_{s0} \sin\psi\cos\psi \ , \\ &\approx -5 \times 10^{-3} \sin\psi\cos\psi \quad \text{Weber/m}^2 \quad \text{(example)} \ . \end{aligned}\right\} \qquad (3\text{-}95)$$

In the example the peak current density was used from Figure 3-2. This result may be compared with the field preceded by the air current at the ground surface,

$$\left.\begin{aligned} B_{x0a} &\approx -\mu_0 \delta_a J_{sy0} \approx -\mu_0 \sqrt{\frac{c}{\varepsilon_0 \sigma_a \alpha}}\, J_{s0} \cos\psi \ , \\ &\approx 2.2 \times 10^{-3} \cos\psi \ \text{Weber/m}^2 \quad \text{(example)} \ . \end{aligned}\right\} \tag{3-96}$$

The field B_x decays in depth d in the ground, and changes sign again due to return conduction current flowing below the Compton current.

When the air conductivity falls below the ground conductivity, after the peak, δ_a soon becomes larger than δ_g, and the ground current and fields are again dominated by sources in the air.

Two cautions should be noted regarding the results of this section. First, the peak E_z estimated in Equation 3-94 is in a range that might lead to breakdown in the soil. Second, the peak dose rate in the example is sufficiently high that it might increase the conductivity of the top layer of the ground. Not much can be said with certainty about the probability of occurrence of either of these effects; experiments with relevant soil samples are needed. Both effects could be expected to result in a decrease in the fields at greater depths in the ground, but relying on this expectation might be risky.

Attention was first called to the importance of the ground Compton currents by R. R. Schaefer and W. R. Graham.

3.12 THE QUASISTATIC PHASE

As stated in Section 3.7, the quasistatic phase begins when the skin depth in the air becomes as large as allowed by the spherical geometry, i.e., when δ exceeds the distance r from the burst point,

$$\delta > r. \tag{3-97}$$

The approximation (3-67) for $\sigma(t)$ is representative if the time origin is suitably chosen, as in Figure 3-3. In that case (our usual example)

$$\sigma_p = 0.5 \text{ mho/m} \quad , \quad t_p \approx 6 \times 10^{-8} \text{ sec} . \tag{3-98}$$

Equation 3-68 then gives the skin depth

$$\delta \approx 3.6 \times 10^{6}\, t \quad \text{(example)} . \tag{3-99}$$

With $r \approx 500$ meters, the quasistatic phase begins at

$$t = 1.4 \times 10^{-4} \text{ sec} . \tag{3-100}$$

Figure 3-3 shows that ion conductivity is beginning to be significant at this time. Over most of the quasistatic phase, ion conductivity is dominant.

It was shown in Reference 1-2 that a fair approximation to the solution of the governing Equation 3-31 for the quasistatic phase is obtained by taking the potential function Φ to be a function of θ alone. Thus the predominant electric field is E_θ; the electric field lines are approximately circular about the burst point as center. The fields E_θ and B_ϕ can be deduced from this model and the conservation of charge, Equation 3-31. If we assume $E_r << E_\theta$, this equation becomes (on writing the divergence operator in spherical coordinates)

$$\frac{1}{r\sin\theta} \frac{\partial}{\partial\theta} \sin\theta\sigma E_\theta = - \nabla \cdot \vec{J}_s = - \frac{1}{r^2} \frac{\partial}{\partial r} r^2 J_s . \tag{3-101}$$

Since σ is approximately independent of θ and since the distance scaling of J_s is approximately that in Equation 3-20, this equation can be written

$$\frac{\sigma}{r\sin\theta} \frac{\partial}{\partial\theta} \sin\theta E_\theta = \frac{J_s}{\lambda} ,$$

or

$$\frac{\partial}{\partial\theta}\sin\theta E_\theta = \frac{r}{\lambda}\frac{J_s}{\sigma}\sin\theta \ . \tag{3-102}$$

Integrating on θ gives

$$\sin\theta E_\theta = \frac{r}{\lambda}\frac{J_s}{\sigma}(1-\cos\theta) \ ,$$

so that

$$E_\theta = \frac{r}{\lambda}\frac{J_s}{\sigma}\frac{1-\cos\theta}{\sin\theta} = \frac{r}{\lambda}\frac{J_s}{\sigma}\tan\frac{\theta}{2} \ . \tag{3-103}$$

In order for the fields to be static, we must have $\nabla \times \vec{E} = 0$, which implies

$$\frac{1}{r}\frac{\partial}{\partial r} rE_\theta = 0 \quad \text{or} \quad E_\theta \sim 1/r \ . \tag{3-104}$$

Comparison of this result with Equation 3-103 shows that we must have

$$\frac{J_s}{\sigma} \sim \frac{1}{r^2} \ . \tag{3-105}$$

If the conductivity were mostly electronic J_s/σ would be independent of r. However, when the conductivity is ionic, $\sigma \sim \sqrt{J_s}$, and the condition 3-105 becomes

$$\frac{e^{-r/2\lambda}}{r} \sim \frac{1}{r^2} \quad , \quad \text{or} \quad re^{-r/2\lambda} \approx \text{constant} \ .$$

This relationship is not accurately valid, but one may compute the following numbers:

$$x \equiv r/\lambda = 0.5, \quad 1, \quad 2, \quad 4, \quad 5,$$

$$xe^{-x/2} = 0.39, \quad 0.61, \quad 0.74, \quad 0.54, \quad 0.41 \ .$$

It can be said that the relation is valid to ±30 percent over the range from $r = 0.5\lambda$ to 5λ. In much of the quasistatic phase, the hard gammas from air capture are strong contributors, for which the effective λ (including build up) is about 400 meters. Thus the model is justified over the range

r = 0.2 to 2 km. Hardening of the gamma spectrum with distance make the relation 3-104 more accurately satisfied, since λ increases with distance. Thus Equation 3-103 gives reasonably good values for E_θ over the range indicated.

Photographs of large yield nuclear explosions show lightning-like discharges developing in the time frame from 10^{-3} to 3×10^{-2} second (Reference 3-3). The discharges rose from sharp objects (antennas) on the ground, and followed quite closely the θ-direction. The inference that they were driven by the quasistatic electric field is hard to resist. The growth rate of the discharges contains information on the magnitude of the electric field, but analysis of the data is not complete at this writing.

The magnetic field can be found from Equation 3-32. The r-component of this equation is

$$\frac{1}{r\sin\theta} \frac{\partial}{\partial\theta} \sin\theta B_\phi = \frac{Z_0}{c} J_s \ . \qquad (3\text{-}105)$$

This equation has the same form as Equation 3-103, and the same integration procedure leads to

$$B_\phi = \frac{Z_0}{c} r J_s \tan\frac{\theta}{2} \ , \qquad (\frac{Z_0}{c} = \mu_0) \ . \qquad (3\text{-}107)$$

The time dependence of E_θ and B_ϕ can be deduced from Equations 3-103 and 3-107. E_θ is independent of time until the conductivity becomes ionic, then falls as $\sqrt{J_s}$. B_ϕ falls as J_s throughout the entire quasistatic phas .

The radial field E_r at the ground can be found from the condition that the entire Compton current passing out through the hemisphere at radius r must return in the ground. The radial dependence of E_r is complicated by a rather complex current flow pattern in the ground, and the time dependence

if affected by the fact that diffusion persists longer in the ground than in the air. Once diffusion is completed, the time dependence of E_r at the ground is the same as that of J_s. Diffusion takes about 3.5×10^{-3} second at r = 500 meters.

REFERENCES FOR CHAPTER 3

3-1. Messier, M. A., "The Propagation of an Electromagnetic Impulse Through Soil: Influence of Frequency Dependent Parameters," to be published.

3-2. Gilbert, J. L., and C. L. Longmire, "EMP Environment Produced by Gammas in Ground," to be published.

3-3. Uman, M. A., D. F. Seacord, G. H. Price and E. T. Peirce, "Lightning Induced by Thermonuclear Detonations," J. Geoph. Res., Vol. 77, 1591 (March 20, 1970).

CHAPTER 4
COUPLING TO SHORT BURIED CABLES

4.1 INTRODUCTION

Ground-based systems hardened to blast often have electrical conductors buried at depths of one to a few meters in the ground for mechanical protection. Burial also affords some protection from EMP, but by no means total protection since the fields penetrate to these depths without strong attenuation, especially in the lower frequency components. It is useful to distinguish two categories of buried cables. The category considered in this chapter includes cables shorter than a few hundred meters, i.e., one gamma-ray absorption length in air. For such cables the EMP fields may be assumed to have roughly constant amplitude along the length of the cable. The phase is not constant, for in general the EMP will sweep over the cable with a speed determined by the angle χ between the cable run and the radial direction from the nuclear burst. (See Figure 4-1.) The phase speed v is

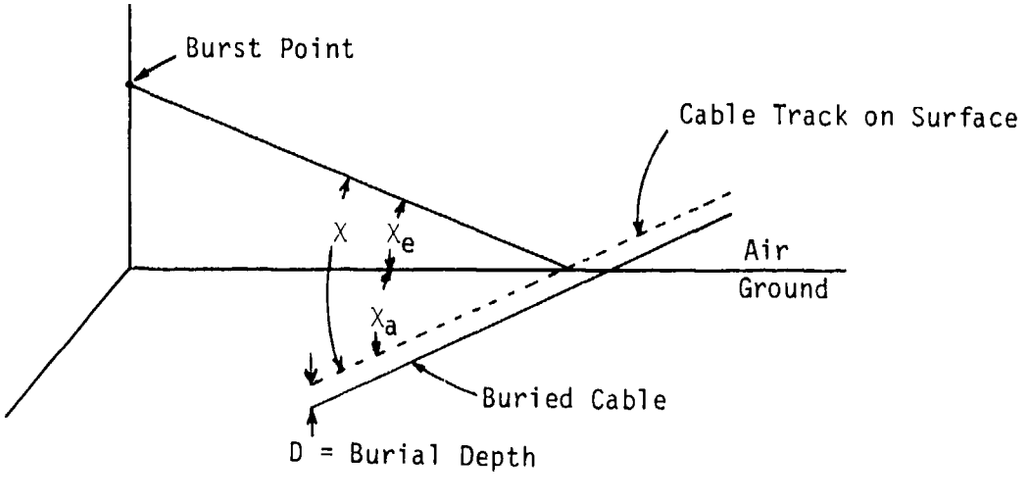

Figure 4-1. Geometry of burst and cable run.

$$v = c/\cos\chi \quad , \quad \cos\chi = \cos\chi_e \cos\chi_a \ . \tag{4-1}$$

In case the burst is above the surface, the angle χ is made up from two angles, the elevation angle χ_e of the burst point as seen from the cable, and the azimuthal angle χ_a in the ground plane. The horizontal EMP electric field E_h at the wire, under the assumptions of constant amplitude and constant phase speed, has the form

$$E_h = E_h(t - \frac{z}{v}) \ , \tag{4-2}$$

where z is the distance along the wire (not the vertical coordinate). The field component of interest is that parallel to the cable, which is related to the horizontal field E_{pr} in the projected radial direction from the burst by

$$E_h = \cos\chi_a E_{pr} \ . \tag{4-3}$$

The cable is most strongly driven when $\chi_a = 0$, and since the location of the burst will not usually be predictable, this case should be assumed.

If E_h is Fourier analyzed in terms of waves of the form $\exp[j(\omega t - kz)]$, then Equation 4-2 leads to the result that k is determined by ω,

$$k = \frac{\omega}{v} = \frac{\omega}{c} \cos\chi \ . \tag{4-4}$$

The fact that $v \geq c$ means that the EMP sweeps over the cables faster than free signals can propagate along it. Since also ε_∞ of the soil is considerably greater than unity, the EMP sweep speed is considerably greater than the free signal speed. In particular, signals arising from effects at the cable ends arrive at most points along the cable with significant delay after the EMP arrives. It is therefore useful to calculate first the response of the cable ignoring end effects, i.e., as if the cable were infinitely long. This problem is taken up in Section 4.2.

The other category of cables includes those that are so long that the EMP environment cannot be assumed to have constant amplitude over the length of the cable. This category is discussed in Chapter 5.

Some of the buried cables of interest will be of multi-wire type. However, these will generally have an outer conducting sheath to shield the wires from EMP, lightning or other electrical interference. The conducting sheath will generally be covered by an insulating sheath for protection against corrosion of the (metallic) conducting sheath. In this chapter, only the insulator and the outermost conductor will be considered. Transfer coupling from the outer conductor to internal wires, if any, is a separable problem, at least approximately. The cable geometry is defined by Figure 4-2. The conductor is drawn as a hollow cylindrical shell of thickness d, but it could be a solid cylinder. The electrical conductivity of the conductor is generally much larger, by a factor of the order of 10^{10}, than that of the soil. Thus the conductor has the same resistance per unit length as a cylinder of soil with radius of the order 10^4 to 10^5 times larger than a_1, depending on the thickness d. The relative permittivity of the

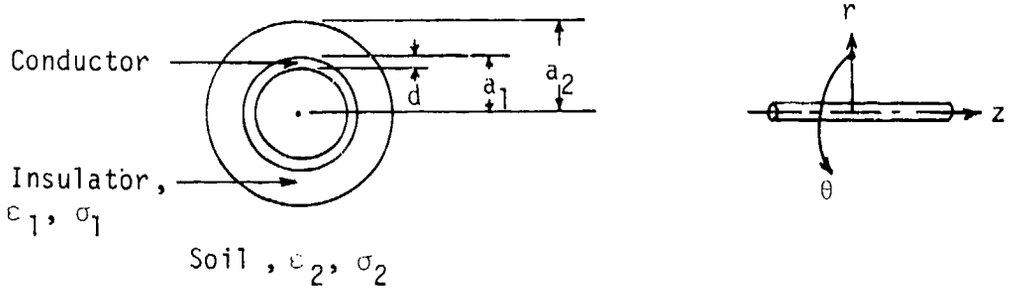

Figure 4-2. Definition of cable parameters and cylindrical parameters.

insulator is a little larger than unity, $\varepsilon_1 \approx 2$ being typical. The conductivity of the insulator, typically very small compared with that of soil, may be enhanced by the gamma radiation penetrating to the burial depth. The peak gamma induced conductivity may be as high as 10^{-6} mho/m, and is time dependent (proportional to the dose rate). The analysis of this chapter will treat σ_1 as constant, but will estimate the importance of gamma-induced conductivity. The soil parameters ε_2 and σ_2 will be treated as independent of time but frequency dependent.

The presence of the air, with its time-varying conductivity, affects the coupling to the cable. The analysis here will first assume that the soil extends to infinity in all directions, and then show how the presence of the air can be taken into account in an approximate way. In addition, the wire initially will be assumed to have perfect conductivity.

4.2 PERFECTLY CONDUCTING WIRE IN INFINITE SOIL

EMP environments are calculated without wires present. Let the Fourier component of the environmental electric field parallel to the wire axis, at the position of the axis, with frequency ω be

$$E_h(\omega) = E_0(\omega)\exp[j(\omega t - kz)] \quad . \tag{4-5}$$

Here k is specified by Equation 4-4. The total parallel electric field must vanish at the wire surface. A current I flows in the wire, such that the additional fields produced by I have a parallel electric field canceling the applied EMP field.

The EMP electric field has components both parallel and perpendicular to the wire axis. The perpendicular component causes the wire to polarize, with positive charge appearing on one side and equal negative charge on the opposite side. The currents involved in this polarization are small when the wire diameter is small compared with the wavelengths in the EMP, a

condition which is generally well satisfied. Further, these currents do not flow along the wire, so are of no consequence for equipment connected to the wire. The EMP field of importance is the component of the electric field parallel to the wire axis, and the variation of this field around the circumference of the wire is negligible.

The usual cylindrical coordinates r, θ, z, right handed in that order and indicated in Figure 4-2, are convenient for the problem at hand. The field components associated with the wire current are E_r, E_z and B_θ, and they are all independent of θ. Maxwell's Equations 1-17 and 1-18 become, for fields with t and z dependence given by Equation 4-5,

$$j\omega B_\theta = jkE_r + \frac{\partial}{\partial r} E_z \ , \tag{4-6}$$

$$\eta E_r = jkcB_\theta \ , \tag{4-7}$$

$$\eta E_z = \frac{c}{r} \frac{\partial}{\partial r} rB_\theta \ , \tag{4-8}$$

where $\eta(\omega)$ is the relative admittance introduced in Section 2.2. Equation 4-7 can be used to express E_r in terms of B_θ,

$$E_r = \frac{jkc}{\eta} B_\theta \ . \tag{4-9}$$

Use of this result in Equation 4-6 allows expression of B_θ in terms of E_z,

$$B_\theta = - \frac{\eta}{c} \frac{1}{\kappa^2} \frac{\partial E_z}{\partial r} \ , \tag{4-10}$$

where κ is defined by

$$\kappa^2(\omega) \equiv - \left(\frac{j\omega\eta}{c} + k^2\right) \ . \tag{4-11}$$

From the definition of η, Equation 2-2, this becomes

$$\kappa = [\frac{\omega}{c}(\frac{\varepsilon\omega}{c} - jZ_0\sigma) - k^2]^{1/2} , \tag{4-12}$$

$$= [(\varepsilon-\cos^2\chi)(\frac{\omega}{c})^2 - jZ_0\sigma\frac{\omega}{c}]^{1/2} . \tag{4-13}$$

In the second line k has been evaluated by Equation 4-4. The choice of sign of the square root here will always be taken such that κ would be real and positive if σ vanished. Thus the imaginary part of κ is negative for $\omega > 0$.

Using Equation 4-10 in Equation 4-8 gives a differential equation for E_z,

$$\frac{1}{r}\frac{\partial}{\partial r} r \frac{\partial E_z}{\partial r} = - \kappa^2 E_z . \tag{4-14}$$

The solutions of this equation are Bessel functions of order zero, $J_0(\kappa r)$, $Y_0(\kappa r)$. (See Reference 4-1.) The value of κ is different in insulator and soil. Let κ_1 apply to the insulator, κ_2 to the soil. In the soil, the field E_z produced by the wire current should approach zero at large r. This requires the combination of J_0 and Y_0,

$$E_z = A[J_0(\kappa_2 r) - jY_0(\kappa_2 r)] \equiv AH_0(\kappa_2 r) , \tag{4-15}$$

where A is an arbitrary constant. Equation 4-10 then gives B_θ in the soil,

$$B_\theta = \frac{\eta_2 A}{c\kappa_2}[J_1(\kappa_2 r) - jY_1(\kappa_2 r)] \equiv \frac{\eta_2 A}{c\kappa_2} H_1(\kappa_2 r) . \tag{4-16}$$

In the insulator, the solution contains two arbitrary constants B and C:

$$E_z = BJ_0(\kappa_1 r) + CY_0(\kappa_1 r) , \tag{4-17}$$

$$B_0 = \frac{\eta_1}{c\kappa_1}[BJ_1(\kappa_1 r) + CY_1(\kappa_1 r)] . \tag{4-18}$$

The constants A, B and C are determined by the requirements that E_z cancel the applied field E_0 at $r = a_1$ and that E_z and B_θ both be continuous at $r = a_2$.

If the two continuity conditions are written out first, they can be solved for the ratios B/A and C/A, with the results:

$$\frac{B}{A} = \frac{H_0 Y_1 - G H_1 Y_0}{W} \quad , \quad \frac{C}{A} = - \frac{H_0 J_1 - G H_1 J_0}{W} \tag{4-19}$$

In these expressions, H_0 and H_1 are evaluated at $\kappa_2 a_2$, and J_0, Y_0, J_1 and Y_1 are evaluated at $\kappa_1 a_2$. The factor G is

$$G \equiv \frac{\kappa_1 \eta_2}{\kappa_2 \eta_1} \ , \tag{4-20}$$

and W is the Wronskian

$$W \equiv J_0 Y_1 - J_1 Y_0 = - \frac{2}{\pi \kappa_1 a_2} \ . \tag{4-21}$$

The condition that E_z cancel E_0 at $r = a$ can be written as

$$- \frac{E_0}{A} = \frac{B}{A} J_0(\kappa_1 a_1) + \frac{C}{A} Y_0(\kappa_1 a_1) \ . \tag{4-22}$$

Since B/A and C/A are known, this equation determines A, and Equation 4-19 then determines B and C, which completes the solution.

The total current in the wire is related to the value of B_0 at $r = a_1$ by Equation 1-19, which becomes

$$\frac{I}{A} = \frac{2\pi a_1 \eta_1}{Z_0 \kappa_1} \left[\frac{B}{A} J_1(\kappa_1 a_1) + \frac{C}{A} Y_1(\kappa_1 a_1) \right] \ . \tag{4-23}$$

The impedance Z_w of the wire is defined as

$$Z_w(\omega) = E_0(\omega)/I(\omega) \quad \text{ohms/meter} \ . \tag{4-24}$$

By use of the result obtained above, Z_w can be found to be

$$Z_w = \frac{Z_0 \kappa_1}{2\pi a_1 \eta_1} \left[\frac{(H_0 J_1 - G H_1 J_0) Y_0^* - (H_0 Y_1 - G H_1 Y_0) J_0^*}{-(H_0 J_1 - G H_1 J_0) Y_1^* + (H_0 Y_1 - G H_1 Y_0) J_1^*} \right] . \qquad (4\text{-}25)$$

Here H_0 and H_1 are evaluated at $\kappa_2 a_2$; J_0, J_1, Y_0 and Y_1 at $\kappa_1 a_2$; and the asterisks indicate evaluation at $\kappa_1 a_1$, not complex conjugation. The functions H_0 and H_1 are defined in Equations 4-15 and 4-16.

4.3 SMALL RADIUS APPROXIMATION FOR WIRE IMPEDANCE

The exact expression for the wire impedance, Equation 4-25, is difficult to deal with, although it can be evaluated numerically. Reference 4-1 gives quite accurate polynomial approximations for the various Bessel functions useful for numerical work. However, it is fortunate that the arguments of all of the Bessel functions are small in cases of interest in this report. The largest argument is $\kappa_2 a_2$. For $\omega = 10^9$, $\varepsilon \approx 10$, $\sigma \approx 0.04$ (see Figures 2-2 and 2-3), Equation 4-13 gives $|\kappa_2| \approx 11\ m^{-1}$. If the radius $a_2 = 0.01$ m, then $|\kappa_2 a_2| \approx 0.11$. For $\omega = 10^8$, $|\kappa_2 a_2| \approx 0.013$, and for smaller ω, the argument is even smaller. Thus it is reasonable to expect that the small-argument expansions of the Bessel functions may yield a sufficiently accurate evaluation of Z_w. These expansions are

$$J_0(x) = 1 - \frac{x^2}{4} + O(x^4) \quad , \quad J_1(x) = \frac{x}{2} - \frac{x^3}{16} + O(x^5) \quad ,$$
$$Y_0(x) = \frac{2}{\pi} \ln \frac{\gamma x}{2} \left(1 - \frac{x^2}{4}\right) + \frac{x^2}{4} + O(x^4) \quad , \quad Y_1(x) = -\frac{2}{\pi x} + \frac{x}{\pi} \ln \frac{\gamma x}{2} - \frac{x}{2} + O(x^3) \qquad (4\text{-}26)$$

where γ is the Euler-Mascheroni constant,

$$\gamma = 1.781 \ldots \quad . \qquad (4\text{-}27)$$

By using these expansions and taking care to collect all of the terms of lowest order, Equation 4-25 can be reduced to

$$Z_w(\omega) \approx \frac{Z_0}{2\pi}\left[-\frac{\kappa_2^2}{\eta_2}\left(\ell n \frac{2}{\gamma\kappa_2 a_2} - \frac{j\pi}{2}\right) - \frac{\kappa_1^2}{\eta_1}\ell n \frac{a_2}{a_1}\right]. \qquad (4\text{-}28)$$

This formula holds for any ω, real or complex, provided $|\omega|$ is not so large that the arguments of the Bessel functions are no longer small. We shall test the accuracy of the formula in the Laplace domain rather than the Fourier domain, i.e., for exponentially rising applied fields of the form

$$E_h(\alpha) = E_0(\alpha)\exp[\alpha t - \tilde{k}z] \ . \qquad (4\text{-}29)$$

The assumption of constant amplitude and phase speed, Equation 4-2, now implies

$$\tilde{k} = \frac{\alpha}{v} = \frac{\alpha}{c}\cos\chi \ . \qquad (4\text{-}30)$$

Comparison of Equations 4-29 and 4-30 with Equations 4-5 and 4-4 respectively shows that the formulae can be written in the Laplace domain by making the replacements

$$\left.\begin{aligned} \omega &\to -j\alpha \ , \\ k &\to -j\tilde{k} \ . \end{aligned}\right\} \qquad (4\text{-}31)$$

Then the media parameters become

$$\eta = Z_0\sigma(\alpha) + \frac{\alpha}{c}\varepsilon(\alpha) \ , \qquad (4\text{-}32)$$

$$\kappa^2 = -\left(\frac{\alpha\eta}{c} - \tilde{k}^2\right) \equiv -\tilde{\kappa}^2 \ . \qquad (4\text{-}33)$$

Thus the replacement

$$\kappa \to -j\tilde{\kappa} \ , \qquad (3\text{-}34)$$

should also be made in the formulae. Equations 4-12 and 4-13 become

$$\tilde{\kappa} = \left[\frac{\alpha}{c}\left(\varepsilon\,\frac{\alpha}{c} + Z_0\sigma\right) - \tilde{\kappa}^2\right]^{1/2} , \tag{4-35}$$

$$= \left[(\varepsilon - \cos^2\chi)\left(\frac{\alpha}{c}\right)^2 + Z_0\sigma\,\frac{\alpha}{c}\right]^{1/2} . \tag{4-36}$$

The exact formula for Z_w, Equation 4-25, could now be rewritten in terms of the modified Bessel functions (Bessel functions of imaginary argument), but we shall leave it as it stands. It is convenient, however, to evaluate the small radius approximation in terms of the Laplace domain parameters. Making the replacements indicated above in Equation 4-28 leads to the totally real result

$$Z_w(\alpha) \approx \frac{Z_0}{2\pi}\left[\frac{\tilde{\kappa}_2^2}{\eta_2}\,\ell n\,\frac{2}{\gamma\tilde{\kappa}_2 a_2} + \frac{\tilde{\kappa}_1^2}{\eta_1}\,\ell n\,\frac{a_2}{a_1}\right] . \tag{4-37}$$

To test the accuracy of the small radius approximation, we have numerically evaluated both Equations 4-25 and 4-37 for the following cable and soil parameters:

$$\begin{aligned} &a_1 = 0.5 \text{ cm} \quad , \quad a_2 = 1.0 \text{ cm} \quad , \quad \cos\chi = 1 \ , \\ &\varepsilon_1 = 2 \quad , \quad \sigma_1 = 0 \quad , \quad \varepsilon_2 = 10 \quad , \quad \sigma_2 = 0.01 \text{ mho/m} \ . \end{aligned} \tag{4-38}$$

The computed results are shown in Table 4-1. The accuracy is quite adequate up to the highest frequencies of interest.

Table 4-1. Comparison of exact formula and small radius approximation for $Z_w(\alpha)$, for perfectly conducting wire.

α	Exact	Approximation	Error	Skin Depth
10^8 sec^{-1}	89.21 ohms/m	89.17 ohms/m	0.04 %	0.74 m
3×10^8	213.1	212.6	0.2	0.31
10^9	506.7	498.8	1.6	0.16

For a typical application of our results, note that an EMP field that rises with $\alpha = 10^8$ sec^{-1} to a peak of about 10^5 V/m would drive a current of about 10^3 A in this wire at the peak of the EMP. The current will continue to rise after the peak, for the impedance is mostly inductive, as will be seen in later sections of this report. Note that wire resistance is negligible compared with the computed impedance, at these frequencies.

In use of the Laplace domain results, it should be noted that $\sigma(\alpha)$ and $\varepsilon(\alpha)$ in Equation 4-32 are not the same as $\sigma(\omega)$ and $\varepsilon(\omega)$, unless σ and α are independent of frequency. Equation 2-21 gives $\eta(\alpha)$ directly for universal soils, and Figure 2-5 gives $\eta(\alpha)$ for our standard soil (10 percent water content).

It should also be noted that the proximity of the conducting air to the cable has not yet been included in the analysis. The effect of the air proximity is not large for $\alpha \approx 10^8$ sec^{-1} and burial depths of 1 meter or more. After the peak, the air proximity will have a larger effect, enhancing the current during that period in which the air conductivity is larger than the ground admittance η/Z_0.

The quantities $2/\gamma\kappa_2$ in Equation 4-28 and $2/\gamma\tilde{\kappa}_2$ in Equation 4-37 are the skin depths in the soil; they give a measure of the depth of penetration of the wire-induced fields into the soil. The skin depth is complex in Fourier domain, in which case its magnitude indicates the depth of penetration. It is real in the Laplace domain, and values are given in Table 4-1.

4.4 THE TRANSFER FACTORS

In addition to the wire current, it is useful to be able to predict the radial fields E_r in the insulator and the voltage across the insulator. Formulae for these quantities can be obtained from Equations 4-9 and the fact that, when the small-argument approximation of the Bessel functions is valid,

$$B_\theta \approx \frac{Z_0 I}{2\pi r c} . \tag{4-39}$$

This is the static approximation, Equation 1-19, and is valid near the wire. The result for E_r is, in the Fourier domain,

$$E_r(\omega) = \frac{jk}{2\pi r\eta} \frac{Z_0}{Z_w} E_0(\omega) \equiv T(\omega) E_0(\omega) , \tag{4-40}$$

and in the Laplace domain,

$$E_r(\alpha) = \frac{\tilde{k}}{2\pi r\eta} \frac{Z_0}{Z_w} E_0(\alpha) \equiv T(\alpha) E_0(\alpha) . \tag{4-41}$$

The name <u>transfer factor</u> will be used for the factors T multiplying E_0 in these equations. They are dimensionless. According to Equations 4-4 and 4-30 for the sweeping EMP, they are

$$T(\omega) = \frac{j(\omega/c)\cos\chi}{2\pi r\eta} \frac{Z_0}{Z_w} , \tag{4-42}$$

$$T(\alpha) = \frac{(\alpha/c)\cos\chi}{2\pi r\eta} \frac{Z_0}{Z_w} . \tag{4-43}$$

In an insulating material, $\sigma = 0$, both of these formulae simplify to

$$T = \frac{\cos\chi}{2\pi r c} \frac{Z_0}{Z_w} . \tag{4-44}$$

In all of the expressions for T, the appropriate η, Z_w and ε is to be used, i.e., $\eta(\omega)$ or $\eta(\alpha)$, etc.

Table 4-2 gives the values of T for the example (4-38) and for points r in the insulator just outside $r = a_1(T_1)$, and in the soil just outside $r = a_2(T_2)$. It is seen that E_r will be much larger than the applied E_0, and that the transfer factors are larger at lower frequency. Indeed, the radial fields are in the breakdown range.

The voltage V across the insulator is obtained by integrating T from a_1 to a_2. Thus

$$V = T_v E_0 \ , \tag{4-45}$$

where

$$T_v = \frac{\cos\chi}{2\pi\varepsilon} \frac{Z_0}{Z_i} \ln \frac{a_2}{a_1} \ . \tag{4-46}$$

The dimensions of T_v are meters. T_v is also given in Table 4-2 for the same example.

The field transfer factor T is smaller for wires of larger radius, as indicated by Equations 4-42 to 4-44. Z_w decreases as the radius increases, but only logarithmicly.

Table 4-2. Transfer factors for the example (4-38).

α	T_1	T_2	T_v
10^8 sec^{-1}	67.2	3.2	0.233 meters
3×10^8	28.2	2.1	0.098
10^9	11.8	1.1	0.047

4.5 R, L EQUIVALENT CIRCUIT OF THE WIRE IMPEDANCE

During the rise of the EMP, the Laplace domain form of the wire impedance can be used directly to calculate the wire current and radial electric field. After the peak in the EMP, this simple procedure is not applicable. Fourier transform techniques are applicable: transform the applied field to the ω domain, use $Z_w(\omega)$ to calculate $I(\omega)$, and invert to find $I(t)$. While this procedure is straightforward, it is time consuming, and the analyst tends to lose contact with the numbers and confidence in the results. This occurs especially since the whole process is usually left in the hands of computational technicians, who may have little feel for electromagnetics.

An alternative approach is to continue to use analytical techniques to construct a simple, approximate method that can be applied directly in the time domain. In this section an R,L circuit will be devised, which has the same impedance Z_w, to good accuracy, as the actual wire.

At low frequencies the impedance Z_w, calculated for a perfectly conducting wire, becomes so small that the finite resistance of the wire is not negligible. We therefore add to Z_w the resistance R_{w0} (ohms/meter) of the outer conductor of the cable. R_{w0} may depend on frequency, as it will if the thickness d of the outer conductor is more than a skin depth in it. Most commonly this will not be the case at those low frequencies for which R_{w0} is significant compared with Z_w. We shall treat R_{w0} as independent of frequency, and take it to be the d.c. resistance of the outer conductor.

A convenient equivalent circuit would have the form shown in Figure 4-3, for then the current in each branch could be computed separately and the total cable current obtained by adding the branch currents. Since the admittance of the network is most easily written, it is desired to make the fit to the wire admittance Y_w,

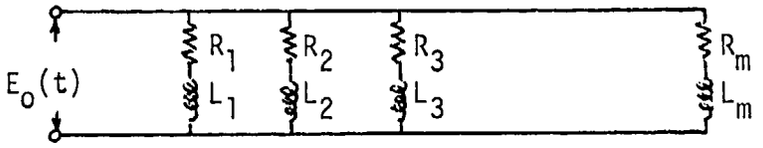

Figure 4-3. Equivalent R,L circuit to fit cable impedance.

$$\frac{1}{R_{w0} + Z_w} \equiv Y_w \approx \sum_{n=1}^{m} \frac{1}{R_n + j\omega L_n} . \tag{4-47}$$

This equation can also be written

$$Y_w(\omega) \approx \sum_{n=1}^{m} \frac{g_n}{1 + j\omega/\beta_n} , \tag{4-48}$$

where

$$g_n = 1/R_n \quad , \quad \beta_n = R_n/L_n . \tag{4-49}$$

The fit can be made by first choosing arbitrarily a set of β_n's, spaced one decade apart, say. The g_n are then determined by requiring Equation 4-48 to hold exactly at a set of ω's, e.g., $\omega = \beta_1, \beta_2, \beta_3, \ldots\beta_m$, which gives a set of m linear equations to solve for the m quantities g_n.

The fit can be made either in the Laplace or Fourier domain. In the Laplace domain, both sides of Equation 4-48 are real. In the Fourier domain, one can fit, say, the imaginary (inductive) part of $Y_w(\omega)$. The real (resistive) part should then fit automatically, since both sides of Equation 4-48 are analytic functions. The fit will not be exact, of course, at frequencies between the fit points.

Lavery (Reference 4-2) used this technique to fit the admittance of a cable with parameters

$$\left.\begin{aligned} &a_1 = 0.5 \text{ cm} \quad , \quad a_2 = 1.0 \text{ cm} \quad , \quad d = 0.05 \text{ cm} \quad , \quad \cos X = 1, \\ &\varepsilon_1 = 2 \quad , \quad \sigma_1 = 0 \quad , \quad R_{w0} = 1.129 \times 10^{-3} \text{ ohm/m} \ , \end{aligned}\right\} \tag{4-50}$$

imbedded in our standard soil. The β_n chosen were

$$\beta_n = 5 \times 10^{1+n} \quad , \quad n = 1 \text{ to } 7 \ . \tag{4-51}$$

The real and imaginary parts of $Y_w(\omega)$ and of the fit are graphed in Figure 4-4 for $10^2 \leq \omega \leq 10^9$ sec^{-1}. It is seen that the fit is quite accurate, except for the real part at $\omega \geq 10^8$. This discrepancy could be removed by adding higher β_n's, but we shall not depend on the fit at these high frequencies. The values of g_n, R_n and L_n for the fit are given in Table 4-3. In this table, an entry a(b) means $a \times 10^b$. The zero frequency conductance G_0 and the infinite frequency inductance L_∞ of the network are

Table 4-3. Fit parameters for the example (4-50) in standard soil.

n	g_n(m/ohm)	R_n(ohm/m)	L_n(henry/m)
1	8.439(2)	1.185(-3)	2.370(-6)
2	2.137(1)	4.679(-2)	9.359(-6)
3	1.306(0)	7.657(-1)	1.531(-5)
4	1.972(-1)	5.071(0)	1.014(-5)
5	2.684(-2)	3.726(1)	7.452(-6)
6	5.002(-3)	1.999(2)	3.998(-6)
7	1.258(-3)	7.949(2)	1.590(-6)

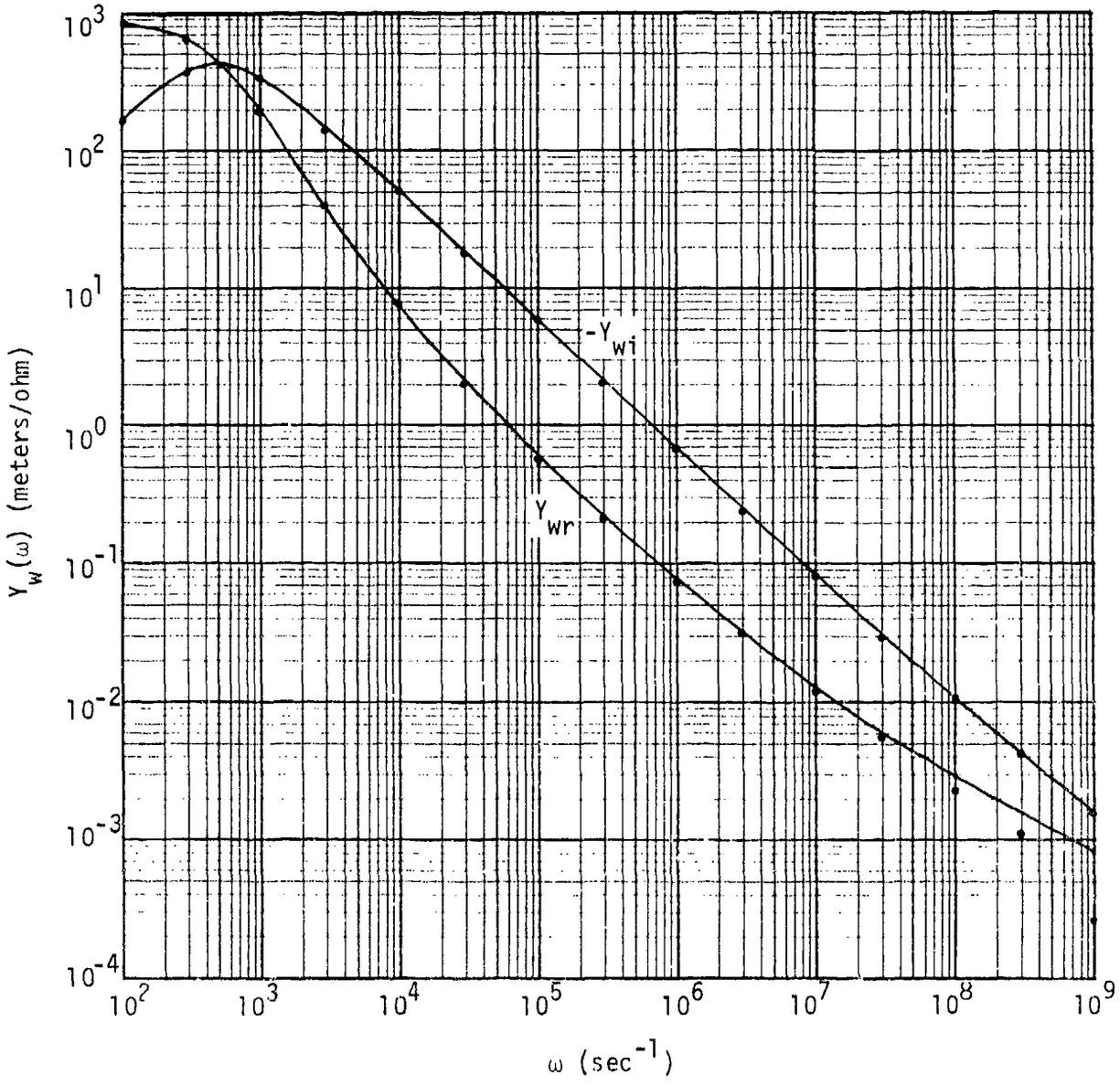

Figure 4-4. Real and imaginary parts Y_{wr} and Y_{wi} of cable admittance as a function of ω. The curves are computed from the definition of Y_w, Equation 4-47, with Z_w given by Equation 4-28. The points are computed from the R,L circuit fit. The fit was made to Y_{wi} at the points $\omega = 10^{n+2}$, n = 1 to 7. The R,L model values for Y_{wr} are also very close to the true values, except at $\omega \geq 10^8$. This discrepancy could be removed by adding R,L branches with higher rates β_n.

$$\left.\begin{aligned} G_0 &= \sum_n g_n = 8.668 \times 10^3 \text{ mho-m} \approx 1/R_{w0} \ , \\ L &= \left(\sum_n g_n \beta_n\right)^{-1} = 5.862 \times 10^{-7} \text{ henry/m} \ . \end{aligned}\right\} \tag{4-52}$$

The admittance in the Laplace domain is

$$Y_w(\alpha) \approx \sum_{n=1}^{m} \frac{g_n}{1 + \alpha/\beta_n} \ . \tag{4-53}$$

Figure 4-5 compares $Y_w(\alpha)$ with the fit for the example (4-50).

The current in the n^{th} branch of the network can be computed by solving the differential equation

$$L_n \frac{dI_n}{dt} + R_n I_n = E_0(t) \ ,$$

or

$$\frac{dI_n}{dt} + \beta_n I_n = g_n \beta_n E_0(t). \tag{4-54}$$

The solution of this equation is

$$I_n(t) = e^{-\beta_n (t-t_0)} I_n(t_0) + g_n \beta_n e^{-\beta_n t} \int_{t_0}^{t} e^{\beta_n t'} E_0(t')dt' \ . \tag{4-58}$$

This solution allows for an arbitrary initial current $I_n(t_0)$ at the starting time t_0, in case it is convenient to approximate $E_0(t)$ by different analytical forms in different time periods. For example, a somewhat crude but useful approximation to the early-time part of the horizontal electric field (see Figure 4-6) is

$$\left.\begin{aligned} E_0(t) &= E_m e^{\alpha t} \quad \text{for} \quad t < 0 \ , \\ &= E_m e^{-\gamma t} \quad \text{for} \quad t > 0 \ . \end{aligned}\right\} \tag{4-56}$$

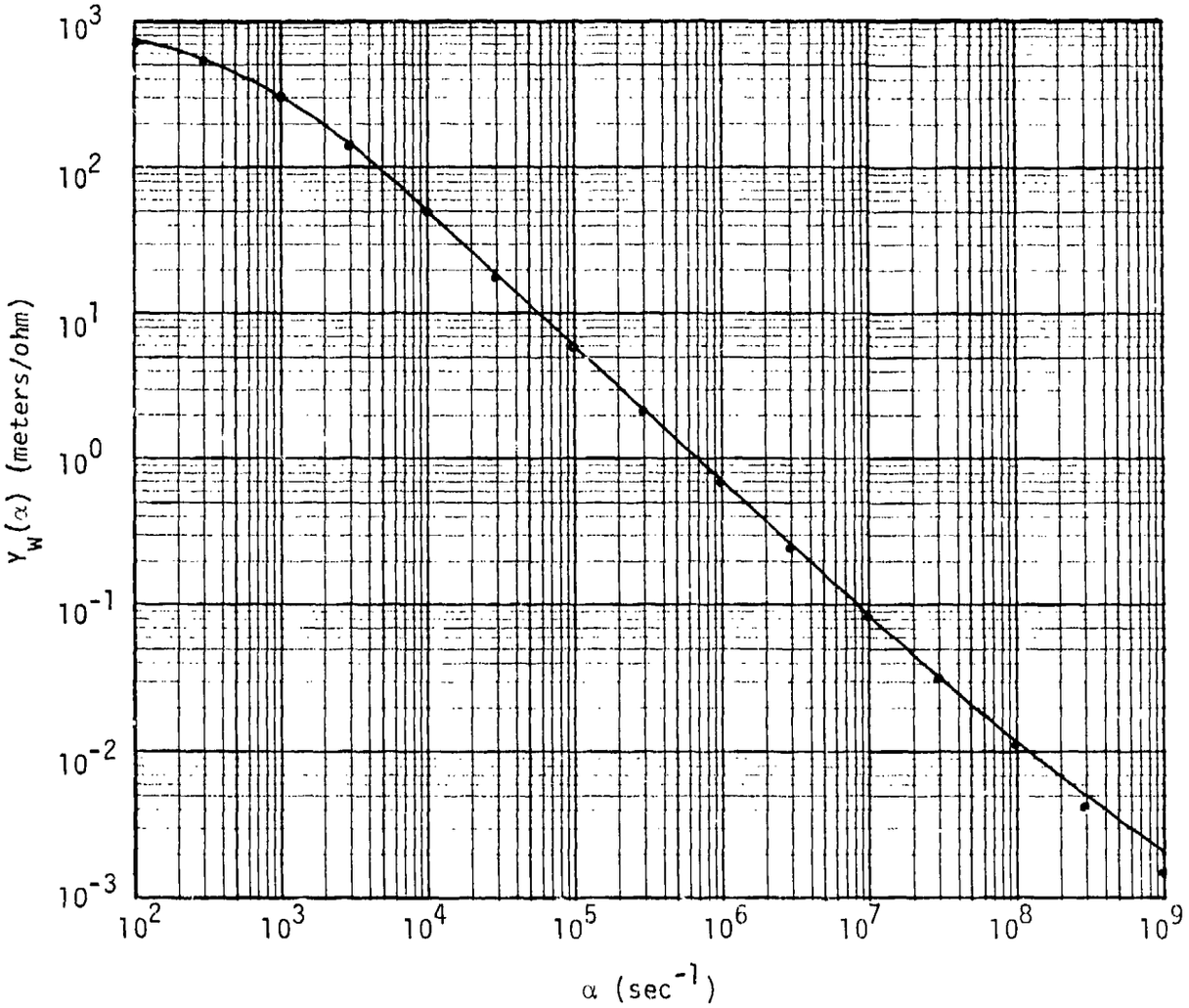

Figure 4-5. Admittance $Y_W(\alpha)$ of cable as a function of α. The curve is computed from the definition of Y_W with Z_W given by Equation 4-37. The points are computed from the R,L circuit fit to $Y_{Wi}(\omega)$. The discrepancy between the curve and the points at $\alpha > 10^8$ could be removed by adding R,L branches with higher rates β_n.

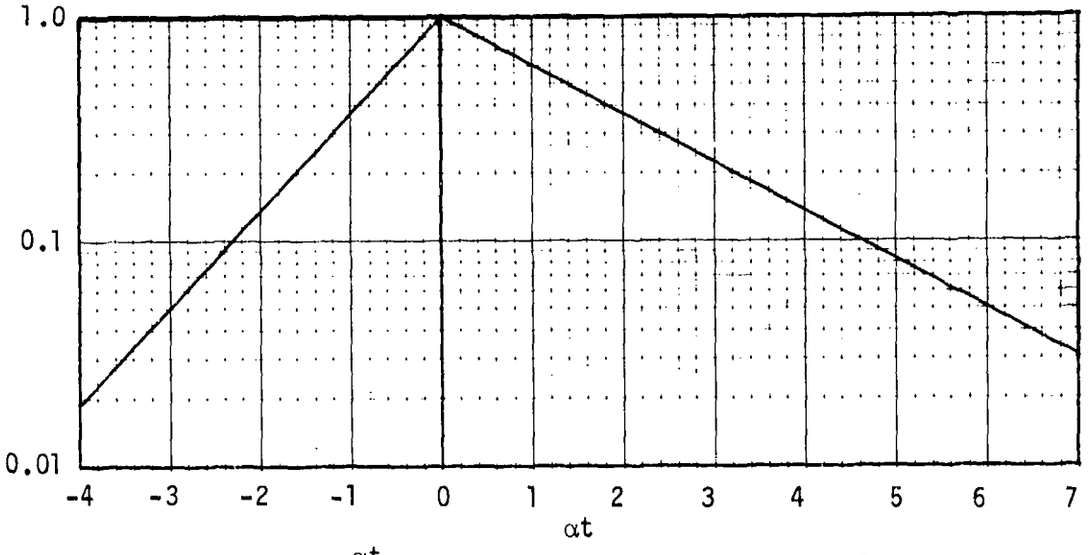

(a) The function $f = e^{\alpha t}$, $t < 0$, for the case $\gamma = \alpha/2$
$= e^{-\gamma t}$, $t > 0$,

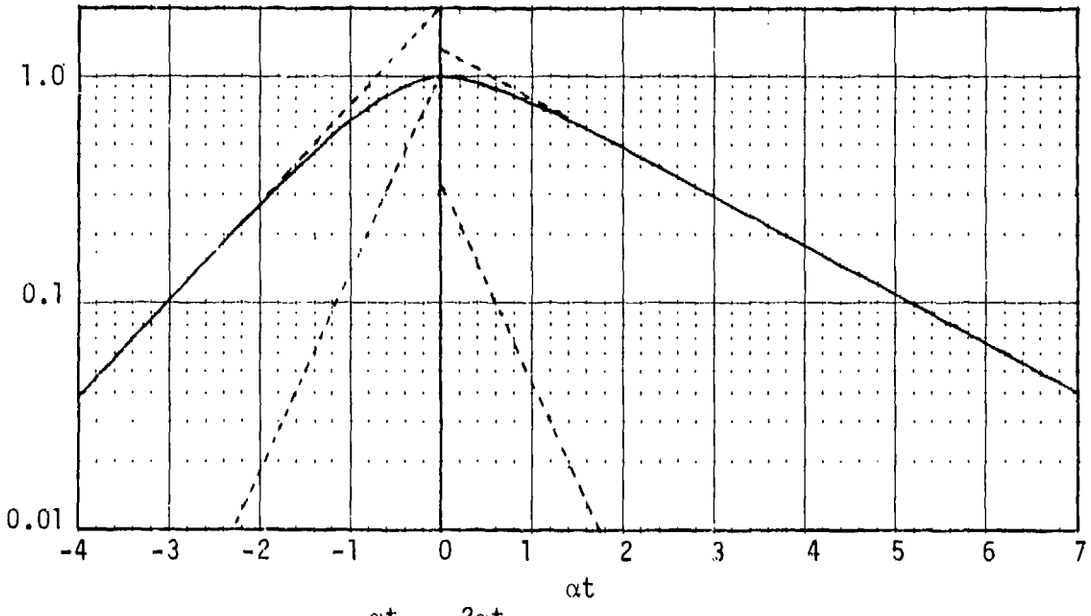

(b) The function $f = 2e^{\alpha t} - e^{2\alpha t}$, $t < 0$, for the case $\gamma = \alpha/2$
$= \frac{2\alpha}{2\alpha-\gamma} e^{-\gamma t} - \frac{\gamma}{2\alpha-\gamma} e^{-2\alpha t}$, $t > 0$.

Figure 4-6. Some simple analytic approximations for the EMP.

Here E_m is the maximum value, achieved at $t = 0$.. If E_m is chosen somewhat larger than the actual peak field, the form (4-56) will bound the actual field, and the computed current will therefore bound the actual current.

For the form (4-56), the current for $t < 0$ can be calculated directly from $Y_w(\alpha)$,

$$I(t) = Y_w(\alpha)E_m e^{\alpha t} \quad \text{for} \quad t < 0 \ . \tag{4-57}$$

For this purpose, either the original $Y_w(\alpha)$ or the fit to it may be used. At $t = 0 = t_0$, there is already a current flowing in the wire, and the part of this current flowing in the n^{th} branch is

$$I_n(0) = \frac{g_n E_m}{1 + \alpha/\beta_n} \ . \tag{4-58}$$

From Equation 4-55, the n^{th} current for $t > 0$ is easily calculated to be

$$I_n(t) = e^{-\beta_n t} I_n(0) + \frac{g_n \beta_n E_m}{\beta_n - \gamma} (e^{-\gamma t} - e^{-\beta_n t}) \ . \tag{4-59}$$

The apparent singularity in the second term here if γ should approach β_n actually does not occur, as the exponentials also cancel in the limit $\gamma \to \beta_n$. Summing $I_n(t)$ over n gives the result, for $t > 0$,

$$I(t) = (\alpha+\gamma)E_m \sum_n \frac{g_n \beta_n e^{-\beta_n t}}{(\alpha+\beta_n)(\gamma-\beta_n)} + Y_w(-\gamma)E_m e^{-\gamma t} \ . \tag{4-60}$$

Here $Y_w(-\gamma)$ is $Y_w(\alpha)$ evaluated at $\alpha = -\gamma$.

The form (4-56) has a discontinuity in slope at its peak, which gives it more high-frequency content than the true EMP. A function with a discontinuity in slope has a Fourier transform which falls off no faster than $1/\omega^2$ at large ω, whereas the transform of the true EMP

(which has all derivatives continuous) falls off faster than any finite power of ω. The form can be improved easily by adding other exponentials. For example, the form

$$\left.\begin{aligned} E_0(t) &= E_m(2e^{\alpha t}-e^{2\alpha t}) \quad , \quad t < 0 \ , \\ &= E_m\left(\frac{2\alpha}{2\alpha-\gamma}\, e^{-\gamma t} - \frac{\gamma}{2\alpha-\gamma}\, e^{-2\alpha t}\right) \quad , \quad t > 0 \ , \end{aligned}\right\} \tag{4-61}$$

has maximum value E_m at $t = 0$ and zero slope there, as is easily verified. This function is graphed in Figure 4-6 for the case $\gamma = \alpha/2$. The function has discontinuous second derivative, and its Fourier transform falls as $1/\omega^3$ at large ω. It is possible, with the rise and decay rates α and γ fixed in the first exponentials on each line, to vary the constants in the last two exponentials and the coefficients of all terms in such a way that continuity is maintained through the fourth derivative. If the N^{th} derivative shows the first discontinuity, the Fourier transform falls as $1/\omega^{N+1}$ asymptotically. The algebra determining the coefficients becomes quite complicated for the very smooth forms. Use of the simple forms bounds the high-frequency content.

The current for the form (4-61) can be written down by applying Equations 4-57 and 4-59 to each of the exponential terms. In this way, all but the final summing of the terms can be done analytically. Alternatively, the differential Equation 4-54 or the integral in Equation 4-55 can be solved or evaluated numerically. Either approach gives a fast and quite accurate way of calculating the cable current.

Note that the transfer factor for the insulating layer, Equation 4-44, displays no frequency dependence except in the factor Z_w. Therefore, on including the d.c. wire resistance, it is possible to write

$$E_r = \frac{Z_0 \cos\chi}{2\pi r\varepsilon} \frac{E_0}{R_{w0} + Z_w} ,$$

$$= \frac{Z_0 \cos\chi}{2\pi r\varepsilon} I , \qquad \text{(insulator)} \tag{4-62}$$

and the la line here holds in either frequency or time domains. Calculation of I therefore imediately yields E_r in the insulator. Unfortunately, this is not true for E_r in the soil. At lower frequencies, where η is approximately constant,

$$E_r \approx \frac{\cos\chi}{2\pi r\sigma_0} \frac{1}{c} \frac{\partial I}{\partial t} . \qquad \text{(soil, near wire)} \tag{4-63}$$

At high frequencies where ε rather than σ dominates η and ε does not vary strongly with frequency, Equation 4-62 applies approximately in the soil near the wire.

4.6 THE TIME-VARYING INDUCTANCE MODEL

The method developed in Section 4.5, while transparent and accurate, still requires a considerable amount of calculation. A simpler method is desirable, even if it is less accurate. Such a method exists for the type of applied fields found in EMP environments.

The expression (4-28) for Z_w can be simplified by making some approximations. Equation 4-11 shows that, if the k^2 term is dropped

$$-\frac{k^2}{\eta} \approx j\frac{\omega}{c} . \tag{4-64}$$

Now, the k^2 term contributes the term $-\cos^2\chi$ in Equation 4-13. In the soil, $\cos^2\chi$ is no more than about 10 percent of ε, where $\varepsilon \gtrsim 10$. In the insulator, dropping $\cos^2\chi$ makes a bigger percentage change. The logarithm factor $\ln(a_2/a_1)$ is usually much smaller than the logarithm for the soil

term, so that the insulator term is not very important. However, if σ is negligible in the insulator, κ^2/η is still simple, and can be retained. The approximate form of Z_w is

$$Z_w \approx \frac{j\omega Z_0}{2\pi c}\left[\ell n\left(\frac{2}{j\gamma\kappa_2 a_2}\right) + \left(1 - \frac{\cos^2\chi}{\varepsilon_1}\right)\ell n\,\frac{a_2}{a_1}\right] . \qquad (4\text{-}65)$$

(Note that $\ell n(-j) = -j\pi/2$.) This expression gives an impedance which is too large, but not by more than about 10 percent.

If the logarithm in Equation 4-65 were independent of frequency and real, it would represent the impedance of a pure inductance. If κ_2 is written in terms of its magnitude and phase,

$$\kappa_2 = |\kappa_2| e^{-j\phi} , \qquad (4\text{-}66)$$

it is clear from Equation 4-13 that ϕ varies between zero and $\pi/4$; ϕ approaches zero when the dielectric term is dominant and approaches $\pi/4$ when the conductivity term is dominant. On separating real and imaginary parts, Z_w becomes

$$Z_w = \frac{j\omega Z_0}{2\pi c}\left[\ell n\,\frac{2}{\gamma|\kappa_2|a_2} + \left(1 - \frac{\cos^2\chi}{\varepsilon_1}\right)\ell n\,\frac{a_2}{a_1}\right] + \frac{|\omega|\eta_0}{2\pi c}\left(\frac{\pi}{2} - \phi\right) . \qquad (4\text{-}67)$$

The absolute value on the factor ω in the real term is demanded, for negative ω, by the reality condition, $Z_w^*(\omega) = Z_w(-\omega)$, and can also of course be derived from the properties of the Bessel functions by carrying through the analysis for negative ω. The second term is resistive and leads to energy dissipation. If the soil is a good dielectric, $\phi \to 0$, and the energy is radiated away. If the soil is a good conductor, $\phi \to \pi/4$, and the energy is dissipated in Joule heating of the soil.

The magnitude of the resistive term is generally fairly small compared with the first or inductive term. The first logarithm is typically between 3 and 12 in cases of interest, whereas $(\frac{\pi}{2} - \phi)$ ranges between $\pi/2$ and $\pi/4$. Dropping the resistive term should increase the calculated current and provide an upper bound. We shall drop it, and compare calculated results with those obtained from the more accurate equivalent circuit method.

In terms of the inductance L of the wire,

$$Z_w = j\omega L \ , \tag{4-68}$$

and

$$L = \frac{Z_0}{2\pi c} \left[\ell n \left(\frac{2}{\gamma |\kappa_2| a_2} \right) + \left(1 - \frac{\cos^2 \chi}{\varepsilon_1} \right) \ell n \frac{a_2}{a_1} \right] . \tag{4-69}$$

Note th t

$$\frac{Z_0}{2\pi c} = \frac{\mu_0}{2\pi} = 2 \times 10^{-7} \text{ Henry/meter} \ . \tag{4-70}$$

The inductance depends on $|\kappa_2|$, but only quite slowly because of the logarithm. Thus an approximate fit to $|\kappa_2|$ would be adequate. According to Equation 4-64,

$$|\kappa_2| \approx \sqrt{\frac{\omega}{c}} |\eta_2| \ . \tag{4-71}$$

A good fit to $\sqrt{|\eta_2|}$ is given by

$$\sqrt{|\eta_2|} \approx \sqrt{\varepsilon_\infty \frac{\omega}{c}} + \sqrt{Z_0 \sigma_0} \ . \tag{4-72}$$

For our standard soil, the exact evaluation of $\sqrt{|\eta_2|}$ and this approximation yield the results:

ω =	10^3	10^4	10^5	10^6	10^7	10^8	10^9
exact =	1.76	1.77	1.79	1.82	2.04	2.90	5.94
approximate =	1.74	1.75	1.78	1.87	2.15	3.03	5.82

(4-73)

The approximation is within 5 perce[illegible] exact result over the entire range. Therefore, a good fit to $2/\gamma$[illegible]

$$\delta \equiv \frac{2}{\gamma|\kappa_2|} \approx \frac{1.1}{\frac{\omega}{c}\left(\sqrt{\varepsilon_\infty} + \sqrt{Z_0\sigma_0 c/\omega}\right)} . \tag{4-74}$$

The quantity δ defined here is the skin depth in the soil for the present cylindrical problem. In terms of δ, the inductance is

$$L = \frac{Z_0}{2\pi c}\left[\ell n \frac{\delta}{a_2} + \left(1 - \frac{\cos^2\chi}{\varepsilon_1}\right) \ell n \frac{a_2}{a_1}\right] . \tag{4-75}$$

Because of the logarithm, the inductance changes only slowly with frequency. For the example (4-50), Equation 4-75 gives the results:

ω =	10^3	10^4	10^5	10^6	10^7	10^8	10^9	sec^{-1}
δ =	353	111	34.5	10.4	2.86	0.641	0.105	meters
L =	2.16	1.93	1.70	1.46	1.20	0.90	0.54	$\mu H/m$.

(4-76)

The relation between the applied $E_0(\omega)$ and the current $I(\omega)$, including now the wire resistance R_{w0}, can be written

$$j\omega[L(\omega)I(\omega)] = E_0(\omega) - R_{w0}I . \tag{4-77}$$

The exceedingly slow variation of $L(\omega)$ suggests that it might be a reasonably good approximation to regard $L(\omega)$ as constant in inverting this equation to the time domain. It would appear appropriate to use the value of L for that range of ω which gives the dominant contribution to the integral of $E_0(\omega)\exp(j\omega t)$ over ω, i.e., to the inverse Fourier transform of Equation 4-77. Since the exponential here oscillates rapidly with ω when $\omega t >> 1$, the appropriate range of ω is

$$\omega \approx 1/t , \tag{4-78}$$

unless $E_0(\omega)$ varies rapidly with ω. The latter possibility depends on

the choice of the time origin. The EMP $E_0(t)$ varies rapidly with t initially, and then more and more slowly at later and later times. If the time origin is chosen at that time when $E_0(t)$ is changing most rapidly, then $E_0(\omega)$ will not vary rapidly with ω. For example, the form (4-56) for $E_0(t)$ has the Fourier transform

$$E_0(\omega) = E_m \frac{\alpha + \gamma}{(\gamma+j\omega)(\alpha-j\omega)} . \tag{4-79}$$

However, if the time origin were shifted to time t_0, then $E_0(\omega)$ would acquire a multiplicative factor $\exp(-j\omega t_0)$. Thus, rapid variation is avoided by choosing the time origin as stated. We agree to make this choice, and use Equation 4-78 (otherwise we would choose $\omega \approx 1/(t-t_0)$).

The suggested approximate time domain equation is therefore

$$\frac{d}{dt}[L(t)I(t)] = E_0(t) - R_{w0}I , \tag{4-80}$$

where $L(t)$ is given by Equation 4-75 with δ evaluated from Equation 4-74 and 4-78, i.e.,

$$\delta \approx \frac{1.12ct}{\sqrt{\varepsilon_\infty} + \sqrt{Z_0\sigma_0 ct}} . \tag{4-81}$$

This prescription would have difficulty if used at $t = 0$. However, the EMP has a finite rise time t_r, which for the exponential rise model is $t_r \approx 1/\alpha$. Thus in using Equation 4-81, t should be set equal to

$$t = t_r = 1/\alpha \quad \text{if} \quad t < t_r , \tag{4-82}$$

and the time origin should be chosen so that $t = t_r$ when the rise rate begins to fall significantly below α. Obviously, this prescription is somewhat imprecise at early times. Note, however that quite accurate evaluation of the current during the rise of the applied field can be had by using the form (4-56) or, better, the form (4-61) and the Laplace domain impedance. For the latter form, the current is

$$I(t) = E_m \left(\frac{2}{Z_w(\alpha)} e^{\alpha t} - \frac{1}{Z_w(2\alpha)} e^{2\alpha t} \right) \quad \text{for} \quad t \leq 0 \ . \quad (4\text{-}83)$$

Lavery (Reference 4-2) has tested the approximate equations against the equivalent circuit model of Section 4.5 for the applied field

$$\left.\begin{aligned} E_0(t) &= 0 \quad \text{for} \quad t < 0 \\ &= E_a(e^{-\gamma t} - e^{-\alpha t}) \quad \text{for} \quad t > 0 \ , \end{aligned}\right\} \quad (4\text{-}84)$$

for which the equivalent circuit equations can be solved analytically. The cable example (4-50) was used, with $\alpha = 10^8$ sec^{-1}. In Equation 4-81, t was set equal to the larger of t and 10^{-8} seconds. Equation 4-80 was integrated numerically for several values of γ as indicated in Figure 4-7, which compares the currents computed by the two methods. The comparison shows that the varying inductance approximation is quite good.

Although Equation 4-80 was integrated numerically in this example to show how good the approximation is, the current can obviously be estimated by crude integration of the equation over blocks of time in each of which $E_0(t)$ and $L(t)$ are regarded as constant. Note that the decay time L/R_{w0} is of the order milliseconds.

Our choice of putting $L(t)$ inside the time derivative in Equation 4-80 instead of outside was somewhat arbitrary, mathematically. The choice made gives better agreement with the accurately calculated currents for the shorter driving pulses. If L were put outside, the current would not decrease immediately after the short pulse, but would decay only on the time scale $L/R_{w0} \approx 10^{-3}$ second. Putting L under the time derivative gives back some of the dissipation associated with the real part of $Y_w(\omega)$, through the term $I dL/dt$. Since dL/dt is positive this term has the effect of a resistance.

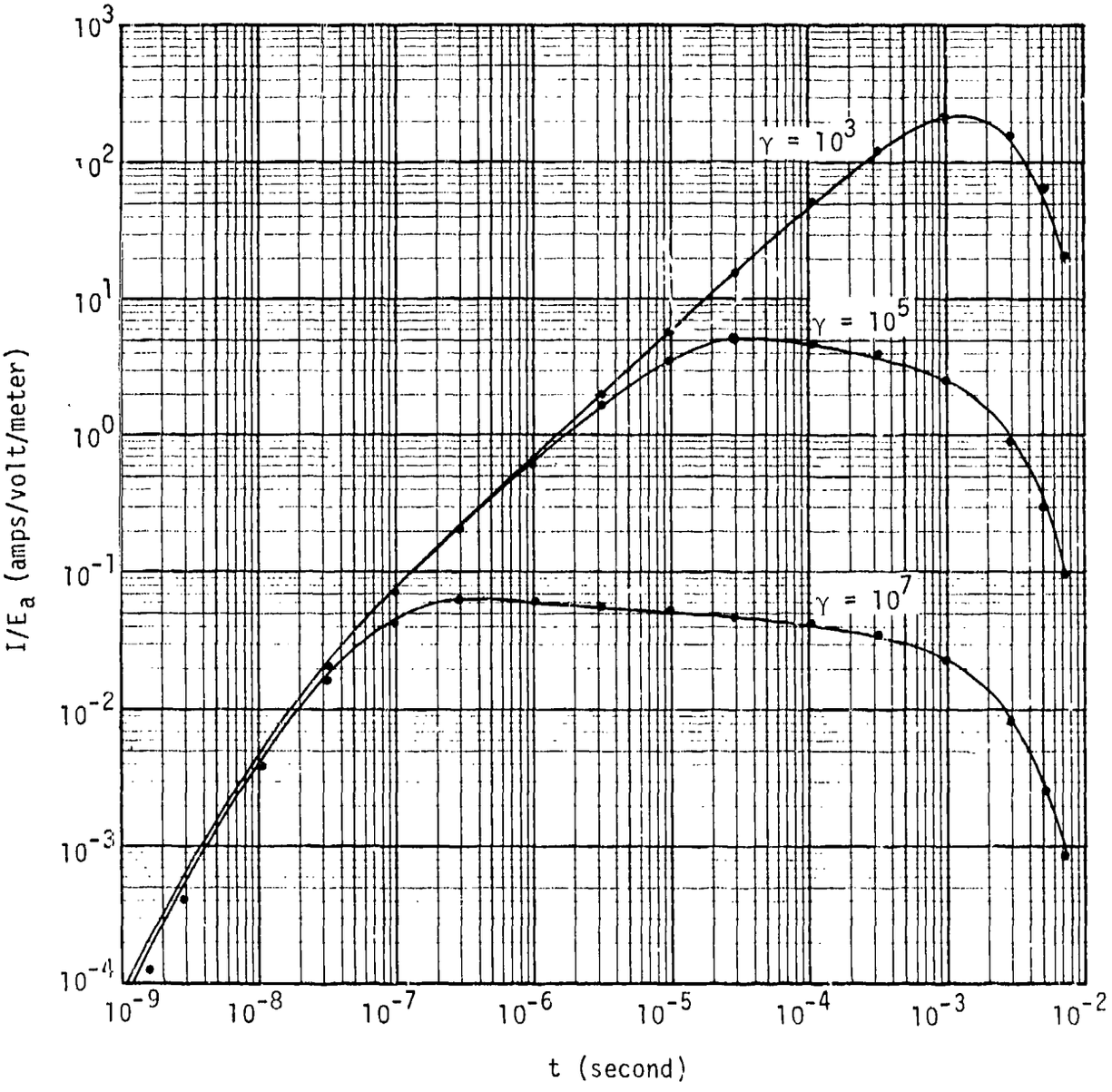

Figure 4-7. Comparison of currents calculated from R,L equivalent circuit (curves) and from time-varying inductance model (points), for the applied field of Equation 4-84. The values of γ are indicated.

4.7 FREELY PROPAGATING SOLUTIONS

The analysis thus far has considered only the particular solution of Maxwell's equations, or that part driven by the applied field. The equations also allow freely propagating solutions, and these are needed to satisfy conditions at the end of the cable. The freely propagating solutions $\sim \exp(j(\omega t - kz))$ occur for ω and k such that

$$Z_w = 0 \ , \tag{4-85}$$

so that a current I can exist without an applied field. Thus k is no longer determined by Equation 4-4, but for each ω is chosen to make Z_w vanish.

Z_w is given by Equation 4-28, and Equation 4-11 gives

$$-\frac{\kappa^2}{\eta} = j\frac{\omega}{c} + \frac{k^2}{\eta} \ , \tag{4-86}$$

for arbitrary k and ω. Ignoring the dependence of the logarithm on k (through κ_2) allows solution of Equation 4-85 for k^2, with the result

$$k^2 = -j\frac{\omega}{c}\eta_1 \frac{\ell n(\delta/a_2) + \ell n(a_2/a_1)}{\ell n(a_2/a_1) + \frac{\eta_1}{\eta_2}\ell n(\delta/a_2)} \ , \tag{4-87}$$

where the skin depth δ for propagation is complex,

$$\delta = 2/\gamma j\kappa_2 \ . \tag{4-88}$$

Since κ_2 and δ depend on k^2 (see Equation 4-12), Equation 4-87 has to be solved by iteration for accurate results, in general.

For $\omega \lesssim 10^6$ sec^{-1} and when the conductivity of the insulator is indeed small (true except in case of high radiation exposure), the first step in the iteration gives approximately correct results. The first step puts $k^2 = 0$ in the calculation of κ_2 and δ. For $\omega \lesssim 10^6$ the dielectric part of η can be neglected and

$$\kappa_2 \approx \sqrt{-jZ_0\sigma_0\omega/c} \ , \tag{4-89}$$

so that

$$\delta \approx \frac{2\sqrt{-j}}{\gamma\sqrt{Z_0\sigma_0\omega/c}} \equiv \delta_m\sqrt{-j} \ . \tag{4-90}$$

Here δ_m is the magnitude of δ. Thus

$$\ell n\left(\frac{\delta}{a_2}\right) = \ell n\left(\frac{\delta_m}{a_2}\right) - j\,\frac{\pi}{4} \ . \tag{4-91}$$

The ratio of the η's is

$$\frac{\eta_1}{\eta_2} \approx -\frac{j\varepsilon_1\omega/c}{Z_0\sigma_0} \ .$$

For the example (4-50) at $\omega = 10^6$, $\ell n(\delta_m/a_2) \approx 7.3$, $\ell n(a_2/a_1) = 0.693$, and $\eta_1/\eta_2 \simeq j/450$. The second term in the denominator of Equation 4-87 can be neglected, with the result

$$k^2 = \varepsilon_1\left(\frac{\omega}{c}\right)^2 \frac{\ell n(\delta_m/a_1) - j\,\frac{\pi}{4}}{\ell n(a_2/a_1)} \ . \tag{4-91}$$

This result verifies that it was proper to neglect k^2 in calculating κ_2. Since $\ell n(\delta_m/a_1)$ is considerably larger than $\pi/4$, the square root can be calculated approximately, giving the formula for k,

$$k \approx \sqrt{\varepsilon_1}\,\frac{\omega}{c}\sqrt{\frac{\ell n(\delta_m/a_1)}{\ell n(a_2/a_1)}}\left(1 - \frac{j\pi/8}{\ell n(\delta_m/a_1)}\right) \ . \tag{4-92}$$

The imaginary part of k gives the attenuation of the propagating wave.

For large ω, the solution for k^2, Equation 4-87, should be iterated by putting this value of k^2 back into the formula (Equation 4-86) for κ_2, and so on. For accuracy, the full η should of course be used, instead of $Z_0\sigma_0$. Figure 4-8 shows the real and imaginary parts of k for

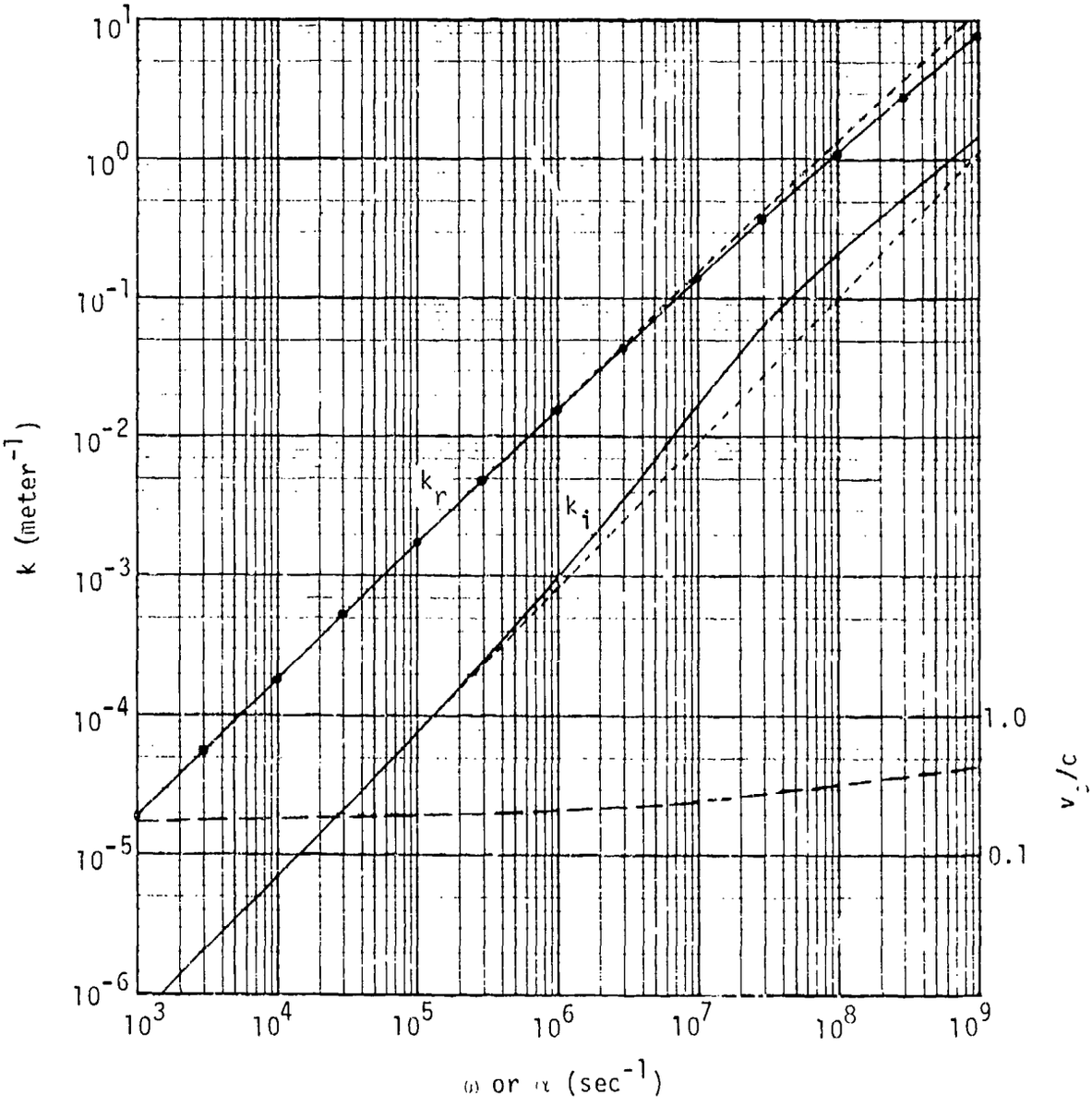

Figure 4-8. Cable propagation constants. Solid curves, real and imaginary parts k_r and k_i as functions of ω. Short dashed curves, the same from the approximate Equation 4-92. Points, $\mathcal{R}(\alpha)$; note that this is virtually the same as $k_r(\omega)$. Long dashed curve, ratio of phase speed to speed of light.

the example (4-50), along with results from the approximate formula Equation 4-92.

In the Laplace domain, one looks for freely propagating solutions of the form

$$I \sim \exp(\alpha t - \tilde{k} z) \quad , \tag{4-93}$$

where $\tilde{k}$ is again determined for given α by requiring that $Z_w = 0$. For this case, Equation 4-87 becomes

$$\tilde{k}^2 = \frac{\alpha}{c} \eta_1 \frac{\ell n(\delta/a_2) + \ell n(a_2/a_1)}{\ell n(a_2/a_1) + \frac{\eta_1}{\eta_2} \ell n(\delta/a_2)} \quad . \tag{4-94}$$

The skin depth is

$$\delta = 2/\gamma \tilde{\kappa}_2 \quad , \tag{4-95}$$

and $\tilde{\kappa}_2$ is to be found from Equation 4-33 or 4-35. Again, iterative solution is generally required. The η's in these equations are of course $\eta(\alpha)$. Figure 4-8 also shows $\tilde{k}(\alpha)$.

As in Section 4.4, E_r can be related to the current I for the freely propagating solutions. By the same procedure it is found that

$$E_r(\omega) = \frac{jkZ_0}{2\pi r \eta} I(\omega) \quad , \tag{4-96}$$

$$E_r(\alpha) = \frac{\tilde{k} Z_0}{2\pi r \eta} I(\alpha) \quad . \tag{4-97}$$

The voltage V across the insulator (σ assumed negligible) is found by integrating these expressions on r. The result is

$$V(\omega) = \frac{kZ_0}{2\pi\varepsilon_1 \omega/c} \ell n\left(\frac{a_2}{a_1}\right) I(\omega) \quad , \tag{4-98}$$

$$V(\alpha) = \frac{\tilde{k} Z_0}{2\pi c_1 \alpha / c} \ln\left(\frac{a_2}{a_1}\right) I(\alpha) \quad . \tag{4-99}$$

Note that the sign of V depends on the sign of k or $\tilde{k}$, i.e., it is different for solutions propagating to right and left. The factors multiplying I in these equations are analogous to the characteristic impedance Z_c of a coaxial transmission line. In the present case, the outer conductor (the soil) does not have perfect conductivity, and there are significant electric fields in it out to radii of the order of δ.

4.8 THE END CONDITIONS: OPEN CIRCUIT

The freely propagating solutions are added to the driven solution to satisfy conditions at the end of the wire. The easiest case to analyze is that in which the end of the wire is insulated from the soil, i.e., the case of open circuit. If the driven and freely propagating currents are denoted by I_d and I_p respectively, the end condition is then that

$$I_p = - I_d \quad . \tag{4-100}$$

The driven current is determined by the applied electric field, and propagating currents are then fed into the ends to cancel the driven current at those points. The propagating currents propagate along the wire, modifying the total current and fields as they go. They eventually reach the opposite end from their origin. At that time, additional propagating currents are fed into the ends to cancel the outgoing propagating currents. The analysis here is the same as in normal transmission line analysis.

This analysis is not exact. While the propagating solution can cancel the wire current of the driven solution, it does not cancel the fields of the latter in detail. The values of k, and therefore of k_z, are different for the driven and propagating solutions for a given frequency. Hence the radial distribution of fields is not the same. Cancellation of

the currents means that the B_θ fields, which are given for both solutions by Equation 4 39 near the wire (out to about one skin depth), will also cancel approximately. However, as will be seen shortly, the fields E_r are substantially different for the driven and propagated solutions, and come nowhere near canceling. It is reasonable to expect an adjustment of the radial electric field over a region of the size of one skin depth near the end of the wire.

Equation 4-9 relates E_r to B_θ. Since B_θ is approximately the same for driven and propagated solutions, given Equation 4-100, out to about one skin depth, the difference in E_r comes from the difference in k. For the driven solution, k_d is given by Equation 4-4. For the propagating solutions, k_p is given by Equation 4-87, or for lower frequencies by the approximate Equation 4-92. It is seen that k_p is typically several times k_d. Thus E_{rp} is several times E_{rd}.

The adjustment of E_r involves propagating solutions with higher radial modes. The k for these modes is again found by requiring $Z_w = 0$, but this time the exact Equation 4-25 must be used instead of the approximate Equation 4-28 resulting from the small argument expansion. These solutions decay rapidly with distance away from the wire end, and carry little current so that Equation 4-100 remains approximately correct. Their role is, roughly, to remove E_r from the soil and increase E_r in the insulator near the end of the wire. They are important, therefore, in considerations of insulator breakdown at the wire end. The total solution depends also on the structure of wire and insulation at the end. The field across the insulation can be reduced by connecting the end of the wire to a larger conducting sphere which is also insulated from the soil. No detailed solutions were available at the time of writing of this report.

The radial field in the insulator is at least as large as the values indicated by Equations 4-96 or 4-97. With the approximation Equation 4-92 for k, these equations become, in the insulator,

$$E_r \approx \frac{Z_0}{2\pi r \sqrt{\epsilon_1}} \sqrt{\frac{\ell n(\delta_m/a_1)}{\ell n(a_2/a_1)}}\, I_p \quad . \tag{4-101}$$

A measure of the importance of the fields in the soil to those in the insulator is given by the ratio of the radial voltage drop $V = \int E_r dr$ in the two regions. On taking $B_\theta \sim 1/r$, Equation 4-9 leads to

$$\frac{V_{soil}}{V_{ins}} \approx \frac{\eta_1}{\eta_2} \frac{\ell n(\delta/a_2)}{\ell n(a_2/a_1)} \quad . \tag{4-102}$$

This ratio was shown to be small for $\omega \leq 10^6$ in Section 4.7. It is graphed as a function of Laplace domain frequency in Figure 4-9 for our usual example, which shows that it is always considerably less than unity. It is to be expected that the increase in E_r in the insulator due to adjustment of fields near the wire end is by a factor $1 + (V_{soil}/V_{ins})$, which is not large.

The phase speed of propagation along the cable is (k_r is the real part of k)

$$v_\phi = \frac{\omega}{k_r} \quad \text{or} \quad \frac{\alpha}{\tilde{k}} \quad . \tag{4-103}$$

This speed is considerably less than c, as shown by Equation 4-92. The ratio v_ϕ/c is graphed in Figure 4-8.

The maximum value of the current at the center of the cable will usually occur, for EMP drive, just before the propagated signals arrive from the two ends. Attenuation and dispersion of the propagated signals must be taken into account. An approximate way of treating this is developed in the following section.

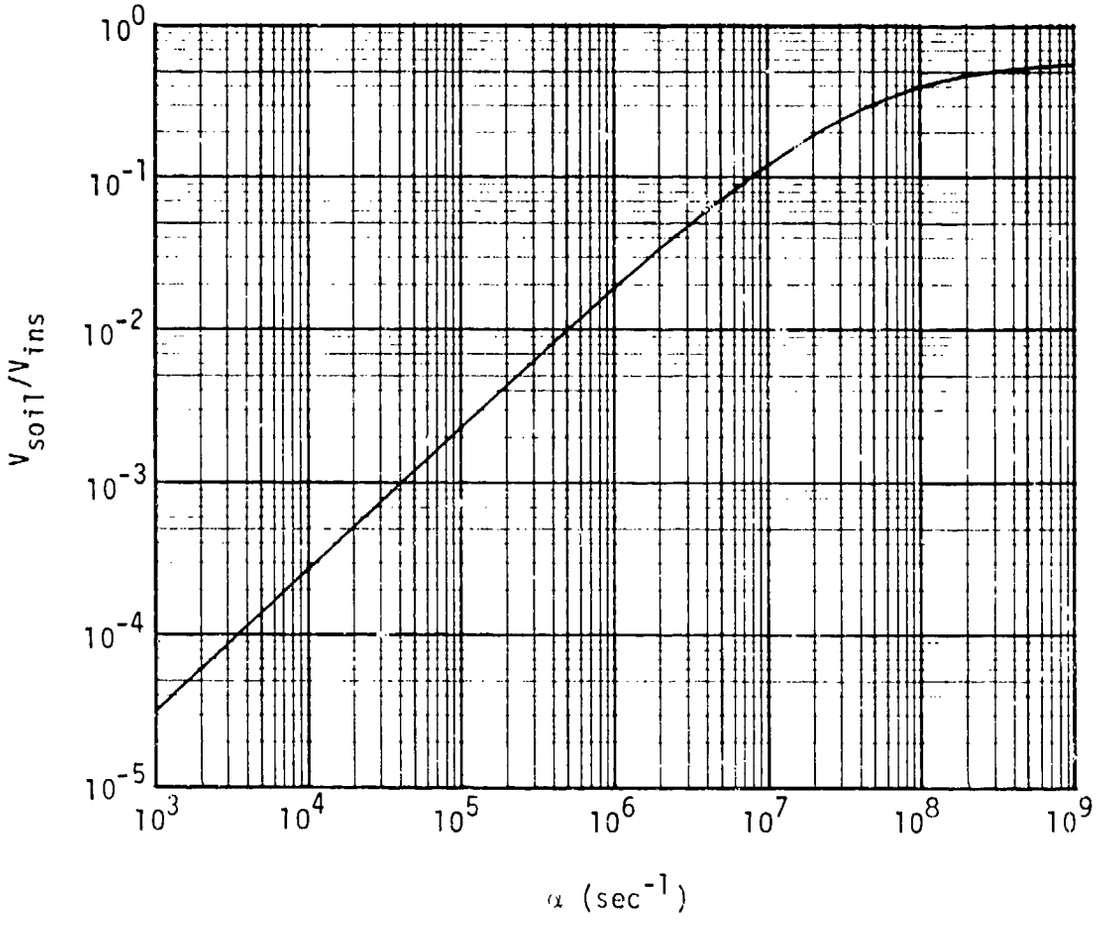

Figure 4-9. Ratio of the radial voltage drops in the soil and in the insulator for the propagating solution in the Laplace domain, as a function of frequency.

4.9 ATTENUATION AND DISPERSION

The factor $\exp(-jkz)$ determines how the signal propagates along the cable. In order to estimate the effects of attenuation and dispersion, an analytic approximation to $k(\omega)$ is needed. Figure 4-8 shows that the real part k_r can be fitted quite well, over a few decades of ω about any point, by a power law. In choosing a fit, care must be taken to maintain the reality and causality conditions (see Section 2.3). A satisfactory approximation is

$$jk = a(j\omega)^p \ , \tag{4-104}$$

where the power p and the factor a are both real constants. For then the complex conjugate of jk is

$$[jk(\omega)]^* = jk(-\omega) \ , \tag{4-105}$$

and reality is guaranteed. Causality requires that jk be analytic in the negative imaginary half of the complex ω plane. The function 4-104 is analytic in any region that does not enclose the origin. A cut along the imaginary axis from $\omega = 0$ to $\omega = j\infty$ prevents encircling the origin. The path of integration in any Fourier inversions must then pass below the origin, as in Figure 4-10a.

Figure 4-8 shows that the exponent p is just slightly less than unity. Thus q, defined as

$$q = 1 - p \ , \tag{4-106}$$

is a small number, of the order 0.05 to 0.1.

Equation 4-104 can also be written, for ω on the positive real axis,

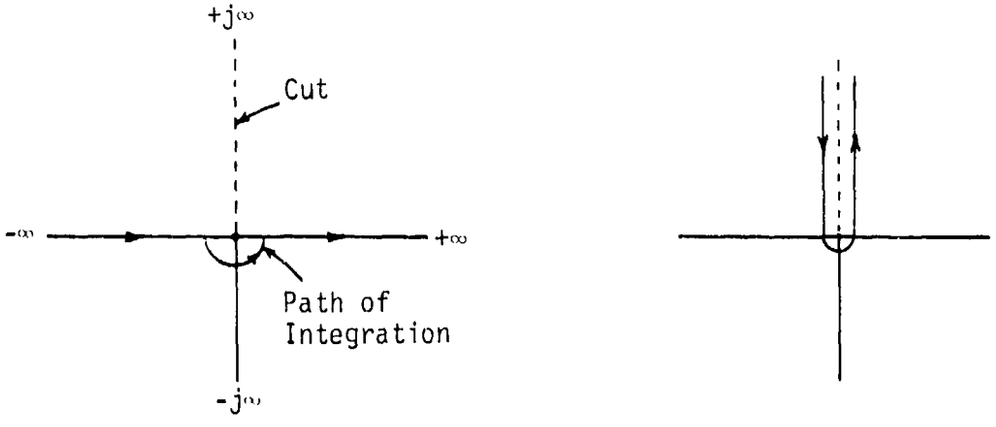

a. Normal Integration Contour

b. Folded Contour

Figure 4-10. Cut and integration path in complex ω plane.

$$k = aj^{-q}\omega^p = a\omega^p \exp(-j\,\frac{q\pi}{2})$$

$$= a\omega^p[\cos(\frac{q\pi}{2}) - j\sin(\frac{q\pi}{2})] \qquad (4\text{-}107)$$

$$\approx a\omega^p[1 - j\,\frac{q\pi}{2}] \quad (\text{for } q << 1) .$$

This shows the relation of the real and imaginary parts of k. The closer p is to unity, the smaller is the ratio of k_i to k_r, which explains the shape of the k_i curve in Figure 4-8. If we choose to fit the k_r curve in the vicinity of some frequency ω_0, where $k_r = k_0$, then the constant a is

$$a \approx k_0/\omega_0^p . \qquad (4\text{-}108)$$

Let an impulse current be injected at $t = 0$ into the end of the cable, which is at $z = 0$. The Fourier transform of the impulse function is unity. The signal at t,z is then

$$I_{im}(t,z) = \frac{1}{2\pi}\int_{-\infty}^{\infty} \exp[j\omega t - az(j\omega)^p]d\omega \ . \qquad (4\text{-}109)$$

The integral here is difficult to evaluate exactly, but it can be estimated by the method of stationary phase (or saddle point). The argument of the exponential is stationary when

$$\frac{\partial}{\partial(j\omega)} \arg = t - paz(j\omega)^{-q} = 0 \ , \qquad (4\text{-}110)$$

or at

$$j\omega = j\omega_{st} = \left(\frac{paz}{t}\right)^{1/q} \ . \qquad (4\text{-}111)$$

This point is on the negative imaginary axis ($\omega = -j \times$ real number), so that the integration contour can be deformed to pass through it. The value of the argument at the stationary point is

$$\arg_0 = t\left(\frac{paz}{t}\right)^{1/q} - az\left(\frac{paz}{t}\right)^{p/q}$$

$$= t\left(\frac{paz}{t}\right)^{1/q}\left[1 - \frac{1}{p}\right] = -qaz\left(\frac{paz}{t}\right)^{(1-q)/q} \ . \qquad (4\text{-}112)$$

The second derivative of the argument is

$$\frac{\partial^2}{\partial\omega^2} \arg = -\frac{\partial^2}{\partial(j\omega)^2} \arg = -qpaz(j\omega)^{-(1+q)} \ , \qquad (4\text{-}113)$$

and evaluation at the stationary point gives

$$\arg_0'' = -qpaz\left(\frac{t}{paz}\right)^{(1+q)/q} \ . \qquad (4\text{-}114)$$

In the vicinity of the stationary point, $\omega = \omega_{st} + \delta\omega$

$$\arg \approx \arg_0 + \frac{1}{2}\arg_0''(\delta\omega)^2 \ . \qquad (4\text{-}115)$$

Thus the exponential in Equation 4-109 is real and decaying if the path of integration passes horizontally ($\delta\omega$ real) through the stationary point. The estimate of I_{im} is then

$$I_{im}(t,z) \approx \frac{1}{2\pi}\sqrt{\frac{2\pi}{qpaz}}\left(\frac{paz}{t}\right)^{(1+q)/2q} \exp\left[-qaz\left(\frac{paz}{t}\right)^{(1-q)/q}\right] . \quad (4\text{-}116)$$

Since $(1-q)/q$ is a large number (≈ 10 to 20), the exponential here makes I very small until t is large enough to make the argument of the exponential near unity. For larger t, the factor $t^{-(1+q)2q}$ makes I decrease rapidly again. Thus the original impulse function is spread out over a short time about that time that makes the argument of the exponential equal to unity.

The form of Equation 4-116 can be simplified by calling the argument of the exponential $-u^2$, i.e.,

$$u(t,z) \equiv \sqrt{qaz}\left(\frac{paz}{t}\right)^{(1-q)/2q} . \quad (4\text{-}117)$$

Note then that

$$\frac{\partial u}{\partial t} = -\frac{1}{2}\frac{1}{\sqrt{qaz}}\left(\frac{paz}{t}\right)^{(1+q)/2q} . \quad (4\text{-}118)$$

Comparison of this expression with Equation 4-116 shows that

$$I_{im} = -\sqrt{\frac{2}{\pi p}}\frac{\partial u}{\partial t}e^{-u^2} . \quad (4\text{-}119)$$

Now, the response I_{st} of the cable to a unit step function is related to I_{im} by

$$I_{st}(t,z) = \int_0^t I_{im}(t,z)dt$$

$$= \sqrt{\frac{2}{\pi p}}\int_{u(t,z)}^{\infty} e^{-u^2}du . \quad (4\text{-}120)$$

Note that $t = \infty$ corresponds to $u = 0$, so that

$$I_{st}(\infty, z) = \sqrt{\frac{2}{\pi p}} \int_0^\infty e^{-u^2} du = \frac{1}{\sqrt{2p}} \quad . \tag{4-121}$$

Actually, $I_{st}(\infty, z)$ should equal unity. The factor $1/\sqrt{2p} \approx 0.73$ is not far from unity, but our estimate is not entirely accurate. It will be shown below that the error comes at late times after most of the pulse has arrived at the point z. For the present we proceed with the formulae as they stand.

The integral in Equation 4-120 attains half of its final value at about $u = 1/2$, and it can be said that the signal arrives at the corresponding time. This time can be evaluated from Equation 4-117, which gives the arrival time

$$t_a = p(4q)^{q/p}(az)^{1/p} \quad . \tag{4-122}$$

If a is evaluated from the reference values k_0 and ω_0, Equation 4-108, this result becomes

$$\frac{v_0 t_a}{z} = p(4qk_0 z)^{q/p} \quad , \tag{4-123}$$

where v_0 is the phase speed at the reference values,

$$v_0 \equiv \omega_0 / k_0 \quad . \tag{4-124}$$

Equation 4-123 shows that the arrival time increases faster than z/v_0 with increasing z; this comes from attenuation of the higher frequencies with increasing z.

The rate of rise of the signal at the arrival time can be estimated from Equation 4-119:

$$\text{rise rate} \approx \sqrt{\frac{2}{\pi p}}\left(-\frac{\partial u}{\partial t}\right)e^{-1/4} = \sqrt{\frac{2}{\pi p}}\,\frac{(1-q)/q}{t_a}\,u_a e^{-1/4}$$

$$\approx 0.62\,\frac{\sqrt{p}}{q t_a} \quad . \tag{4-125}$$

The rise time t_r is the ratio of the final value to the rise rate,

$$t_r \approx 1.14\,\frac{q}{p}\,t_a \quad . \tag{4-126}$$

Thus t_r is a small fraction of t_a.

Equations 4-128 and 4-125 have a very simple and useful interpretation, from which they could have been foreseen. First, note that no specific choice of ω_0 and k_0 has been made, except that they go together. Thus in Equation 4-123, k_0 can be set equal to any value of k_r (the real part of k) if v_0 is set equal to the phase speed v_ϕ going with k_r. The equation can then be written

$$t_a = \frac{z}{v_\phi}\left(p^{p/q}\,4qk_r z\right)^{q/p} \quad . \tag{4-127}$$

Now,

$$p^{p/q} = (1-q)^{p/q} \approx e^{-p} \qquad (q \ll 1) \quad .$$

For $0.9 < p < 0.95$, $4e^{-p}$ is quite close to $\pi/2$ (within 3 percent). Next, note that according to Equation 4-107,

$$\frac{\pi}{2}\,qk_r \approx k_i \quad . \tag{4-128}$$

Thus Equation 4-127 is equivalent to

$$t_a = \frac{z}{v_\phi}\left(k_i z\right)^{q/p} \quad . \tag{4-129}$$

The interpretation is now clear: find that ω_1, from Figure 4-8 for example, for which

$$k_i(\omega_1)\,z = 1 \quad ; \tag{4-130}$$

the arrival time is then

$$t_a = z/v_\phi(\omega_1) \ . \tag{4-131}$$

The interpretation of the rise rate, Equation 4-125 is equally simple. The value of k_r for the case (4-130) is

$$\begin{aligned} k_r(\omega_1) &= 2k_i/\pi q \\ &= 2/\pi qz \ . \end{aligned} \tag{4-132}$$

The frequency going with $k_r(\omega_1)$ is

$$\begin{aligned} \omega_1 &= v_\phi k_r = 2v_\phi/\pi qz \\ &= \frac{2}{\pi q t_a} \ . \end{aligned} \tag{4-133}$$

Now $2/\pi = 0.64$, quite close to the factor $0.62\sqrt{p}$ in Equation 4-125. Thus the rise rate of the signal at z is equal to that frequency ω_1 for which the attenuation is e^{-1}.

These results hold for a step function input current. Figure 4-7 shows that short EM pulses produce step-like currents, but with finite rise rates. The rise rate at z cannot be faster than that at the input. Long EM pulses produce ramp-like currents. The response of the cable to a ramp is the time integral of the step-function response. The arrival time for a ramp is essentially the same as for a step function. The rise time of the step corresponds to the time for the ramp to acquire its final slope.

The failure of I_{st} to reach unity, Equation 4-121, comes from the fact that the expansion of the argument, Equation 4-115, is not accurate at late times. For $t > 0$, the integral in Equation 4-109 can be evaluated by folding the contour of integration about the cut as in Figure 4-10b. The result is

$$I_{im}(t,z) = \frac{1}{\pi}\int_0^\infty e^{-st} e^{\cos(q\pi)azs^p} \sin[\sin(q\pi)azs^p]ds \ . \qquad (4\text{-}134)$$

For large t, most of the contribution to this integral comes from small s, so that the functions of s^p can be replaced by the first terms in their power series expansions. Thus for large t,

$$I_{im}(t,z) \approx \frac{1}{\pi}\int_0^\infty e^{-st}\sin(q\pi)azs^p ds$$

$$\approx qaz(p!)/t^{p+1} \qquad (t \text{ large}) \ . \qquad (4\text{-}135)$$

This result shows that the impulse response falls to zero somewhat more slowly at late times than was indicated by Equation 4-116. This explains why the time integral of Equation 4-116 did not quite reach unity. The behavior of I_{st} is sketched in Figure 4-11. The current rises rapidly at t near t_a, but not quite to unity. The final rise to unity takes a few t_a's.

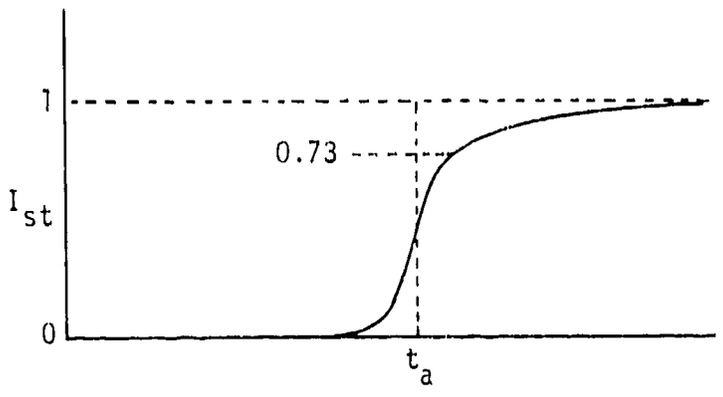

Figure 4-11. Shape of the step function response.

CHAPTER 5
COUPLING TO LONG BURIED CABLES; AN EXAMPLE

5.1 INTRODUCTION

In this chapter the theory of Chapter 4 will be extended to buried wires that are long enough that the amplitude of the EMP changes appreciably over the length of the wire. In most of this chapter, attention is given to a particular example, namely that of a buried power line which terminates at a buried facility. In order to maximize the coupling, the nuclear burst is assumed to occur directly on the power line, at a distance of 1 kilometer from the facility. The geometry is sketched in Figure 5-1.

The air in the fireball is very hot, with temperatures in the range 1 to 10 eV, and is therefore thermally ionized. The electrical conductivity in the fireball is in excess of 10^4 mho/meter. The fireball is a very good conductor compared with the soil and with the air outside the fireball. The radius R of the fireball increases with time as

$$R(\text{meters}) \approx 1300\ t^{2/5} Y^{1/5}\ , \qquad (5\text{-}1)$$

where t is the time in seconds and Y is the yield in megatons. This formula is valid for $t \gtrsim 0.1\ Y^{1/3}$ second.

Buried power lines typically have a central "hot" wire surrounded by insulation, then wrapped with several return conductors which are approximately at ground potential. Often a partially conducting plastic sheath protects the return wires from corrosion by the soil. We shall assume that the return wires are in electrical contact with the soil, and take the

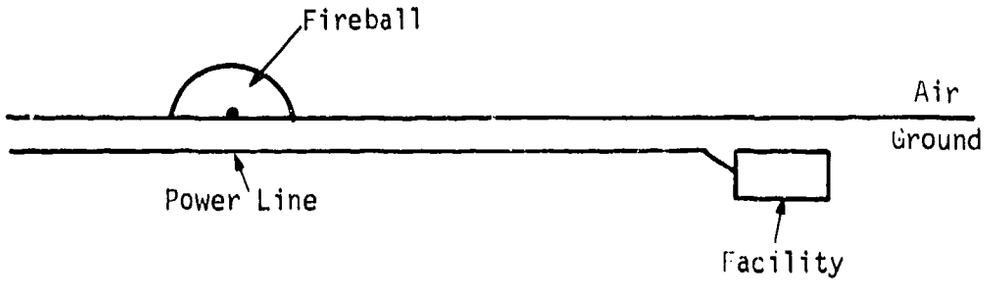

Figure 5-1. Geometry of burst, power line and facility.

resistance of the return wires to be

$$\rho \approx 0.3 \text{ milliohm/meter} . \qquad (5\text{-}2)$$

The integral of the radial EMP electric field in the ground between the fireball and the facility would be of the order of 1 to 10 megavolts, if the power line were not present. After a period of inductive limitation of current in the wire, this voltage appears partly between the wire and the fireball at one end, and partly between the wire and the facility at the other end. It is likely that these voltages are large enough to drive arcs between the wire and the fireball and between the wire and the facility walls. It is assumed here that the latter are reinforced concrete, and have a low impedance to distant ground. The fireball, which is in contact with the soil, also has a low impedance to distant ground. The current in the wire is limited, after the inductive phase, by these two impedances. It is likely also that the soil will break down in the vicinity of the wire along its length, reducing to some extent the voltage and current delivered to the facility.

The question as to whether ground shock destroys the power line is immaterial. There is no shock wave outside the fireball (at the times of interest here), so the power line must be intact at the fireball radius. If the power line is opened at some point underneath the fireball, the arc can still strike near its edge.

5.2 THE DRIVING ELECTRIC FIELD

Figure 5-2 shows a crude representation of the time and radius dependence of the radial electric field in the ground within a few meters of the surface. The times T labeling the curves are retarded times,

$$T = t - \frac{r}{c} . \tag{5-3}$$

Actual calculated fields do not fall precisely exponentially with distance, but the representation shown is not a bad one. The fields given are most appropriate for a few megaton explosion over soil of conductivity (at low frequency)

$$\sigma_0 \approx 10^{-3} \text{ mho/meter.} \tag{5-4}$$

The ends of the curves are placed at the fireball radius obtained from Equation 5-1 with Y = 5 MT.

The behavior of the field can be understood from the theory presented in Chapter 3. At early times the air conductivity is larger than the soil conductivity, and the radial electric field is approximately equal to the saturated field $J_s/\sigma(\text{air})$, which varies little with distance out to 1 kilometer. At late times, in the quasistatic phase, the Compton current passing outwards through the hemisphere of radius r in the air returns as conduction current through the hemisphere of radius r in the ground, so that

$$E_r \approx - J_s/\sigma_0 \sim e^{-r/\lambda}/r^2 . \tag{5-5}$$

This formula indicates that E_r should fall by about a factor of 10 between r = 300 and 600 meters ($\lambda \approx 300$ meters), in agreement with the curve at $T = 10^{-2}$ second. At intermediate times, the curves can be understood by assuming that the Compton current within one skin depth in the air returns as conduction current within one skin depth in the ground.

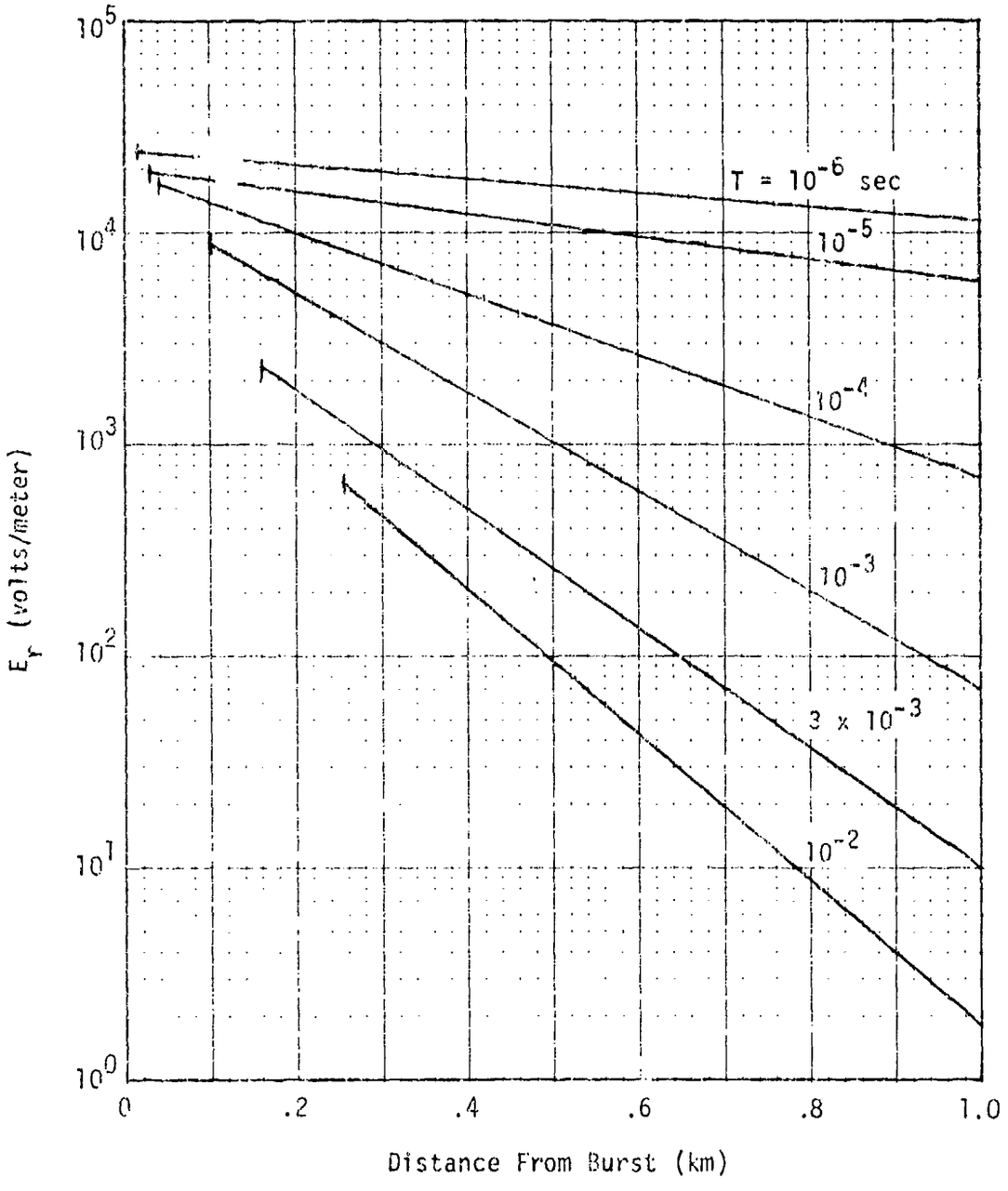

Figure 5-2. Radial electric field in the ground as a function of distance, for various retarded times.

The fields of Figure 5-2 are represented analyticaly by the formula

$$E_r(r,t) = \mathcal{E}(t - \frac{r}{c})e^{-\beta r} \quad . \tag{5-6}$$

Here $\mathcal{E}$ is a function only of retarded time. The parameter β is not independent of time, because the slope of the curves in Figure 5-2 varies. From the slopes we obtain the following table:

$$\left.\begin{array}{lllllll} t = & 10^{-6} & 10^{-5} & 10^{-4} & 10^{-3} & 10^{-2} & \text{sec} \\ \beta = & 0.007 & 0.0012 & 0.0034 & 0.0054 & 0.0079 & m^{-1} \end{array}\right\} \tag{5-7}$$

It is seen that β changes only slowly with time.

If β is regarded as independent of time, then the Fourier expansion of $E_r(r,t)$ contains terms of the form

$$E_z \sim e^{j(\omega t - kz)} \quad , \tag{5-8}$$

where

$$k = \frac{\omega}{c} - j\beta \quad . \tag{5-9}$$

Note that the horizontal coordinate (along the power line) is now called z, in order not to confuse it with the cylindrical coordinate r of Chapter 4.

5.3 THE WIRE IMPEDANCE

The impedance of the power line to driving fields of the type of Equation 5-8 is given by Equation 4-28. The absence of an insulating layer in the present case can be accounted for by putting $a_1 = a_2$. The impedance Z_w is then

$$Z_w(\omega) \approx \frac{Z_0}{2\pi}\left[-\frac{\kappa_2^2}{n_2}\left(\ell n \frac{2}{\gamma \kappa_2 a_2} - \frac{j\pi}{2}\right)\right] \quad . \tag{5-10}$$

The quantity κ_2 is given by Equation 4-11, which with Equation 5-9 becomes

$$-\kappa_2^2 = \frac{j\omega\eta_2}{c} + \left(\frac{\omega}{c} - j\beta\right)^2 , \tag{5-11}$$

where the relative soil admittance is

$$\eta_2 = Z_0\sigma + j\,\frac{\omega\varepsilon}{c} . \tag{5-12}$$

In deriving the time-varying inductance model in Section 4.6, we showed that the second (k^2) term on the right in Equation 5-11, with $\beta = 0$, was small compared with the first term and could be neglected. This approximation must now be reexamined. Writing out Equation 5-11 gives

$$-\kappa_2^2 = -\frac{\omega^2}{c^2}(\varepsilon - 1) + j\,\frac{\omega}{c}(Z_0\sigma - 2\beta) - \beta^2 . \tag{5-13}$$

The contributions of the k^2 term are evident. First, there is the term -1 in the factor $\varepsilon - 1$, which can be neglected as in Section 4.6. Second, there is the term -2β in the factor $Z_0\sigma - 2\beta$. Now $Z_0\sigma \approx 0.377$ while $2\beta < 0.016$; thus 2β can also be neglected. Finally, there is the term $-\beta^2$. This term is negligible if

$$\beta^2 < \frac{\omega}{c} Z_0\sigma ,$$

or, since $Z_0/c = \mu_0$, if

$$\frac{1}{\beta} > \frac{1}{\sqrt{\mu_0\sigma\omega}} \approx \text{skin depth} . \tag{5-14}$$

Thus the time-varying inductance model is still valid if the distance of diffusion of fields along the wire is small compared with the distance $1/\beta$ in which the amplitude of the driving field varies appreciably. In the time domain, the inductance model is valid for times

$$t < \frac{\mu_0\sigma}{\beta^2} \approx 10^{-4} \text{ sec in present example} . \tag{5-15}$$

In order to find an approximate evaluation of Z_w, it is necessary to evaluate both the factor κ_2^2/η_2 and the logarithm in Equation 5-10. For the log term, the variation of which is not sensitive, we take

$$\frac{2}{\gamma|\kappa_2|a_2} = \frac{\delta}{a_2} , \tag{5-16}$$

where δ is given by Equations 4-74 or 4-81 if Equation 5-15 is satisfied, and

$$\delta = \frac{1.12}{\beta} \quad \text{for} \quad t > \frac{\mu_0\sigma}{\beta^2} . \tag{5-17}$$

For the factor κ_2^2/η_2, note that the neglection, in Equation 5-13, of -1 compared with ε and of -2β compared with $Z_0\sigma$ is equivalent to writing Equation 5-11 as

$$-\kappa_2^2 \approx \frac{j\omega\eta_2}{c} - \beta^2 ,$$

or

$$-\frac{\kappa_2^2}{\eta_2} \approx j\frac{\omega}{c} - \frac{\beta^2}{\eta_2} \approx j\frac{\omega}{c} - \frac{\beta^2}{Z_0\sigma} . \tag{5-18}$$

The second form here recognizes the dominance of $Z_0\sigma$ over $\varepsilon\omega/c$ at late times when the β^2 term is significant.

With these results and with the inclusion of the resistance R_{w0} of the wire, the impedance of the wire can be written

$$Z_w(s) = j\omega L + R_{w0} - R_\beta , \tag{5-19}$$

where

$$L = \frac{\mu_0}{2\pi} \ln\left(\frac{\delta}{a_2}\right) \text{ Henry/meter} , \tag{5-20}$$

and

$$R_\beta = \frac{\beta^2}{2\pi\sigma} \ln\left(\frac{\delta}{a_2}\right) \text{ ohm/meter} . \qquad (5\text{-}21)$$

As in Section 4.6, the time domain equation for the wire current I is

$$\frac{d}{dt}\left[L(t)I(t)\right] = E(t) - \left[R_{w0} - R_\beta(t)\right]I . \qquad (5\text{-}22)$$

Note that the resistance R_β represents a negative resistance, which accounts for the increase in current at a given z due to larger driving field at smaller z. The e-folding time of the current due to this negative resistance is

$$\tau = \frac{L}{R_\beta} = \frac{\mu_0\sigma}{\beta^2} . \qquad (5\text{-}23)$$

For the example considered in this chapter, $\tau \approx 10^{-4}$ second at $t = 10^{-4}$ second. Thus diffusion along the wire accounts for most of the increase in current after $t = 10^{-4}$ second.

The solution of Equation 5-22 can be written in terms of integrals. Let

$$g(t) = \int_0^t \frac{R_\beta - R_{w0}}{L}\, dt' = \int_0^t \left[\frac{\beta^2}{\mu_0\sigma} - \frac{R_{w0}}{L}\right]dt' . \qquad (5\text{-}24)$$

Then Equation 5-22 can be written as

$$\frac{d}{dt}\left[e^{-g(t)}L(t)I(t)\right] = e^{-g}E(t) ,$$

and the solution of this equation is

$$I(t) = \frac{e^{g(t)}}{L(t)} \int_0^t e^{-g(t')}E(t')dt' . \qquad (5\text{-}25)$$

5.4 DIFFUSION ALONG THE WIRE

The physical origin of the term $R_\beta I$ is made clearer by writing

$$R_\beta I = \frac{R_\beta}{L} LI = \frac{\beta^2}{\mu_0 \sigma} LI \ . \tag{5-26}$$

Now it was assumed in Equation 5-6 that the dependence of the driving field on z and t is $\mathscr{E}(t - z/c)e^{-\beta z}$, and it was shown above that the dependence of $\mathscr{E}$ on z produces negligible effects when, as in the case of interest here, the wire is in electrical contact with the soil. Thus the essential dependence of E on z is $e^{-\beta z}$, and I will have the same dependence, apart from end effects which are considered below. Therefore,

$$\frac{\partial}{\partial z} = - \beta \ , \tag{5-27}$$

so that Equation 5-22 is equivalent to

$$\frac{\partial}{\partial t} [LI] = E - R_{w0} I + \frac{1}{\mu_0 \sigma} \frac{\partial^2}{\partial z^2} [LI] \ . \tag{5-28}$$

This diffusion equation shows explicitly that the magnetic flux LI per unit length of wire diffuses along the wire, and is valid for any dependence of E on z, not just exponentials.

Equation 5-28 can be derived directly from Maxwell's equations for the present case. These are, in the cylindrical coordinates of Figure 4-2,

$$\frac{\partial B_0}{\partial t} = \frac{\partial E_z}{\partial r} - \frac{\partial E_r}{\partial z} \ , \tag{5-29}$$

$$\mu_0 \sigma E_r = - \frac{\partial B_0}{\partial z} \ , \tag{5-30}$$

$$\mu_0 \sigma E_z = \frac{1}{r} \frac{\partial}{\partial r} r B_0 \ . \tag{5-31}$$

In the last two equations the displacement current has been neglected, a good approximation in most soils except at the highest frequencies or very early times. Using Equation 5-30 in Equation 5-29 gives

$$\frac{\partial B_\theta}{\partial t} = \frac{\partial E_z}{\partial r} + \frac{1}{\mu_0 \sigma} \frac{\partial^2 B_\theta}{\partial z^2} . \tag{5-32}$$

Let the fields indicated here be those due to the current in the wire, not including the incident fields applied to the wire. Then B_θ and E_z vanish at sufficiently large r. Integrating Equation 5-32 over r from the radius a_2 of the wire to large r yields

$$\frac{\partial \phi}{\partial t} = - E_z(a_2) + \frac{1}{\mu_0 \sigma} \frac{\partial^2 \phi}{\partial z^2} , \tag{5-33}$$

where ϕ is the magnetic flux per unit length of wire. If the wire were perfectly conducting, then $E_z(a_2) = - E$ (the applied field); for resistive wire,

$$E_z(a_2) = - E + R_{w0} I . \tag{5-34}$$

The flux ϕ is estimated by assuming that B_0 is the field of the current I out to the skin depth δ,

$$\phi = \frac{\mu_0}{2\pi} I \int_{a_2}^{\delta} \frac{dr}{r} = \frac{\mu_0}{2\pi} \ell n \left(\frac{\delta}{a_2}\right) I \cong L I \tag{5-35}$$

When Equations 5-34 and 5-35 are used in Equation 5-33, the result is Equation 5-28. This derivation does not give the formula for δ, which comes only from the complete solution of the equations developed in previous sections. The complete solution also makes clearer the effects of approximations made.

5.5 TERMINATION CONDITIONS

In order to determine a solution of Equation 5-28 for a wire of finite length, an additional equation is needed at each end of the wire. This

equation can be obtained by integrating Equation 5-30 over r from a_2 to δ. The result is

$$\mu_0 \sigma V = - \frac{\partial \phi}{\partial z} = - \frac{\partial}{\partial z} [LI] , \tag{5-36}$$

where

$$V = \int_r^{\delta} E_r dr , \tag{5-37}$$

is the voltage between the end of the wire and distant ground associated with the current I in the wire; i.e., V does not include the incident electric field. Usually, V is related to I by a simple impedance, which at all but the earliest times is well approximated by a resistance. If the facility in Figure 5-1 is approximated as a conducting sphere of radius a_f, its resistance to distant ground is

$$R_f \approx 2 \int_{a_f}^{\delta} \frac{dr}{4\pi r^2 \sigma} \approx \frac{1}{2\pi a_f \sigma} . \quad (\delta >> a_f) \tag{5-38}$$

The factor 2 here comes from the fact that the facility is located near the surface of the semi-infinite soil medium. The resistance of the fireball to distant ground is that of a disc of radius a_{fb},

$$R_{fb} \approx \frac{1}{4 a_{fb} \sigma} . \quad (\delta >> a_{fb}) . \tag{5-39}$$

If the load resistance is designated by R_L (= R_f or R_{fb}), then the relation between V and I is

$$V = I R_L , \tag{5-40}$$

where I is the current flowing <u>out</u> of the wire into the soil. Combining this equation with Equation 5-36 yields the termination condition

$$\begin{aligned} \frac{\partial}{\partial z} [LI] &= - \mu_0 \sigma R_L I \\ &= - \frac{2\pi\sigma R_L}{\ell n(\frac{\delta}{a_2})} [LI] . \end{aligned} \tag{5-41}$$

5.6 METHOD OF SOLUTION OF THE EQUATIONS

The flux function has been defined (by Equation 5-35) as

$$\phi(z,t) = L(t)I(z,t) \ . \tag{5-42}$$

Here L is given by Equation 5-20, with $\delta(t)$ given by Equation 4-81 or Equation 5-17; the t in $\delta(t)$ is really the retarded time, or time after the arrival of the driving field at the position z. The difference between using real time or retarded time in the rest of the equations was shown in Section 5.3 to be negligible. We therefore think of t as retarded time in the remainder of this chapter.

In terms of ϕ, the differential Equation 5-28 and the end condition 5-41 are

$$\frac{\partial\phi}{\partial t} = E - \frac{R_{w0}}{L}\phi + \frac{1}{\mu_0\sigma}\frac{\partial^2\phi}{\partial z^2} \ , \tag{5-43}$$

$$\left.\begin{aligned} \frac{\partial\phi}{\partial z} &= -\zeta_r(t)\phi \qquad \text{at right-hand end} \ , \\ &= +\zeta_\ell(t)\phi \qquad \text{at left-hand end} \ . \end{aligned}\right\} \tag{5-44}$$

Here the factors ζ are defined by

$$\zeta(t) = \frac{2\pi\sigma R_L}{\ell n\left(\frac{\delta}{a_2}\right)} \ , \tag{5-45}$$

with the appropriate load resistance R_L at each end. The positive direction of E and I is to the right.

These equations can be solved quite readily by finite-difference methods. However, approximate solutions can also be found analytically, and these are useful for providing understanding and checks on the finite-difference results.

The first step in the analytical solution is to eliminate the term $R_{w0}\phi/l$ by defining

$$g_1(t) = \int_0^t \frac{R_{w0}}{L(t')} dt' \ , \tag{5-46}$$

and letting

$$\phi = e^{-g_1(t)} \phi_1 \ . \tag{5-47}$$

Then Equation 5-43 becomes

$$\frac{\partial \phi_1}{\partial t} = e^{g_1(t)} E + \frac{1}{\mu_0 \sigma} \frac{\partial^2 \phi_1}{\partial z^2} \ , \tag{5-48}$$

Equations 5-44 are left unchanged except that ϕ is replaced by ϕ_1.

A general method of solving Equation 5-48, subject to the end conditions is: first, find a particular solution of Equation 5-48 ignoring the end conditions; second, find solutions to the homogeneous equation obtained by setting $E = 0$, again ignoring the end conditions; third, choose a linear combination of the particular and homogeneous solutions which satisfies the end conditions.

If

$$E = \mathscr{E}(t) e^{-\beta z} \ , \tag{5-49}$$

then a particular solution of Equation 5-48 can be found by assuming

$$\phi_1(z,t) = \phi_2(t) e^{-\beta z} \ . \tag{5-50}$$

Substitution of this form leads to

$$\frac{d\phi_2}{dt} = e^{g_1(t)} \mathscr{E}(t) + \frac{\beta^2}{\mu_0 \sigma} \phi_2 \ . \tag{5-51}$$

Strictly speaking, this procedure is valid only if β is a constant. However, Equation 5-51 is approximately correct if β changes slowly with time, which we assume. Then if $g_2(t)$ is defined by

$$g_2(t) = \int_0^t \frac{\beta^2(t')}{\mu_0 \sigma} dt' , \tag{5-52}$$

the solution of Equation 5-51 is

$$\phi_2(t) = e^{g_2(t)} \int_0^t \exp[g_1(t') - g_2(t')] \mathscr{E}(t') dt' . \tag{5-53}$$

This completes the particular solution of Equation 5-48.

5.7 HOMOGENEOUS SOLUTIONS

In finding solutions of the homogeneous form of Equation 5-48, it is convenient to redefine the space variable as

$$y = \sqrt{\mu_0 \sigma} z , \tag{5-54}$$

Then the equation becomes simply

$$\frac{\partial \psi}{\partial t} = \frac{\partial^2 \psi}{\partial y^2} , \tag{5-55}$$

where we have designated the homogeneous solution by ψ in order to distinguish it from the particular solution ϕ_1. A very simple solution of Equation 5-55 is

$$\psi = e^{st} e^{\pm \sqrt{s}\, y} , \tag{5-56}$$

where s is an arbitrary positive constant. This would be a useful homogeneous solution to add to the particular solution ϕ_1 if ϕ_1 increased exponentially with time. Equation 5-53 indicates that ϕ_2 and ϕ_1 will increase approximately exponentially with time at late times.

At each end of the wire, we should choose that solution that decays with increasing distance into the wire. Thus at the ends of the wire for the solution going as e^{st}, we have the relation between ψ and $\partial\psi/\partial z$.

$$\left.\begin{aligned} \frac{\partial\psi}{\partial z} &= \sqrt{s\mu_0\sigma}\,\psi \quad \text{at right-hand end} , \\ &= -\sqrt{s\mu_0\sigma}\,\psi \quad \text{at left-hand end} . \end{aligned}\right\} \tag{5-57}$$

It will turn out that only the relation between ψ and $\partial\psi/\partial z$ at the end of the wire is needed to calculate the total current at the end of the wire, at those times before diffusion can occur over the entire length of the wire.

At early times, Equation 5-53 indicates that ϕ_2 will vary more like a power of the time than exponentially. Hence it would be useful to find homogeneous solutions ψ such that

$$\psi(t,y=0) = t^n , \tag{5-58}$$

where n is a positive constant. Such solutions are conveniently found by Laplace transform of the time variable in Equation 5-55. It is easily shown that the general solution, appropriate to the right-hand end of the wire, in the Laplace domain is

$$\psi(s,y) = f(s)e^{\sqrt{s}\,y} , \tag{5-59}$$

where $f(s)$ is an arbitrary function of the Laplace variable s. This function is fixed by Equation 5-58. At $y = 0$, $f(s)$ must be the Laplace transform of t^n,

$$f(s) = \int_0^\infty t^n e^{-st} dt = n!/s^{n+1} . \tag{5-60}$$

The Laplace transform of $\partial\psi/\partial y$ can be found by taking the derivative of Equation 5-59. At $y = 0$,

$$\left.\frac{\partial\psi(s,y)}{\partial y}\right)_{y=0} = \sqrt{s}\, f(s) = n!/s^{n+1/2} \quad . \tag{5-61}$$

Comparing Equations 5-60 and 5-61 makes it clear that in the time domain

$$\left.\frac{\partial\psi(t,y)}{\partial y}\right)_{y=0} = \frac{n!}{(n-\frac{1}{2})!}\, t^{n-1/2} \quad . \tag{5-62}$$

Thus the relation between ψ and $\partial\psi/\partial z$ at the right-hand end, for power law time dependence, is

$$\frac{\partial\psi}{\partial z} = \frac{n!}{(n-\frac{1}{2})!}\sqrt{\mu_0\sigma/t}\;\psi \quad . \tag{5-63}$$

At the left-hand end, a minus sign should be inserted in this equation. Figure 5-3 contains a graph of the ratio of factorials that occurs in Equation 5-63.

The time dependence of ϕ_2, Equation 5-53, will rarely be purely exponential or purely power law. However, the relation between ψ and $\partial\psi/\partial z$ is not very sensitive to the precise form of the time dependence. For example, the exponential function e^{st} is tangent to varying power laws at varying times. Since

$$e^{s(t+\delta t)} \approx e^{st}(1+s\delta t) \quad , \tag{5-64}$$

and

$$(t+\delta t)^n \approx t^n\left(1+\frac{n}{t}\,\delta t\right) \quad , \tag{5-65}$$

it is clear that at time t the exponential is tangent to a power law with

$$n = st \quad \text{or} \quad s = n/t \quad . \tag{5-66}$$

If in the end relation 5-57 for exponentials we make the replacement $s = n/t$, we obtain the approximate power law result

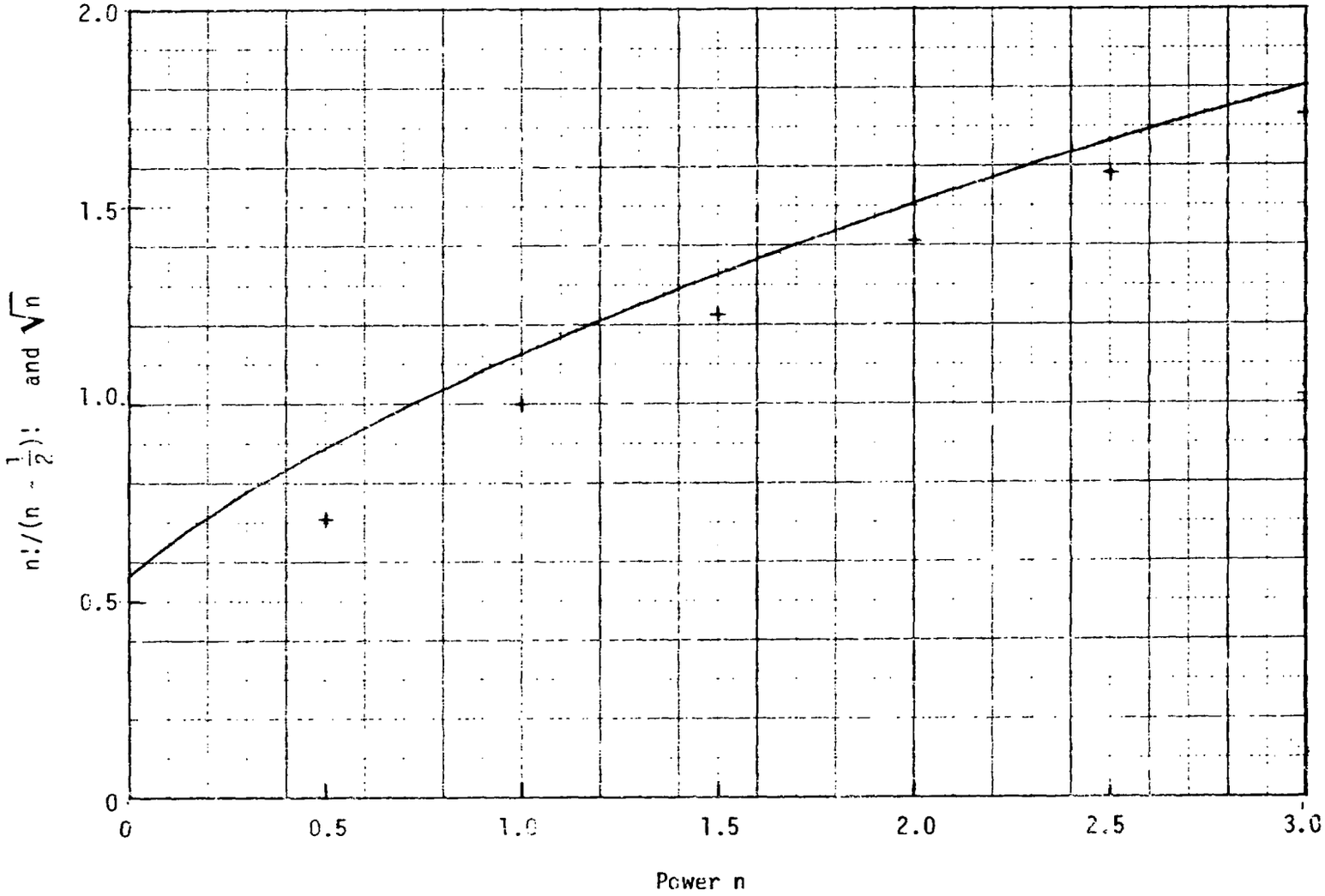

Figure 5-3. Factor occurring in Equation 5-63 for logarithmic derivative of homogeneous solution, solid curve. Power law approximation to exponential case, Equation 5-67, crosses.

$$\frac{\partial \psi}{\partial z} = \sqrt{n}\sqrt{\mu_0 \sigma / t}\ \psi \ . \qquad (5\text{-}67)$$

The crosses plotted in Figure 5-3 are $\sqrt{n}$, which is to be compared with the ratio of factorials of Equation 5-63. It is seen that treating the exponential case by power law fits at various times leads to only a small error.

We shall write the relation between ψ and $\partial\psi/\partial z$ as

$$\frac{1}{\psi}\frac{\partial \psi}{\partial z} = \pm \Lambda(t) \ , \qquad (5\text{-}68)$$

where the plus sign is for the right-hand end, the minus sign is for the left. The formulae for Λ are

$$\left.\begin{aligned} \Lambda &= \sqrt{s\mu_0\sigma} \quad \text{for} \quad \phi_2 \sim e^{st} \ , \\ &= \frac{n!}{(n-\frac{1}{2})!}\sqrt{\mu_0 \sigma / t} \quad \text{for} \quad \phi_2 \sim t^n \ . \end{aligned}\right\} \qquad (5\text{-}69)$$

Note that $1/\Lambda$ is approximately the distance diffused along the wire.

5.8 SOLUTION OF THE TERMINATION CONDITION FOR EARLY TIMES

At times sufficiently early that the diffusion distance $1/\Lambda$ is small compared with the length of the wire the contribution of ψ_ℓ, the homogeneous solution associated with the left-hand end, to the flux at the right-hand end is small and vice versa for ψ_r. The solution of the termination condition Equation 5-45 is then relatively simple. Having evaluated Equation 5-53 for the particular solution $\phi_2(t)$ at the right-hand end, we find the power $n(t)$ appropriate for each value of t. Let $\psi_r(t)$ be the value of the right-hand homogeneous solution, including an arbitrary constant multiplier which is absorbed into ψ_r. We then consider the total solution

$$\phi_T = \phi_2 + \psi_r \ . \tag{5-70}$$

The z-derivative of ϕ_T at the right-hand end is

$$\frac{\partial \phi_T}{\partial z} = \phi_2' + \psi_r' \ , \tag{5-71}$$

where, from Equation 5-50,

$$\phi_2' = - \beta \phi_2 \ , \tag{5-72}$$

and, from Equation 5-68,

$$\psi_r' = \Lambda \psi_r \ . \tag{5-73}$$

The termination condition 5-44 then becomes

$$- \beta \phi_2 + \Lambda \psi_r = - \zeta_r [\phi_2 + \psi_r] \ . \tag{5-74}$$

This equation can be solved for ψ_r, with the result

$$\psi_r = \left(\frac{\beta - \zeta_r}{\Lambda + \zeta_r} \right) \phi_2 \ . \tag{5-75}$$

The flux ϕ_T is then, from Equation 5-70,

$$\phi_T = \left(\frac{\Lambda + \beta}{\Lambda + \zeta_r} \right) \phi_2 \quad \text{(right-hand end)} \ , \tag{5-76}$$

and the current into the termination is

$$I = e^{-g_1(t)} \phi_T / L \ . \tag{5-77}$$

At the left-hand end, $\Lambda \rightarrow -\Lambda$ and $\zeta_r \rightarrow -\zeta_\ell$, so that

$$\phi_T = \left(\frac{\Lambda - \beta}{\Lambda + \zeta_\ell} \right) \phi_2 \quad \text{(left-hand end)} \ . \tag{5-78}$$

It would appear from Equation 5-78 that ϕ_T could change sign at times when Λ becomes less than β, or when the diffusion distance $1/\Lambda$

exceeds the decay length $1/\beta$ of the driving electric field. No change of sign occurs because Λ approaches β at these times. Equations 5-53 and 5-52 show that

$$\phi_2 \approx \exp\left(\frac{\beta^2}{\mu_0\sigma}\, t\right), \tag{5-79}$$

when $\beta^2 t/\mu_0\sigma >> 1$, or when the diffusion distance $\sqrt{t/\mu_0\sigma} >> 1/\beta$. Thus at these times ϕ_2 is approximately exponential in t with $s \approx \beta^2/\mu_0\sigma$, and from Equation 5-69,

$$\Lambda \approx \beta \ . \tag{5-80}$$

The factor $\Lambda-\beta$ in Equation 5-78 becomes small as ϕ_2 becomes large (exponentially), and the result for ϕ_T is not clear.

In order to resolve the uncertainty, it is necessary to examine Equation 5-78 more carefully in the Laplace domain, since ϕ_2 is not exactly exponential in time. In the Laplace domain, the equation

$$\phi_T(s) = \frac{\sqrt{\mu_0\sigma s - \beta}}{\sqrt{\mu_0\sigma s} + \zeta_\ell}\, \phi_2(s) \ , \tag{5-81}$$

is correct provided $\phi_2(s)$ is properly evaluated. This can be achieved from the Laplace transform of Equation 5-51, which is

$$s\phi_2 = F(s) + \frac{\beta^2}{\mu_0\sigma}\, \phi_2 \ , \tag{5-82}$$

where $F(s)$ is the Laplace transform of the function

$$F(t) \equiv e^{g_1(t)} \mathscr{E}(t) \ . \tag{5-83}$$

The solution of Equation 5-82 is

$$\phi_2(s) = \frac{\mu_0\sigma}{\mu_0\sigma s - \beta^2}\, F(s) \ , \tag{5-84}$$

and Equation 5-81 becomes

$$\phi_T(s) = \frac{\mu_0\sigma}{(\sqrt{\mu_0\sigma s} + \zeta_\ell)(\sqrt{\mu_0\sigma s} + \beta)} F(s) \quad . \tag{5-85}$$

Note that the factor $\sqrt{\mu_0\sigma s} - \beta$, which tended to zero in the previous analysis, has canceled out of the equation.

The inversion of Equation 5-85 to the time domain can be done approximately for those times at which the diffusion distance is larger than $1/\beta$, where Equation 5-78 is insufficient. At these times $\sqrt{\mu_0\sigma s}$ can be neglected compared with β. In practical cases ζ_ℓ is comparable to β or larger, so that $\sqrt{\mu_0\sigma s}$ can also be neglected compared with ζ_ℓ. Then

$$\phi_T(s) \approx \frac{\mu_0\sigma}{\zeta_\ell\beta} F(s) \quad ,$$

which leads immediately to

$$\phi_T(t) \approx \frac{\mu_0\sigma}{\zeta_\ell\beta} \mathscr{E}(t) e^{g_1(t)} \quad . \tag{5-86}$$

The current at the left-hand end is

$$I(t) = e^{-g_1(t)} \phi_T/L$$

$$\approx \mathscr{E}(t)/\beta R_L \quad , \tag{5-87}$$

where R_L is the load resistance at the left-hand end. According to Equation 5-49, $\mathscr{E}(t)/\beta$ is the integral of the electric field along the wire, or total voltage. Most of the voltage drop occurs near the left-hand end. The current is approximately equal to the voltage drop divided by the load resistance in the time frame assumed in this paragraph.

At the right-hand end, Equation 5-76 contains no such cancellations. This equation is correct until diffusion from the left-hand end can reach the right-hand end.

5.9 QUASISTATIC SOLUTION AT LATE TIMES

At late times the end effects generated at each end can diffuse to the other end, and this interaction of the end effects must be taken into account. To do this we return to the general equations for ϕ, Equations 5-43 and 5-44, and go to the limit in which diffusion is rapid compared with the time t. Since E varies more and more slowly as time increases, the term $\partial\phi/\partial t$ in Equation 5-43 becomes small compared with other terms, and can be neglected in first order. This procedure yields the static solution appropriate to the E and L at each time. We therefore need to solve the equation

$$\frac{\partial^2\phi}{\partial z^2} - \gamma^2\phi = -\mu_0\sigma E \ , \tag{5-88}$$

where the quantity γ is defined by

$$\gamma = \sqrt{\mu_0\sigma R_{w0}/L}$$

$$= \left(\frac{2\pi\sigma R_{w0}}{\ell n\left(\frac{\delta}{a_2}\right)}\right)^{1/2} \ . \tag{5-89}$$

We again use the form of Equation 5-19 for E, and choose the origin of the z coordinate to be at the left-hand end of the wire. Let d be the distance from the fireball edge to the facility, or length of wire exposed to the field E.

The general solution of Equation 5-88 is

$$\phi = \frac{\mu_0\sigma E}{\beta^2 - \gamma^2}\left[-e^{-\beta z} + C_1 e^{-\gamma z} + C_2 e^{+\gamma z}\right] \ , \tag{5-90}$$

where C_1 and C_2 are arbitrary constants which can be chosen to satisfy the end conditions, Equation 5-44. These end conditions are

$$\left.\begin{aligned} \beta - \gamma C_1 + \gamma C_2 &= \zeta_\ell [-1 + C_1 + C_2] \ , \\ \beta e^{-\beta d} - \gamma e^{-\gamma d} C_1 + \gamma e^{\gamma d} C_2 &= - \zeta_r [-e^{-\beta d} + C_1 e^{-\gamma d} + C_2 e^{\gamma d}] . \end{aligned}\right\} \quad (5\text{-}91)$$

These equations can be solved for C_1 and C_2, with the results

$$\left.\begin{aligned} C_1 &= [(\zeta_\ell+\beta)(\zeta_r+\gamma)e^{\gamma d} - (\zeta_\ell-\gamma)(\zeta_r-\beta)e^{-\beta d}]/D \ , \\ C_2 &= [(\zeta_\ell+\gamma)(\zeta_r-\beta)e^{-\beta d} - (\zeta_\ell+\beta)(\zeta_r-\gamma)e^{-\gamma d}]/D \ , \\ D &= (\gamma_\ell+\gamma)(\zeta_r+\gamma)e^{\gamma d} - (\zeta_\ell-\gamma)(\zeta_r-\gamma)e^{-\gamma d} \ . \end{aligned}\right\} \quad (5\text{-}92)$$

When C_1 and C_2 have been evaluated, the flux ϕ can be calculated from Equation 5-90, as a function of z. The fluxes ϕ_ℓ and ϕ_r at the left and right-hand ends can be evaluated directly, with the results

$$\phi_\ell = \frac{\Pi_0 \mathscr{E}}{\beta^2 - \gamma^2} [(\beta-\gamma)(\zeta_r+\gamma)e^{\gamma d} - (\beta+\gamma)(\zeta_r-\gamma)e^{-\gamma d} + 2\gamma(\zeta_r-\beta)e^{-\beta d}]/D \ , \quad (5\text{-}93)$$

$$\phi_r = \frac{\Pi_0 \mathscr{E} e^{-\beta d}}{\beta^2 - \gamma^2} [-(\beta+\gamma)(\zeta_\ell+\gamma)e^{\gamma d} + (\beta-\gamma)(\zeta_\ell-\gamma)e^{-\gamma d} + 2\gamma(\zeta_\ell+\beta)e^{\beta d}]/D \ . \quad (5\text{-}94)$$

Note that the brackets in these equations transform into each other when ζ_ℓ and ζ_r are interchanged and β is replaced by $-\beta$, as is required by symmetry.

The expressions derived above are fairly complicated and the results are not easy to visualize. However, considerable simplification occurs for a case that is of practical importance. This case is

$$\beta d \gg 1 \ , \ \gamma d \ll 1 \ , \ \gamma \ll \zeta_\ell \ , \ \zeta_r \ . \quad (5\text{-}95)$$

When these conditions hold, terms containing a factor $e^{-\beta d}$ can be dropped and the approximation

$$e^{\pm\gamma z} \approx 1 \pm \gamma z \ , \tag{5-96}$$

can be made. Then $\phi(z)$ can be shown to be

$$\phi(z) \approx \frac{\mu_0 \sigma \mathcal{E}}{\beta^2} \left[-e^{-\beta z} + \frac{(1+\beta x_\ell)(d+x_r-z)}{d + x_\ell + x_r} \right] , \tag{5-97}$$

where we have defined the "extrapolation lengths"

$$x_\ell = 1/\zeta_\ell \ , \ x_r = 1/\zeta_r \ . \tag{5-98}$$

The boundary conditions (5-44) are equivalent to the statement that if ϕ is extrapolated with constant slope to a distance $1/\zeta_r$ or $1/\zeta_\ell$ beyond the ends of the wire, the extrapolated ϕ must vanish. Equation 5-97 satisfies this extrapolation condition approximately. At $z = d + x_r$, ϕ vanishes in the approximation that $e^{-\beta d}$ is negligible. At $z = -x_\ell$, the extrapolated value of $e^{-\beta z}$ is $1 + \beta x_\ell$, so that the bracket vanishes exactly. A sketch of the geometrical relation of the exponential and linear terms in the bracket is shown in Figure 5-4, along with the shape of $\phi(z)$. The value of the current at the right-hand end is

$$I(d) = \frac{\phi(d)}{L} \approx \frac{2\pi\sigma\mathcal{E}}{\beta^2 \ell n(\frac{\delta}{a_2})} \frac{(1+\beta x_\ell) x_r}{d + x_\ell + x_r} = \frac{\mathcal{E}}{\beta R_L} \cdot \frac{1 + \beta x_\ell}{\beta(d+x_\ell+x_r)} \ , \tag{5-99}$$

where R_L is the termination resistance of the right-hand end. Note again that $\mathcal{E}/\beta$ is the total voltage applied along the wire.

5.10 APPLICATION OF FORMULAE TO EXAMPLE

The approximate theory developed above is applied in this section to the example defined in this chapter. The parameters of this example are, in summary:

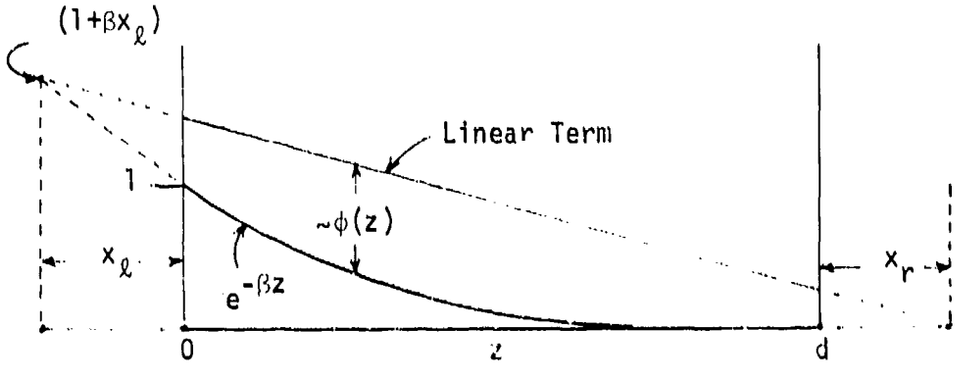

Figure 5-4. Sketch showing relation of exponential and linear terms in Equation 5-97, extrapolation lengths and flux $\phi(z)$.

$$\left.\begin{aligned}
&\text{wire resistance} = R_{w0} = 0.3 \text{ ohms/km};\\
&\text{ground conductivity} = \sigma = \sigma_0 = 10^{-3} \text{ mho/m};\\
&\text{ground permittivity} = \varepsilon_\omega = 10;\\
&\text{radius of wire} = a_2 = 0.01 \text{ m};\\
&\text{resistance, facility to distant ground} = R_f = 10 \text{ ohms};\\
&\text{distance from burst point to facility} = 1000 \text{ m};\\
&\text{driving electric field given by Figure 5-2}.
\end{aligned}\right\} \quad (5\text{-}100)$$

From these input parameters the derived parameters calculated at the indicated times are listed in the Table 5-101. In this table, β is calculated from the slope of the curves in Figure 5-2. The skin depth δ_1 comes from Equation 4-81, which takes into account approximately the frequency variation of σ and ε for typical soils. Equation 5-17 determines δ_2. The smaller of δ_1 and δ_2 is used in Equation 5-20 to determine the inductance L. The resistance R_{fb} between the fireball and distant ground comes from Equation 5-39, with the fireball radius a_{fb} read off Figure 5-2. The logarithmic derivatives ζ_ℓ and ζ_r come from Equation 5-45, and the extrapolation lengths x_ℓ and x_r come from Equation 5-98.

t, sec	10^{-6}	10^{-5}	10^{-4}	10^{-3}	10^{-2}
$10^3\ \beta$, m^{-1}	0.7	1.2	3.4	5.4	7.9
δ_1, m	24.3	91.3	307	990	5150
δ_2, m	1600	933	329	207	142
$\ell n(\frac{\delta_1}{\delta_2})$	7.80	9.12	10.33	9.94	9.56
L, μH/m	1.56	1.82	2.07	1.99	1.91
R_{fb}, ohms	20	10	6.3	2.5	1.0
$10^3\ \sigma_\ell$, m^{-1}	16.1	6.9	3.83	1.58	0.66
$10^3\ \sigma_r$, m^{-1}	8.1	6.9	6.1	6.3	6.6
x_ℓ, m	92	145	261	653	1520
x_r, m	124	145	164	138	152

(5-101)

The next step is to calculate the exponential arguments $g_1(t)$ and $g_2(t)$, defined by Equations 5-46 and 5-52. It is clear from Equations 5-47, 5-48 and 5-53 that these arguments need to be calculated accurately only when they are not small compared with unity. If we take $L = 2.0 \times 10^{-6}$ H/m, a value appropriate to the period 10^{-4} to 10^{-2} second, Equation 5-46 gives

$$g_1(t) \approx 150\ t\ , \qquad \approx 0.15 \text{ at } t = 10^{-3},\ 1.5 \text{ at } t = 10^{-2} \text{ sec}\ . \tag{5-102}$$

Equation 5-102 is therefore an adequate approximation up to 10^{-2} sec. From Equation 5-52 it can be seen that $g_2(t)$ reaches the value unity approximately when

$$\frac{\beta^2 t}{\mu_0 \sigma} \approx 1 \quad \text{or} \quad t \approx \mu_0\sigma/\beta^2 = 1.25 \times 10^{-9}/\beta^2\ . \tag{5-103}$$

With β read from the Table 5-101, trial and error leads to $t \approx 10^{-4}$ second as the time when g_2 nears unity. A simple formula representing β^2 within 20 percent in the time interval from 4×10^{-5} to 10^{-3} second is

$$\beta^2 \approx 10^3 \sqrt{t} ,$$

from which the result follows,

$$g_2(t) \approx 0.53 \left(\frac{t}{10^{-4}}\right)^{3/2} . \qquad (5\text{-}104)$$

In order to calculate the early-time current at the right-hand end of the wire, $\phi_2(t)$ must next be evaluated from Equation 5-53. The ϕ in that equation is to be read from Figure 5-2 at 1 kilometer from the burst point. The points read off are graphed in Figure 5-5 and a smooth curve is drawn through them. This curve is then multiplied by $\exp(g_1-g_2)$, and the result is graphed, and integrated numerically, yielding the integral curve shown. Finally this curve is multiplied by $\exp(g_2)$ to yield $\phi_2(t)$. All of these operations can be done graphically and with the aid of a pocket calculator in a half hour or so.

The next step is to apply the end condition, Equation 5-76, to obtain ϕ_1. To determine the logarithmic derivative A we use the power law approximation in Equation 5-69. From the slope of ϕ_2 in Figure 5-5, the values of the power n are determined; A is then calculated from Figure 5-3 and Equation 5-69. Next, the factor $(A+B)/(A+G_1)$ is evaluated and ϕ_1 is determined from Equation 5-76. Finally, the current I is calculated from Equation 5-77. The numbers obtained in these operations are:

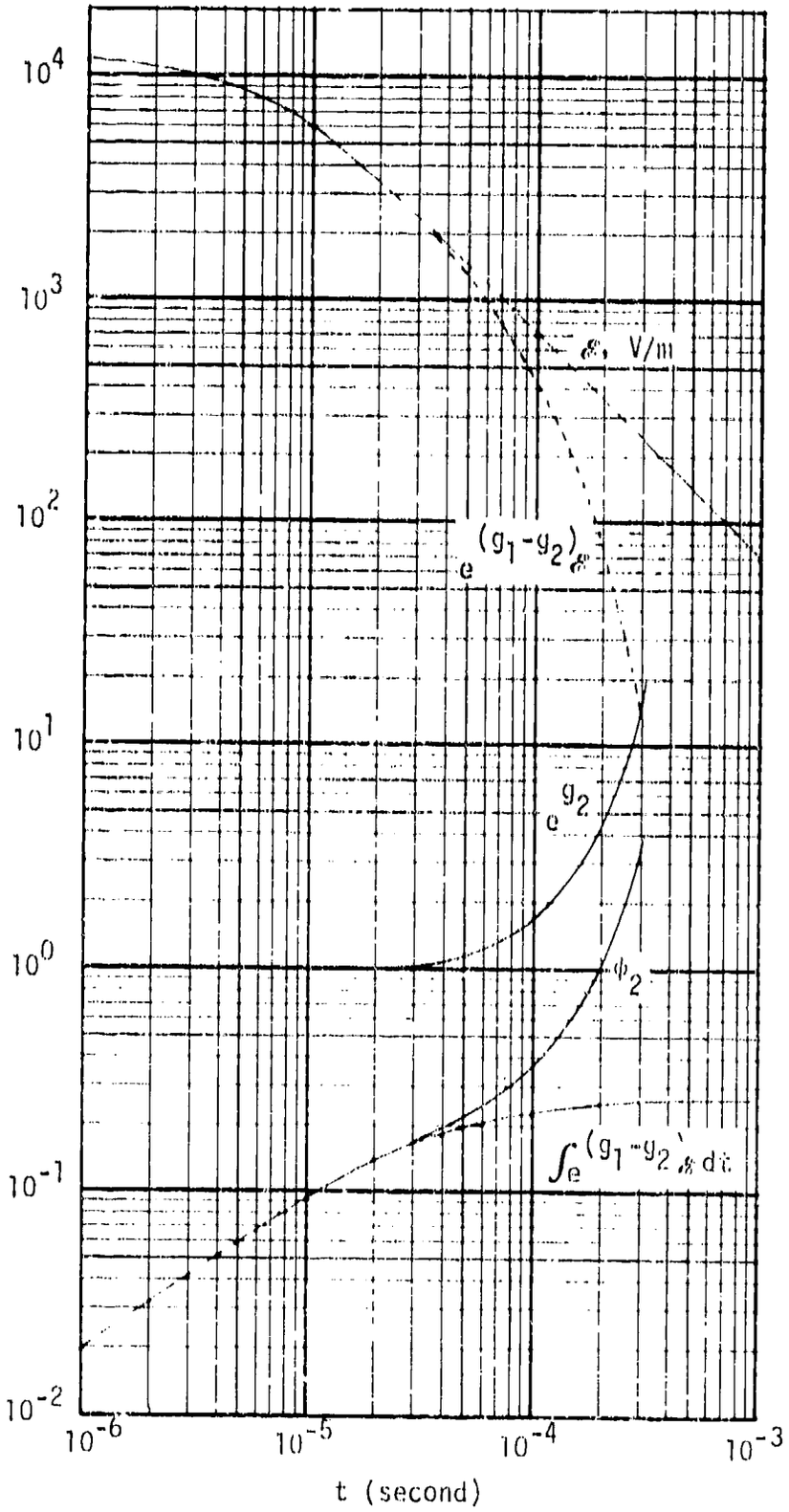

Figure 5-5. Quantities in the early time solution.

t, sec	10^{-6}	10^{-5}	10^{-4}	3×10^{-4}
n	0.65	0.65	1.0	3.0
n!/(n-1/2)!	0.96	0.96	1.12	1.8
Λ, m^{-1}	0.034	0.0107	0.0040	0.0037
$(\Lambda+\beta)/(\Lambda+\zeta_T)$	0.82	0.68	0.73	0.81
ϕ_T, V · sec/m	0.016	0.062	0.27	3.04
I, Amps	1.02×10^4	3.4×10^4	1.30×10^5	1.43×10^6

(5-105)

The early-time current computed here is graphed in Figure 5-6. It begins to rise exponentially, due to diffusion along the wire, at about 10^{-4} second, as expected.

The late-time, or quasistatic approximation for the current is given by Equation 5-99. In that equation, $\mathcal{E}$ is the electric field at the fireball end of the wire, and d is the distance from the fireball edge to the facility, which is read from Figure 5-2. All of the other parameters in Equation 5-99 have been calculated above. The numbers are:

t, sec	10^{-4}	10^{-3}	10^{-2}
$\mathcal{E}$, V/m	1.7×10^4	8.8×10^3	6.5×10^2
d, m	960	900	745
I, Amps	1.97×10^5	7.9×10^4	5.6×10^3

(5-106)

This quasistatic current is also graphed in Figure 5-6, where it is seen that the quasistatic current is less than the early-time (inductively limited) current after $t = 1.3 \times 10^{-4}$ seconds, at about the same time that the early-time current becomes exponential. This result may seem surprising. The time to go into the exponential phase is the time to diffuse a distance $1/\beta = 300$ meters (at 10^{-4} second), and this time is

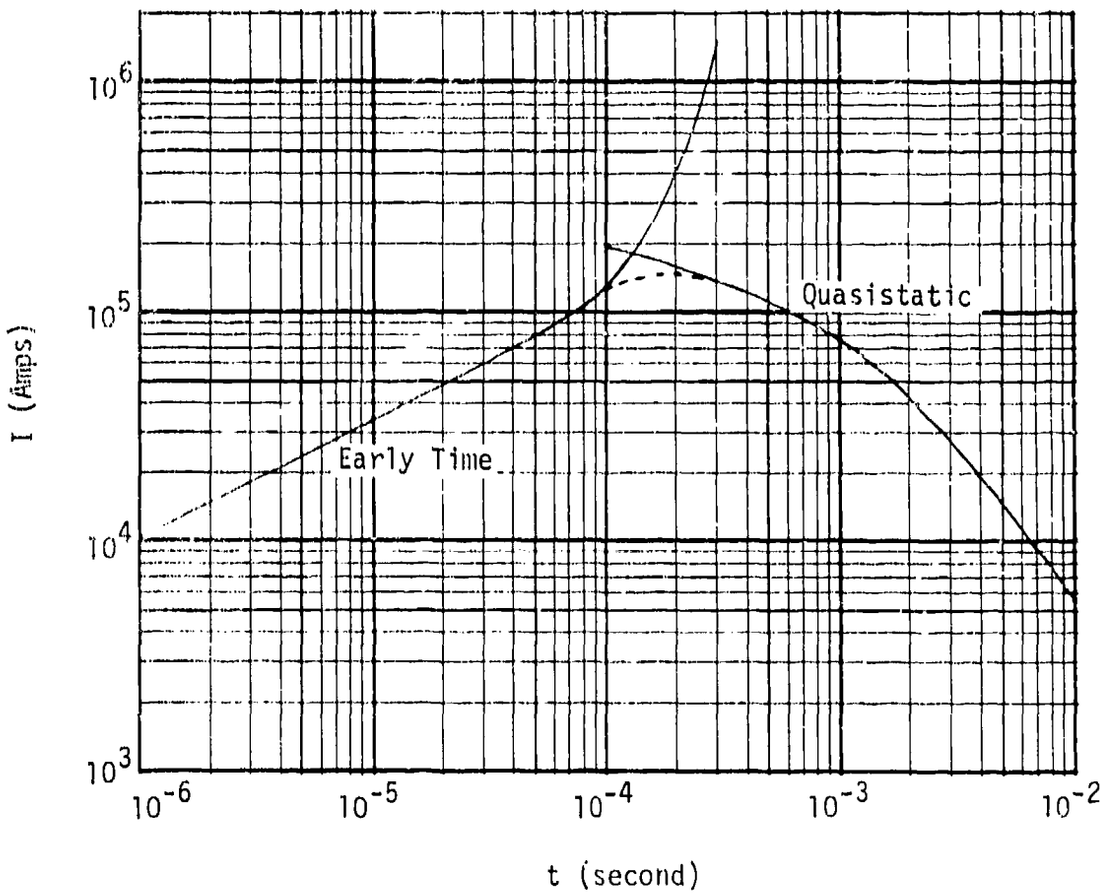

Figure 5-6. Current into the facility.

$$t \approx \mu_0 \sigma / \beta^2 \approx 10^{-4} \text{ second} . \tag{5-107}$$

The time to diffuse a distance d is

$$t \approx \mu_0 \sigma d^2 \approx 10^{-3} \text{ second} , \tag{5-108}$$

so that one might have expected the quasistatic phase to start only at 10^{-3} second. However, because the driving field is much larger at the left-hand end, only a small part of the left-hand end effect needs to diffuse to the right-hand end to make a noticeable effect there.

The actual current is estimated by joining the early-time and quasistatic currents smoothly, as indicated by the dashed curve in Figure 5-6. Note, however, that in the decade between 10^{-4} and 10^{-3} second, where the peak current occurs, the quasistatic approximation has not been shown to be reliable. A better treatment of the diffusion of the left-hand end effect is needed. Such a treatment could be devised.

Note that the energy delivered into the assumed 10-ohm load at the facility is of the order of 10^8 Joules. This explains the extensive electrical damage that occurred in bunkers that had long wires going into them in the early days of nuclear testing.

CHAPTER 6
COUPLING TO OVERHEAD LINES

6.1 INTRODUCTION

Ground-based systems often employ overhead lines for power instead of buried lines as they are substantially cheaper to build than buried lines. These lines are not intended to operate after an attack, as they are relatively easily damaged by air blast. However, their presence can result in large EMP signals which are generated along their length and transmitted to equipment which does have a post-attack survivability requirement. Overhead power lines often consist of a set of several wires carrying power and a neutral wire elevated above the rest which is periodically grounded for protection against lightning—for simplicity in this section we will discuss coupling to a single line located at a height of 10 meters above the ground.

Two features complicate the theory of coupling to overhead lines compared to buried lines.

1. The conductivity of the medium surrounding the wire varies as a function of both time and distance from the burst.

2. The boundaries of the wire and the ground-air interface do not fit as coordinate surfaces in a system where the Helmholtz equation

$$(\nabla^2+k^2)\phi = 0 \ , \qquad (6\text{-}1)$$

is separable. The Laplace equation in the two transverse

dimensions (where the z axis is parallel to the wire)

$$\left(\frac{\partial^2}{\partial x^2} + \frac{\partial^2}{\partial y^2}\right)\phi = 0 \ , \qquad (6\text{-}2)$$

is separable in bipolar coordinates and we will exploit this feature in deriving transmission line equations suitable for late-time calculations.

The discussion of current on the overhead line system breaks naturally into two physical regimes—the first of these encompasses early times when the skin depth in the air is less than the height of the wire over the ground. In this regime we can calculate the electromagnetic fields about the wire in cylindrical coordinates centered on the wire axis and ignore the effects of the ground. This regime is further subdivided into two phases depending on whether the displacement current is greater than the conduction current in the air or vice-versa. In analogy to the discussion of surface-burst EMP, we will call the first of these the wave phase and the second the early diffusion phase. In the second regime, which we will call the late-diffusion phase, the skin depth in the air is larger than the height of the line and it is possible to derive a set of transmission line equations for the current on the overhead line. These three phases will be treated in separate sections of this chapter.

6.2 WAVE PHASE

In this section we derive the current on the overhead wire at early times when the displacement current is much greater than the conduction current in the air. Neglecting the field dependence of the air conductivity, we can separate the electromagnetic fields into incident and scattered parts. For example the electric field parallel to the wire, oriented for convenience along the z axis, is

$$E_z^{total} = E_z^{inc} + E_z^{scattered} \quad . \tag{6-3}$$

The incident field is calculated without including the presence of the wire (but including the effect of the air-ground interface). The scattered field obeys homogenous Maxwell's equations (without the Compton current). The effect of the wire is incorporated by setting the sum of the scattered and incident electric fields (the total field) equal to zero at the surface of the wire. We will only be concerned with the response of the wire to that portion of the incident electric field parallel to the wire axis; the portion which lies in the plane perpendicular to the wire axis results in a polarization of the wire across its width which is inconsequential for system survivability. We will also ignore the variation in the parallel component of the incident electric field across the wire as the width of the wire is much smaller than the spatial variation of this field. In the wave phase, where

$$\frac{\alpha}{c} >> Z_0\sigma \quad , \tag{6-4}$$

Equations 1-17 and 1-18 for the scattered field around the wire are

$$\frac{\partial \vec{B}}{\partial t} = - \nabla \times \vec{E} \quad , \tag{6-5}$$

$$\frac{1}{c}\frac{\partial \vec{E}}{\partial t} = c\nabla \times \vec{B} \quad . \tag{6-6}$$

The component of the incident electric field parallel to the wire at a height 10 meters above the ground varies at early times as

$$E_z^{inc} = \cos\chi E_0(z) e^{\alpha(t-z\cos\chi/c)} \quad , \tag{6-7}$$

where χ is the angle between the radial from the burst and the cable, as shown in Figure 4-1. $E_0(z)$ varies slowly as a function of distance along the line--the variation results from attenuation of gammas and the $1/r^2$ decrease from a point source. If we assume that the scattered fields have the same variation in z and t and ignore the slow variation of E_0 in

z, Maxwell's equations become

$$\alpha B_\theta = \frac{\alpha\cos\chi}{c} E_r + \frac{\partial E_z}{\partial r} , \tag{6-8}$$

$$\frac{\alpha}{c} E_r = \alpha\cos\chi B_\theta , \tag{6-9}$$

$$\frac{\alpha}{c} E_z = \frac{c}{r}\frac{\partial}{\partial r} r B_\theta . \tag{6-10}$$

Eliminating E_r and B_θ we arrive at the following equation for E_z

$$\frac{\alpha^2\sin^2\chi}{c^2} E_z = \frac{1}{r}\frac{\partial}{\partial r} r \frac{\partial E_z}{\partial r} , \tag{6-11}$$

for which the solution vanishing at large r is

$$E_z \sim K_0\left(\frac{r\alpha\sin\chi}{c}\right) , \tag{6-12}$$

where K_0 is a modified (hyperbolic) Bessel function of the second kind. Since $E_z = - E_z^{inc}$ at $r = a$

$$E_z = - E_z^{inc} \frac{K_0(r\alpha\sin\chi/c)}{K_0(a\alpha\sin\chi/c)} . \tag{6-13}$$

As K_0 behaves for large argument as

$$K_0(\xi) \to \sqrt{\frac{\pi}{2\xi}}\, e^{-\xi} , \tag{6-14}$$

we associate the distance

$$\delta = \frac{c}{\alpha\sin\chi} , \tag{6-15}$$

with a skin depth about the wire. The magnetic field can be obtained from

$$\alpha\sin^2\chi B_\theta = + \frac{\partial E_z}{\partial r}$$

$$= + \frac{\alpha}{c}\sin\chi E_z^{inc} \frac{K_1(r\alpha\sin\chi/c)}{K_0(a\alpha\sin\chi/c)} , \tag{6-16}$$

The current on the wire is given by

$$I = \frac{2\pi a}{\mu_0} B_\theta(a) \ . \tag{6-17}$$

For the usual case where

$$a << \delta \ , \tag{6-18}$$

we can use the small argument limits of the Bessel functions

$$K_0(\xi) \to - \ln \frac{\gamma\xi}{2} \ , \ \gamma = 1.781 \ , \tag{6-19}$$

$$K_1(\xi) \to \frac{1}{\xi} \ , \tag{6-20}$$

so

$$I = \frac{2\pi}{\mu_0 \alpha} \frac{1}{\sin^2\chi} \frac{E_z^{inc}}{\ln\left(\frac{2c}{\gamma a \alpha \sin\chi}\right)} \ . \tag{6-21}$$

This equation is similar to the equation governing the rise in current in an inductor where

$$L \frac{\partial I}{\partial t} = E_z^{inc} \ , \tag{6-22}$$

with

$$L = \frac{\mu_0}{2\pi} \sin^2\chi \ln\left(\frac{2c}{\gamma a \alpha \sin\chi}\right) \ . \tag{6-23}$$

The only unusual term in the equation for the inductance is the $\sin^2\chi$ which is do to the buildup of propagating waves near the wire.

We now return to the examination of our assumption that the electromagnetic fields near the wire have the same spatial and temporal variation as the local incident electric field. This assumption will be invalid when χ is sufficiently small that the variation of $E_0(z)$ becomes

important and currents at a given position are strongly influenced by the stronger electric fields nearer the source. Consider the geometry of Figure 6-1. The time difference of arrival between currents generated at the observer location 0 and currents generated at C and propagating to 0 is

$$\Delta t = \frac{\Delta z}{c} (1-\cos\chi) \ , \tag{6-24}$$

so that when the conductivity is small and there is little attenuation of propagating fields near the wire, we can ignore the variation of E_0 in z as long as

$$\frac{\alpha}{c} (1-\cos\chi) >> \frac{1}{E_0} \frac{\partial E_0}{\partial z} \ , \tag{6-25}$$

everywhere along the line. When the burst is sufficiently close to the line that either this condition or the condition that the skin depth is smaller than the height of the line

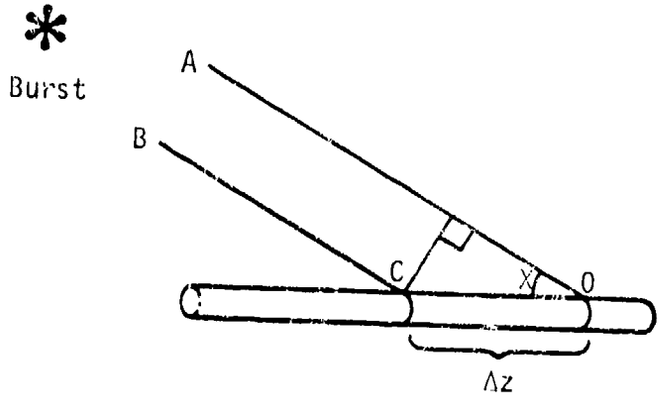

Figure 6-1. Geometry used in calculation of limits of validity of Equation 6-21.

$$\frac{c}{\alpha \sin\chi} \lesssim h \ , \tag{6-26}$$

is violated, the situation becomes substantially more complicated. The case of a short wire high above the ground with the burst located on the wire axis is calculated in Reference 6-1; for a long wire with the burst near the wire axis, the presence of the finite ground conductivity becomes important and this case has not been calculated.

6.3 EARLY DIFFUSION PHASE

At most locations close to the burst, the rising conductivity will cause the conduction current to rise above the displacement current. In this section, we will calculate the wire current when

$$Z_0 \sigma >> \frac{\alpha}{c} \ , \tag{6-27}$$

following the derivation of Reference 6-2. The current on the wire generated during this phase should simply be added to the current on the wire at the end of the wave phase as long as the skin depth is smaller than the wave phase skin depth (Equation 6-15). Ignoring the displacement current, and assuming that the fields vary only as a function of retarded time from the burst

$$t' = t - z\cos\chi/c \ . \tag{6-28}$$

Maxwell's equations become

$$\frac{\partial}{\partial t'} B_0 = \frac{\cos\chi}{c} \frac{\partial E_r}{\partial t'} + \frac{\partial E_z}{\partial r} \ , \tag{6-29}$$

$$Z_0 \sigma E_r = \cos\chi \frac{\partial B_0}{\partial t'} \ , \tag{6-30}$$

$$Z_0 \sigma E_z = \frac{c}{r} \frac{\partial}{\partial r} r B_\theta \ , \tag{6-31}$$

which can be combined into a single equation for B_θ

$$\frac{\partial}{\partial t'}\left(B_\theta - \frac{\cos^2\chi}{Z_0 c}\frac{\partial B_0}{\partial t'}\right) = \frac{c}{Z_0\sigma}\frac{\partial}{\partial r}\frac{1}{r}\frac{\partial}{\partial r}rB_\theta \ . \tag{6-32}$$

Dropping the second term in parenthesis on the left-hand side of (6-32) by virtue of (6-27), using the fact that $c/Z_0 = 1/\mu_0$ and expanding the right-hand side we obtain

$$\frac{\partial^2 B_0}{\partial r^2} + \frac{1}{r}\frac{\partial B_0}{\partial r} - \frac{B_0}{r^2} = \mu_0\sigma\frac{\partial B_0}{\partial t'} \ . \tag{6-33}$$

Changing to the scaled variables

$$R = r/a \ , \tag{6-34}$$

$$\tau = \frac{1}{\mu_0 a^2}\int_{t_0'}^{t'}\frac{dt''}{\sigma(t'')} \ , \tag{6-35}$$

where t_0' is the time at the end of the wave phase, we have

$$\frac{\partial^2 B_0}{\partial R^2} + \frac{1}{R}\frac{\partial B_0}{\partial R} - \frac{B_0}{R^2} = \frac{\partial B_0}{\partial \tau} \ , \tag{6-36}$$

subject to the boundary conditions.

$$\frac{\partial}{\partial R}(RB_0)\Big|_{R=1} = F(\tau) = -\mu_0 a\sigma(t')E_{inc}(t') \ , \tag{6-37}$$

$$\lim_{R\to\infty} B_0 = 0 \ . \tag{6-38}$$

We first determine the Green's function $G(R,\tau-\tau')$ which is the magnetic field resulting from an impulse in F at $\tau = \tau'$. Since Equation 6-36 possesses translational invariance in τ, we exploit this fact by writing G as a Fourier transform.

$$G(R,\tau) = \int_{-\infty}^{\infty} G(R,\omega) e^{i\omega\tau} d\omega \ , \tag{6-39}$$

and the impulse function can be written

$$\delta(\tau) = \frac{1}{2\pi} \int_{-\infty}^{\infty} e^{i\omega\tau} d\omega \ . \tag{6-40}$$

The equation for $G(R,\omega)$ is

$$\frac{\partial^2 G}{\partial R^2} + \frac{1}{R} \frac{\partial G}{\partial R} - \left(\frac{1}{R^2} + i\omega \right) G = 0 \ , \tag{6-41}$$

which has the solution

$$G(R,\omega) = G_1(\omega) I_1(\sqrt{i\omega} R) + G_2(\omega) K_1(\sqrt{i\omega} R) \ , \tag{6-42}$$

where I_1 and K_1 are modified Bessel functions of the first and second kinds. In the Fourier domain, the boundary conditions on G imply

$$G_1(\omega) I_0(\sqrt{i\omega}) - G_2(\omega) K_0(\sqrt{i\omega}) = - \frac{1}{2\pi\sqrt{i\omega}} \ , \tag{6-43}$$

$$\lim_{R \to \infty} G_1(\omega) I_1(\sqrt{i\omega} R) + G_2(\omega) K_1(\sqrt{i\omega} R) = 0 \ , \tag{6-44}$$

The asymptotic limits of the Bessel functions for large arguments are

$$I_1(z) \sim \frac{e^z}{\sqrt{2\pi z}} \qquad |\arg z| < \frac{\pi}{2} \ , \tag{6-45}$$

$$K_1(z) \sim \sqrt{\frac{\pi}{2z}}\, e^{-z} \qquad |\arg z| < \frac{3\pi}{2} \ , \tag{6-46}$$

so if we choose the argument of $\sqrt{i\omega}$ so that

$$\arg(\sqrt{i\omega}) = - \frac{\pi}{4} \qquad \omega < 0 \ , \tag{6-47}$$

$$\arg(\sqrt{i\omega}) = + \frac{\pi}{4} \qquad \omega > 0 \ , \tag{6-48}$$

(which will keep the integrand on the same sheet when we transform back to τ) G_1 must vanish and

$$G_2(\omega) = \frac{1}{2\pi \sqrt{i\omega}\, K_0(\sqrt{i\omega})} . \tag{6-49}$$

Transforming back to the τ domain

$$G(R,\tau) = \frac{1}{2\pi}\int_{-\infty}^{\infty} \frac{d\omega}{\sqrt{i\omega}}\, e^{i\omega\tau}\, \frac{K_1(\sqrt{i\omega}\, R)}{K_0(\sqrt{i\omega})} , \tag{6-50}$$

The integration can be transformed into one over positive real values by deforming the contour in the complex ω plane as shown in Figure 6-2. The integrand has no singularities except a branch point at the origin from which we may run the branch cut along the $+ i\omega$ axis. As the integrand vanishes exponentially for $\tau > 0$, $R > 1$ at large positive imaginary ω, we may ignore the contribution from the axis C_2 and C_6. Near the origin, the integrand behaves as

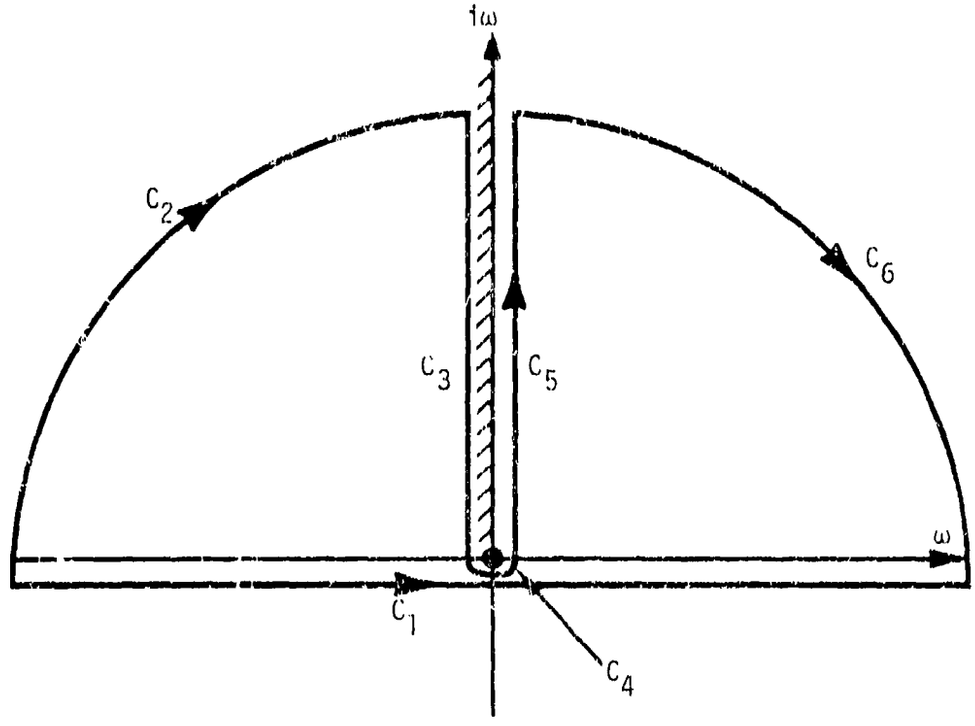

Figure G-2. Integration path for Green's function.

$$I \sim \frac{e^{i\omega\tau}}{i\omega R} \frac{1}{\ell n\,(\gamma\sqrt{i\omega})}\,, \tag{6-51}$$

so that we may ignore the contribution from C_4, and the Green's function is now

$$G(R,\tau) = \frac{1}{2\pi}\int_{C_3+C_5} \frac{d\omega}{\sqrt{i\omega}}\, e^{i\omega\tau}\, \frac{K_1(\sqrt{i\omega}\,R)}{K_0(\sqrt{i\omega})}\,, \tag{6-52}$$

setting $\omega = \rho e^{i0}$ this can be written

$$G(R,\tau) = \frac{-1}{2\pi}\int_0^\infty \frac{d\rho}{\sqrt{\rho}}\, e^{-\tau\rho}\left[\frac{K_1(i\sqrt{\rho}\,R)}{K_0(i\sqrt{\rho})} + \frac{K_1(-i\sqrt{\rho}\,R)}{K_0(-i\sqrt{\rho})}\right]. \tag{6-53}$$

Expressing the modified Bessel functions in terms of Hankel functions of real arguments, this is equal to

$$G(R,\tau) = \frac{i}{2\pi}\int_0^\infty \frac{d\rho}{\sqrt{\rho}}\, e^{-\tau\rho}\left[\frac{H_1^{(1)}(\sqrt{\rho}\,R)}{H_0^{(1)}(\sqrt{\rho})} - \frac{H_1^{(2)}(\sqrt{\rho}\,R)}{H_0^{(2)}(\sqrt{\rho})}\right]. \tag{6-54}$$

Further simplification is possible if we look at $R = 1$ which will give us the magnetic field at the surface of the wire. Using the Wronskian

$$H_1^{(1)}(z)H_0^{(2)}(z) - H_0^{(1)}(z)H_1^{(2)}(z) = -\frac{4i}{\pi z}\,, \tag{6-55}$$

we obtain

$$G(1,\tau) = \frac{2}{\pi^2}\int_0^\infty \frac{d\rho}{\rho}\, \frac{e^{-\tau\rho}}{H_0^{(1)}(\sqrt{\rho})H_0^{(2)}(\sqrt{\rho})}\,. \tag{6-56}$$

Setting $x = \sqrt{\rho}$ and expressing the Hankel functions in terms of ordinary Bessel functions

$$G(1,\tau) = \frac{4}{\pi^2}\int_0^\infty \frac{dx}{x}\, \frac{e^{-\tau x^2}}{J_0^2(x) + Y_0^2(x)}\,, \tag{6-57}$$

which is suitable for machine computation. It is found that a fit to G(1,R) which is accurate to within 2 percent for all τ is

$$G(1,\tau) = 0.425 + \sqrt{\frac{1}{\pi\tau}} \qquad \tau < 1.3 ,$$

$$G(1,\tau) = \frac{\ell n\tau + 5.16}{\ell n^2\tau + 5.64\ell n\tau + 10.23} \qquad \tau > 1.3, \tag{6-58}$$

The magnetic field is, in terms of G,

$$B_0(R,\tau) = \int_{\tau_0}^{\tau} G(R,\tau-\tau')F(\tau')d\tau' , \tag{6-59}$$

so that the current on the wire, obtained from

$$I = \frac{2\pi a}{\mu_0} B_0(a,t') , \tag{6-60}$$

is given by

$$I = 2\pi a^2 \int_{\tau_0}^{\tau} G(1,\tau-\tau') \ (\tau')E_{inc}(\tau')d\tau' . \tag{6-61}$$

We have made a comparison between this accurate calculation and two simplified time-dependent inductance models where we merely set

$$L(t) \frac{\partial I(t)}{\partial t} = E_{inc}(t) , \tag{6-62}$$

for the first model and

$$\frac{\partial}{\partial t} L(t)I(t) = E_{inc}(t) , \tag{6-63}$$

as the second model. The second model is analogous to that used in Chapter 4 (Equation 4-80) and Chapter 5 (Equation 5-33) in that, in the absence of E_{inc}, the current on the wire falls as the magnetic flux ϕ diffuses radially away from the wire. (This effect is absent in the first model.) The simple, approximate forms of the air conductivity and the incident electric field used in the comparison are

$$a = 1 \text{ cm} ,$$

$$E_{inc} = 1.57 \times 10^5 \frac{e^{\alpha t}}{1 + e^{\beta t}} \qquad \text{v/m}$$

$$\sigma = 1.57 \frac{e^{\alpha t}}{1 + e^{\beta t}} \qquad \text{mho/m}$$

where

$$\alpha = 2 \times 10^8 \text{ sec}^{-1} ,$$

$$\beta = 2.4 \times 10^8 \text{ sec}^{-1} ,$$

so that the peak electric field is 10^5 volts/m and the peak conductivity is 1 mho/m. The inductance used in the comparison is

$$L = \frac{\mu_0}{2\pi} \ell n \left(\sqrt{\frac{1}{\mu_0 \sigma(t) \alpha}} / a \right) \qquad t < t_{pk} , \tag{6-64}$$

$$L = \frac{\mu_0}{4\pi} \ell n \left(\int_{t_{pk}}^{t} \frac{dt}{\mu_0 \sigma(t) a^2} + \frac{1}{\mu_0 \sigma(t_{pk}) \alpha a^2} \right) \qquad t > t_{pk} , \tag{6-65}$$

where t_{pk} is the time at which the conductivity peaks. The term inside the logarithm for $t < t_{pk}$ is the ratio of the skin depth in the air to the wire radius for an exponentially rising conductivity. Inside the logarithm for $t > t_{pk}$ is the square of the ratio of the skin depth to the wire radius as defined by the substitution (6-35) which gave rise to the dimensionless τ in the Green's function. The second term in this logarithm ensures continuity of L at t_{pk}. The comparison shown in Figure 6-3 emphasizes the importance of including the reduction in the current due to the diffusion of magnetic flux away from the wire. (We have terminated the curves in Figure 6-3 when the skin depth equals 10 meters.)

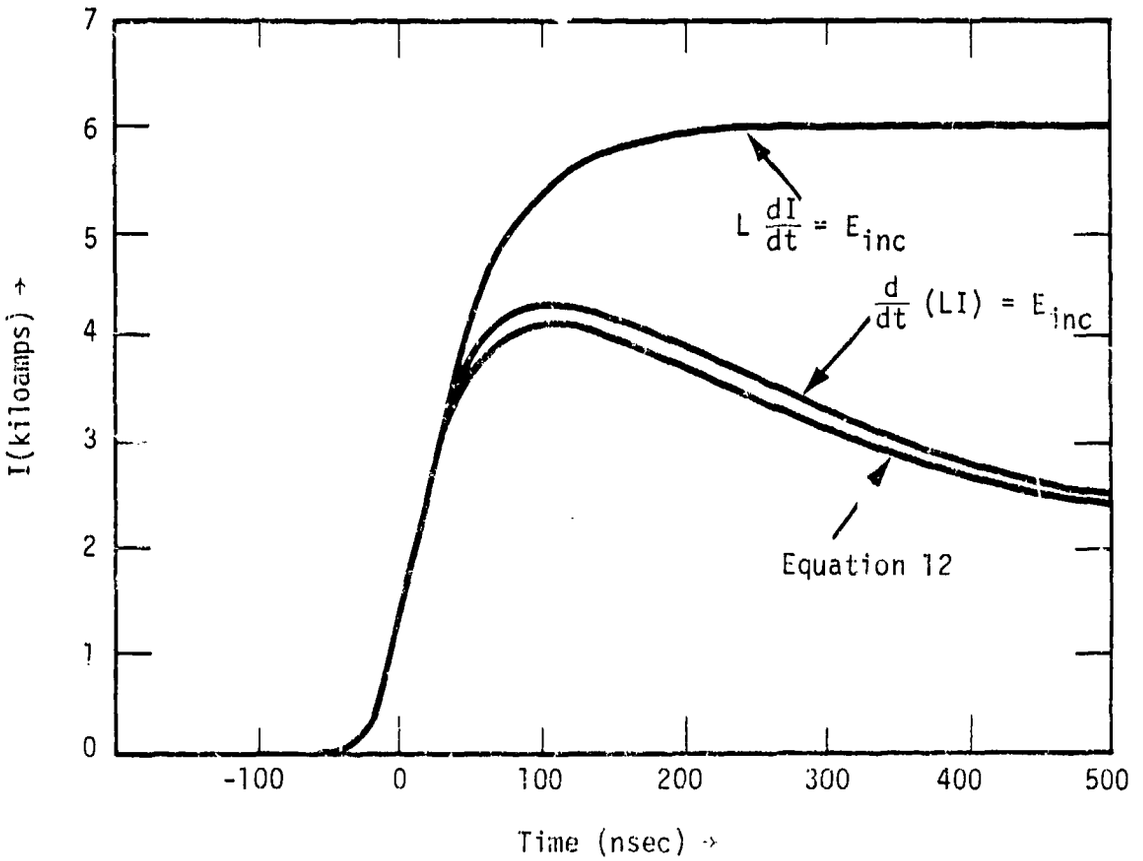

Figure 6-3. Comparison between Green's function and simple models for early diffusion phase.

At late times when the skin depth becomes larger than the wave phase skin depth the wave phase current contribution to the total current should be decreased according to

$$I_{wave}(t)L(t) = I^0_{wave}L^0 , \qquad (6\text{-}66)$$

where I^0_{wave} is the current at the end of the wave phase and L^0 is the inductance calculated with the wave phase skin depth.

6.4 LATE DIFFUSION PHASE

In this section we will develop a model for the late-time portion of the diffusion phase when the skin depth in the air is greater than the height of the overhead line. Where the last two sections of this chapter have dealt with local phenomena where the current on the line was only a function of the time histories of the incident electric field and conductivity at that point, the current on the line at a given point in the late diffusion phase involves the time histories of the conductivity and incident field at other locations on the line. We will assume a perfectly conducting ground in this section—the effects of finite ground conductivity on low-frequency signals on overhead lines was first investigated by J. R. Carson in 1926 and is reviewed in Sunde's text (Reference 6-3). The features of his theory which are relevant to us are the two modifications to the inductance of an overhead line which result from finite soil conductivity—the first of these is that the inductance is increased by the skin depth in the ground. This modification is less than a factor of two change because the ratio of the line radius to twice the height is less than the ratio of twice the height to the skin depth. (The reason we use twice the height will be apparent shortly.) The second modification is that there is a series resistance which results from the diffusion of energy into the ground. At a time of 10^{-4} seconds, this series resistance is less than 10^{-3} ohms/m and falls as 1/t at later times. With this value, the series resistance of the line is usually much less than the termination resistance represented by facilities (as in Chapter 5) if the burst to facility distance

is less than a few kilometers. If it is not, numerical solutions of the transmission line equations wit the effects of finite ground conductivity may be performed.

The transmission line equations are derived by evaluating two sets of integrals of Maxwell's equations. Applying Stoke's theorem to (1-17) for the scattered fields, we obtain

$$\oint \vec{E} \cdot ds = -\int da \cdot \frac{\partial \vec{B}}{\partial t} , \tag{6-67}$$

where $\oint ds$ is the path enclosing the surface a.

If we apply this to the path shown in Figure 6-4 and designate

$$\int_1 Eds = V(z+\delta z/2) , \tag{6-68}$$

$$\int_2 Eds = - E_{inc}\delta z , \tag{6-69}$$

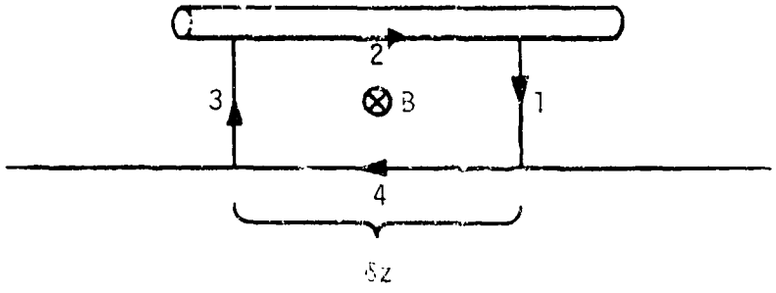

Figure 6-4. Integration path for derivation of first transmission line equation.

$$\int_3 E ds = - V(z-\delta z/2) \ , \tag{6-70}$$

$$\int \vec{B} \cdot da = L_0 I \delta z \ , \tag{6-71}$$

so that V is the voltage between the line and ground and this defines the inductance L_0. $\int_4 E ds$ is zero as the scattered field vanishes at the surface of the ground. As δz approaches zero

$$V(z+\delta z/2) - V(z-\delta z/2) \rightarrow \delta z \frac{\partial V}{\partial z} \ , \tag{6-72}$$

and we obtain the transmission line equation

$$L_0 \frac{\partial I}{\partial t} + \frac{\partial V}{\partial z} = E_{inc} \ . \tag{6-73}$$

The second transmission line equation is derived by applying Stokes' theorem to (1-18), neglecting the displacement current

$$Z_0 \sigma \int \vec{E} \cdot da = c \oint ds \cdot \vec{B} \ . \tag{6-74}$$

Using the path shown in Figure 6-5, we have

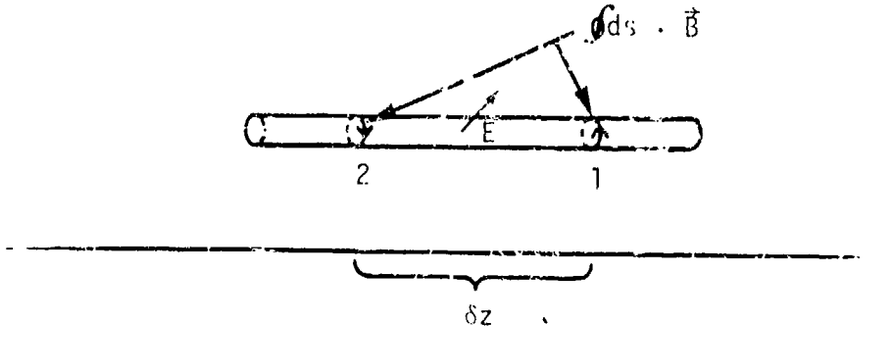

Figure 6-5. Integration path for the derivation of second transmission line equation.

$$\frac{c}{Z_0}\int_1 \vec{B}\cdot d\vec{s} = -\, I(z+\delta z/2)\ , \tag{6-75}$$

$$\frac{c}{Z_0}\int_2 \vec{B}\cdot d\vec{s} = I(z-\delta z/2)\ , \tag{6-76}$$

$$\sigma\int \vec{E}\cdot d\vec{a} = \delta z C V\ , \tag{6-77}$$

where we have used (1-19) in (6-75) and (6-76) and (6-77) defines C. These and (6-74) provide the second transmission line equation

$$\frac{\partial I}{\partial z} = -\, GV\ . \tag{6-78}$$

If the skin depth in the air and the scale length over which variations in I and V occur along z are much larger than the height of the wire then the derivatives with respect to x and y are much larger than those with respect to z and ct and we may make use of two-dimensional electrostatic and magnetostatic models to determine L_0 and G. The electric field is defined as the gradient of a scalar potential

$$E = -\nabla\phi\ , \tag{6-79}$$

(when the air conductivity is uniform in the plane perpendicular to the z axis) and the magnetic field as the curl of the z component of a vector potential.

$$\vec{B} = \nabla \times \vec{A}_z\ . \tag{6-80}$$

The requirements that E tangential to conductors and B perpendicular to conductors vanish are set if ϕ and A_z are constant on each conducting surface. In the air

$$\nabla^2\phi = \nabla^2 A_z = 0\ , \tag{6-81}$$

where the Laplacians are in the two dimensions perpendicular to z. These

conditions can be met for a wire of radius a located a height h above a ground plane by using bipolar coordinates (see Figure 6-6) (Reference 6-4).

The transformation to bipolar coordinates is given by

$$x = \frac{h'\sinh\xi}{\cosh\xi + \cos\theta} \quad , \tag{6-82}$$

$$y = \frac{h'\sin\theta}{\cosh\xi + \cos\theta} \quad , \tag{6-83}$$

and Laplace's equation becomes

$$\frac{\partial^2\phi}{\partial x^2} + \frac{\partial^2\phi}{\partial y^2} = \frac{(\cosh\xi+\cos\theta)^2}{h'^2}\left(\frac{\partial^2\phi}{\partial\xi^2} + \frac{\partial^2\phi}{\partial\theta^2}\right) = 0 \quad . \tag{6-84}$$

The line $\xi = 0$ is $x = 0$, $\xi = \xi_0$ is a circle centered at

$$x = h = h' \coth \xi_0 \qquad y = 0 \quad , \tag{6-85}$$

with radius

$$a = h' \operatorname{csch} \xi_0 \quad . \tag{6-86}$$

The solution to our electrostatics problem is

$$\begin{aligned} \phi &= C_1\xi \quad , \\ A_z &= C_2\xi \quad . \end{aligned} \tag{6-87}$$

From (6-71) and (6-68)

$$\begin{aligned} I_0 l &= C_2\xi_0 \quad , \\ V &= C_1\xi_0 \quad . \end{aligned} \tag{6-88}$$

The normal derivative of ϕ on ξ_0 is

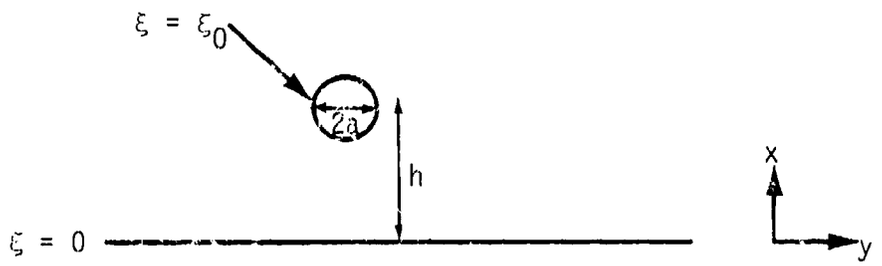

Figure 6-6. Coordinate system used for calculation of inductance and conductance terms in transmission line equations.

$$\frac{\partial \phi}{\partial \eta} = - \frac{\cosh \xi_0 + \cos\theta}{h'} C_1 \ , \tag{6-89}$$

and the normal derivative of A_z is the same with C_1 replaced by C_2. GV can be found by integrating this around the wire

$$\begin{aligned} GV &= - \int_0^{2\pi} \frac{\partial \phi}{\partial \eta} \frac{oh' d\theta}{\cosh \xi_0 + \cos\theta} \\ &= + 2\pi\sigma C_1 \ , \end{aligned} \tag{6-90}$$

so that

$$\begin{aligned} G &= \frac{2\pi\sigma}{\xi_0} \\ &= \frac{2\pi\sigma}{\cosh^{-1}(h/a)} \ . \end{aligned} \tag{6-91}$$

A similar development of L_0 yields

$$L_0 = \frac{\mu_0}{2\pi} \cosh^{-1}(h/a) \ . \tag{6-92}$$

If h/a is large, we can use

$$\cosh^{-1}(h/a) \rightarrow \ell n\,(\frac{2h}{a}) \quad . \tag{6-93}$$

The two transmission line equations may be combined to obtain

$$L_0 \frac{\partial I}{\partial t} - \frac{\partial}{\partial z} \frac{1}{G} \frac{\partial I}{\partial z} = E_{inc} \quad . \tag{6-94}$$

We will assume a simple form for the late-time shunt conductance, that it is separable in space and time and decreases exponentially in distance

$$G = f(t)e^{-\alpha z} \quad , \tag{6-95}$$

and we will examine an infinite line running from $-\infty$ to $+\infty$ in z.

To determine the Green's function for the current on the line, we examine the current which results from an incident electric field of the form

$$E_{inc} = \delta(z-z_0)\delta(t-t_0) \quad , \tag{6-96}$$

or

$$L_0 f(t) \frac{\partial \mathcal{G}}{\partial t} - \frac{\partial}{\partial z} e^{\alpha z} \frac{\partial \mathcal{G}}{\partial z} = f(t)\delta(z-z_0)\delta(t-t_0) \quad . \tag{6-97}$$

This equation may be simplified by the substitution

$$\tau = \int_{t_{pk}}^{t} \frac{dt'}{f(t')} \quad , \tag{6-98}$$

$$\frac{\partial}{\partial t} = \frac{d\tau}{dt} \frac{\partial}{\partial \tau} = \frac{1}{f(t)} \frac{\partial}{\partial \tau} \quad , \tag{6-99}$$

$$\delta(t-t_0) = \frac{d\tau}{dt} \delta(\tau-\tau_0) = \frac{1}{f(t)} \delta(\tau-\tau_0) \quad . \tag{6-100}$$

Equation 6-97 becomes

$$L_0 \frac{\partial \mathscr{G}}{\partial \tau} - \frac{\partial}{\partial z} e^{\alpha z} \frac{\partial \mathscr{G}}{\partial z} = \delta(z-z_0)\delta(\tau-\tau_0) \ , \tag{6-101}$$

which is invariant under translations in τ, so that a frequency domain technique such as a Laplace transform is a useful technique. The Laplace transform of Equation 6-101 is

$$\left(sL_0 - \frac{\partial}{\partial z} e^{\alpha z} \frac{\partial}{\partial z}\right) g = \delta(z-z_0) \ , \tag{6-102}$$

where $g(z,s)$ is the Laplace transform of $\mathscr{G}(z,t)$. The last equation can be reduced to a variation of Bessel's equation by the substitution

$$y = e^{-\alpha z/2} \ , \tag{6-103}$$

$$\frac{dy}{dz} = -\frac{\alpha y}{2} \ , \tag{6-104}$$

and it becomes, for $z \neq z_0$

$$y^2 \frac{\partial^2 g}{\partial y^2} - y \frac{\partial g}{\partial y} - \frac{4sL_0}{\alpha^2} y^2 g = 0 \ . \tag{6-105}$$

The solution (in terms of z) of this is, from Reference 6-5,

$$\begin{aligned} g = {} & C_1 e^{-\alpha z/2} I_1\left(\frac{2}{\alpha} \sqrt{sL_0}\, e^{-\alpha z/2}\right) \\ & + C_2 e^{-\alpha z/2} K_1\left(\frac{2}{\alpha} \sqrt{sL_0}\, e^{-\alpha z/2}\right) \ , \end{aligned} \tag{6-106}$$

where I_1 and K_1 are modified Bessel functions. We now need to determine the values of C_1 and C_2 to use for $z \gtrless z_0$ to produce the discontinuity in the spatial derivative of g and satisfy physical boundary conditions as $z \to \pm \infty$. As $z \to -\infty$ the argument of the modified Bessel functions become large. If χ is the argument, the Bessel functions behave as

$$I_1 \to \frac{e^{\chi}}{\sqrt{2\pi\chi}} , \tag{6-107}$$

$$K_1 \to \sqrt{\frac{\pi}{2\chi}}\, e^{-\chi} , \tag{6-108}$$

for large χ so we use the solution that causes small currents for $z \to -\infty$, or

$$g_< = C_2 e^{-\alpha z/2} K_1\left(\frac{2}{\alpha}\sqrt{sL_0}\, e^{-\alpha z/2}\right) , \tag{6-109}$$

for $z < z_0$. As $z \to +\infty$, the argument of the modified Bessel functions becomes small, and they behave as

$$I_1 \to \frac{\chi}{2} , \tag{6-110}$$

$$K_1 \to \frac{1}{\chi} , \tag{6-111}$$

where χ is again the argument. At the present point in the derivation, we have no a priori justification for choosing the combination of C_1 and C_2 for $z > z_0$. Ultimately, we will find that the choice is determined by the termination resistance at large z. For the present, we set g for $z > z_0$ equal to

$$g_> = C_1 e^{-\alpha z/2} I_1\left(\frac{2}{\alpha}\sqrt{sL_0}\, e^{-\alpha z/2}\right) , \tag{6-112}$$

and, after transforming back to the time domain, we will find that this choice is appropriate for an infinite termination resistance at large z. We will then determine the modification necessary for finite termination resistances, which will involve a term proportional to K_1. The solution of Equation 6-102 at $z = z_0$ can be determined by making the first derivative of g discontinuous at that point so that

$$g_<|_{z_0} = g_>|_{z_0} , \tag{6-113}$$

$$\frac{dg_>}{dz}\Big|_{z_0} - \frac{dg_<}{dz}\Big|_{z_0} = - e^{-\alpha z_0} \quad , \tag{6-114}$$

The derivatives of g are easily found with the use of the relations

$$\frac{d}{d\chi}\left[\chi I_1(\chi)\right] = \chi I_0(\chi) \quad , \tag{6-115}$$

$$\frac{d}{d\chi}\left[\chi K_1(\chi)\right] = - \chi K_0(\chi) \quad , \tag{6-116}$$

to be

$$\frac{dg_>}{dz} = - C_1 \sqrt{sL_0}\, e^{-\alpha z} I_0\left(\frac{2}{\alpha}\sqrt{sL_0}\, e^{-\alpha z/2}\right) \quad , \tag{6-117}$$

$$\frac{dg_<}{dz} = C_2 \sqrt{sL_0}\, e^{-\alpha z} K_0\left(\frac{2}{\alpha}\sqrt{sL_0}\, e^{-\alpha z/2}\right) \quad , \tag{6-118}$$

and the solutions for $g_>$ and $g_<$ which satisfy Equation 6-102 are

$$g_> = \sqrt{\frac{1}{sL_0}}\, \frac{K_1(\chi_0) I_1(\chi)}{K_1(\chi_0) I_0(\chi_0) + K_0(\chi_0) I_1(\chi_0)}\, e^{-\alpha z/2} \quad , \tag{6-119}$$

$$g_< = \sqrt{\frac{1}{sL_0}}\, \frac{K_1(\chi) I_1(\chi_0)}{K_1(\chi_0) I_0(\chi_0) + K_0(\chi_0) I_1(\chi_0)}\, e^{-\alpha z/2} \quad , \tag{6-120}$$

where

$$\chi = \frac{2}{\alpha}\sqrt{sL_0}\, e^{-\alpha z/2} \quad . \tag{6-121}$$

This can be simplified by using the Wronskian

$$K_1(\chi) I_0(\chi) + K_0(\chi) I_1(\chi) = 1/\chi \quad , \tag{6-122}$$

and the notation

$$\text{if} \quad z > z_0 \qquad z_> = z \qquad z_< = z_0 \quad ,$$

$$\text{if} \quad z < z_0 \qquad z_> = z_0 \qquad z_< = z \quad ,$$

so that

$$g = \frac{2}{\alpha} e^{-\alpha(z+z_0)/2} K_1\left(\frac{2}{\alpha}\sqrt{sL_0}\, e^{-\alpha z_</2}\right) I_1\left(\frac{2}{\alpha}\sqrt{sL_0}\, e^{-\alpha z_>/2}\right). \tag{6-123}$$

It is possible to find the inverse Laplace transform of this function using the tabulated pair (Reference 6-6).

$$\tilde{f} = K_\nu(a^{1/2}s^{1/2}+b^{1/2}s^{1/2}) I_\nu(a^{1/2}s^{1/2}-b^{1/2}s^{1/2}) , \tag{6-124}$$

$$\begin{aligned} f &= \frac{1}{2\pi i}\int_{c-i\infty}^{c+i\infty} e^{st}\tilde{f}(s)ds \\ &= \frac{1}{2t} e^{-(a+b)/2t} I_\nu\left(\frac{a-b}{2t}\right) . \end{aligned} \tag{6-125}$$

The inverse transform of g is, substituting back to the time t as the variable,

$$\begin{aligned} \mathcal{G} = \frac{1}{\alpha} \frac{e^{-\alpha(z+z_0)/2}}{\int_{t_0}^{t}\frac{dt'}{f(t')}} \exp\left\{-\frac{L_0}{\alpha^2}(e^{-\alpha z_<}+e^{-\alpha z_0})\Big/\int_{t_0}^{t}\frac{dt'}{f(t')}\right\} \\ \times I_1\left\{\frac{2L_0}{\alpha^2} e^{-\alpha(z+z_0)/2}\Big/\int_{t_0}^{t}\frac{dt'}{f(t')}\right\} , \end{aligned} \tag{6-126}$$

and the current distribution resulting from an arbitrary incident electric field is

$$I(z,t) = \int_{-\infty}^{\infty} dz_0 \int_{-\infty}^{t} dt_0\ \mathcal{G}(z,t;z_0,t_0) E_{inc}(z_0,t_0) , \tag{6-127}$$

The Green's function has two interesting limits—if we take the large argument limit of the Bessel function we obtain

$$\mathscr{G} \sim \frac{1}{\sqrt{4\pi L_0}} \frac{e^{-\alpha(z+z_0)/4}}{\sqrt{\int_{t_0}^{t} \frac{dt'}{f(t')}}} \exp\left\{ - \frac{L_0 \left(e^{-\alpha z/2} - e^{-\alpha z_0/2} \right)^2}{\alpha^2 \int_{t_0}^{t} \frac{dt'}{f(t')}} \right\} . \quad (6\text{-}128)$$

This reduces to the usual Green's function for diffusion in the limit

$$z \to z_0 ,$$

$$t \to t_0 .$$

The second limit results from taking the small argument limit of the Bessel function and is

$$\mathscr{G} \sim \frac{L_0}{\alpha^3} \frac{e^{-\alpha(z+z_0)}}{\left[\int_{t_0}^{t} \frac{dt'}{f(t')} \right]^2} \exp\left\{ - \frac{L_0 \left(e^{-\alpha z} + e^{-\alpha z_0} \right)}{\alpha^2 \int_{t_0}^{t} \frac{dt'}{f(t')}} \right\} . \quad (6\text{-}129)$$

This limit of the Green's function tells us how sources within the source region at early times produce currents outside the source region at late times. If z_0 is much smaller than z and $f(t)$ is such that

$$\int_{t_{pk}}^{t} \frac{dt'}{f(t')} >> \int_{t_{pk}}^{t_0} \frac{dt'}{f(t')} , \quad (6\text{-}130)$$

then the exponential factor in Equation 6-129 is small for

$$\frac{L_0 e^{-\alpha z_0}}{\alpha^2 \int_{t_{pk}}^{t} \frac{dt'}{f(t')}} \gtrsim 1 , \quad (6\text{-}131)$$

or

$$\left[\int_{t_{pk}}^{t} \frac{dt'}{L_0 G(z_0,t')}\right]^{1/2} \lesssim \frac{1}{\alpha} \ . \tag{6-132}$$

The quantity on the left-hand side can be interpreted as the skin depth at the point z_0 at the time t and shows that the energy is trapped by the air conductivity until the skin depth becomes greater than the conductivity attenuation length $1/\alpha$. The time of the peak current can be calculated directly from Equation 6-129, by setting the derivative equal to zero, and occurs when

$$2\int_{t_0}^{t} \frac{dt'}{f(t')} = \frac{L_0(e^{-\alpha z_0}+e^{-\alpha z})}{\alpha^2} \ . \tag{6-133}$$

The voltage on the power line may be determined by

$$V = -\frac{1}{G}\frac{\partial I}{\partial z} = -\frac{L_0}{\alpha^2}\frac{e^{\alpha z}}{f(t)}\frac{e^{-\alpha(z+z_0)/2}}{\left[\int_{t_0}^{t}\frac{dt'}{f(t')}\right]^2}\exp\left\{-\frac{e^{-\alpha z}+e^{-\alpha z_0}}{\int_{t_0}^{t}\frac{dt'}{f(t')}}\right\}$$

$$\times \left[e^{-\alpha z} I_1 - e^{-\alpha(z+z_0)/2} I_0\right] \ , \tag{6-134a}$$

where the arguments of the Bessel functions are the same as in Equation 6-126. When we take the small argument limit of the Bessel functions and let $z \to \infty$, the term proportional to I_0 dominates as it is constant in z while the other term approaches zero as $e^{-\alpha z/2}$. The resulting limit for V is

$$V \sim + \frac{L_0}{\alpha^2}\frac{1}{f(t)}\frac{e^{-\alpha z_0}}{\left[\int_{t_0}^{t}\frac{dt'}{f(t')}\right]^2}\exp\left\{-\frac{L_0 e^{-\alpha z_0}}{\alpha^2\int_{t_0}^{t}\frac{dt'}{f(t')}}\right\} \ , \tag{6-134b}$$

and it shares with the current the property that it is small for

$$\left[\int_{t_{pk}}^{t} \frac{dt'}{L_0 G(\chi_0, t)}\right]^{1/2} \lesssim \frac{1}{\alpha} . \tag{6-135}$$

The peak of V occurs when

$$\frac{df}{dt}\left[\int_{t_0}^{t} \frac{dt'}{f(t')}\right]^2 + 2\int_{t_0}^{t} \frac{dt'}{f(t')} = \frac{L_0(e^{-\alpha z_0}+e^{-\alpha z})}{\alpha^2} , \tag{6-136}$$

which will be later than the peak of I for monotonically decreasing $f(t)$, as the first term on the left-hand side is negative. The time integral of Equation 6-134b from t_0 to ∞ may be evaluated directly by substituting

$$\chi = \frac{L_0 e^{-\alpha z_0}}{\alpha^2 \int_{t_0}^{t} \frac{dt'}{f(t')}} , \tag{6-137}$$

$$d\chi = -\frac{L_0 e^{-\alpha z_0}}{\alpha^2\left[\int_{t_0}^{t} \frac{dt'}{f(t')}\right]^2} \frac{dt}{f(t)} , \tag{6-138}$$

$$V = \int_0^{\infty} e^{-\chi} d\chi = 1 , \tag{6-139}$$

provided $f(t)$ is monotonically decreasing. To summarize the results of our investigation so far, we have derived the Green's function appropriate for an infinite line with an infinite termination impedance at $z = +\infty$ because the voltage (Equation 6-134b) approaches a constant value as $z \to \infty$ and the current approaches zero. We have discovered the interesting fact that the energy is trapped on the line whenever the local skin depth is smaller than the conductivity attenuation length $1/\alpha$. When the skin depth approaches $1/\alpha$, the incident electric field appears as a voltage across the line at large values of z with a relatively narrow pulse and a time integral equal to

$$\int V dt = \int dz \int dt \; E_{inc} \; . \tag{6-140}$$

If we look at the voltage and current at a large but finite value of z we find that the ratio between the two is

$$\begin{aligned} \frac{I}{V} &= \frac{1}{\alpha} f(t) e^{-\alpha z} \\ &= \int_z^\infty G(z',t) dz' \; . \end{aligned} \tag{6-141}$$

We now want to determine the modifications needed to the Green's function to represent a finite termination resistance at large z. This may be determined by examining the response of Equation 6-94 to a step current at large z. Using the term proportional to C_2 in Equation 6-106, the solution which results in a step function in time at t_0 current at z_0 and vanishes as $z \to -\infty$ at finite s is

$$I(z,s) = \frac{1}{s} \frac{e^{-\alpha z/2} K_1\left(\frac{2}{\alpha}\sqrt{sL_0}\; e^{-\alpha z/2}\right)}{e^{-\alpha z_0/2} K_1\left(\frac{2}{\alpha}\sqrt{sL_0}\; e^{-\alpha z_0/2}\right)} \; , \tag{6-112}$$

where we have used the face that the Laplace transform of a step function is $1/s$. If we look at I for $z < z_0$, we can let $z_0 \to \infty$ and expand the Bessel function in the denominator as

$$K_1\left(\frac{2}{\alpha}\sqrt{sL_0}\, e^{-\alpha z_0/2}\right) \to \frac{\alpha}{2\sqrt{sL_0}}\, e^{\alpha z_0/2}\,, \tag{6-143}$$

$$I(z,s) = \frac{2}{\alpha}\sqrt{\frac{L_0}{s}}\, e^{-\alpha z/2} K_1\left(\frac{2}{\alpha}\sqrt{sL_0}\, e^{-\alpha z/2}\right)\,, \tag{6-144}$$

for which the Laplace inverse is

$$I(z,t) = \exp\left\{-\frac{L_0 e^{-\alpha z}}{\alpha^2 \int_{t_0}^{t} \frac{dt'}{f(t')}}\right\}. \tag{6-145}$$

Taking the spatial derivative of I

$$\frac{\partial I}{\partial z} = +\sqrt{\frac{L_0}{s}}\, \frac{e^{-\alpha z} K_0\left(\frac{2}{\alpha}\sqrt{sL_0}\, e^{-\alpha z/2}\right)}{e^{-\alpha z_0/2} K_1\left(\frac{2}{\alpha}\sqrt{sL_0}\, e^{-\alpha z_0/2}\right)}\,, \tag{6-146}$$

if we now again let $z_0 \to +\infty$ so we take the small argument limit of K_1

$$\frac{\partial I}{\partial z} \to +\frac{2L_0}{\alpha}\, e^{-\alpha z} K_0\left(\frac{2}{\alpha}\sqrt{sL_0}\, e^{-\alpha z/2}\right)\,. \tag{6-147}$$

The Laplace inverse of this is

$$\frac{\partial I}{\partial z} = \frac{L_0 e^{-\alpha z}}{\alpha \int_{t_0}^{t} \frac{dt'}{f(t')}} \exp\left\{-\frac{L_0 e^{-\alpha z}}{\alpha^2 \int_{t_0}^{t} \frac{dt'}{f(t')}}\right\}\,, \tag{6-148}$$

where t_0 is the time of the applied current and the voltage resulting from the step current is

$$V = -\frac{1}{G}\frac{\partial I}{\partial z}$$

$$\to -\frac{L_0}{\alpha f(t) \int_{t_0}^{t} \frac{dt'}{f(t')}} \exp\left\{-\frac{L_0 e^{-\alpha z}}{\alpha^2 \int_{t_0}^{t} \frac{dt'}{f(t')}}\right\}\,, \tag{6-149}$$

The physical interpretation of the early time response is clarified by examining the time integral of $V(z,t)$ from 0 to t. This integral is simplified by the substitution

$$\chi = \frac{L_0 e^{-\alpha z}}{\alpha^2 \int_{t_0}^{t} \frac{dt'}{f(t')}} , \tag{6-150}$$

$$d\chi = - \frac{L_0 e^{-\alpha z}}{\alpha^2 \left[\int_{t_0}^{t} \frac{dt'}{f(t')} \right]^2} \frac{dt}{f(t)} , \tag{6-151}$$

and we obtain

$$\begin{aligned} \int_{t_0}^{t} V dt' &= - \frac{L_0}{\alpha} \int_{\chi_0}^{\omega} \frac{d\chi}{\chi} e^{-\chi} \\ &= - \frac{L_0}{\alpha} E_1(\chi_0) , \end{aligned} \tag{6-152}$$

where

$$\chi_0 = \frac{L_0 e^{-\alpha z}}{\alpha^2 \int_{t_0}^{t} \frac{dt'}{f(t')}} , \tag{6-153}$$

and $E_1(\chi_0)$ is the exponential integral. For small χ_0 (large z) the limit of the exponential integral is

$$E_1(\chi_0) \sim - \ln(\gamma \chi_0) \qquad \gamma = 1.781 , \tag{6-154}$$

so

$$\int_{t_0}^{t} V dt \sim \frac{L_0}{\alpha} \ln\left[\frac{\gamma L_0 e^{-\alpha z}}{\alpha^2 \int_{t_0}^{t} \frac{dt'}{f(t')}}\right]$$

$$= - L_0(z-z_0) + 0.577\ L_0/\alpha \ , \tag{6-155}$$

where z_0 is defined by the edge of the source region where the skin depth equals the exponential conductivity scale length

$$\left[\int_{t_0}^{t} \frac{dt'}{L_0 G(z_0,t)}\right]^{1/2} = \frac{1}{\alpha} \ , \tag{6-156}$$

The late-time response can also be understood in the same manner—for late times and f decreasing sufficiently rapidly that

$$\int_{t_{pk}}^{t} \frac{dt'}{f(t')} >> \int_{t_{pk}}^{t_0} \frac{dt'}{f(t')} \ , \tag{6-157}$$

we are looking into a resistance with the value

$$R = - \frac{V}{I} = \frac{L_0}{\alpha f(t) \int_{t_{pk}}^{t} \frac{dt'}{f(t')}} \ , \tag{6-158}$$

which is

$$R = - L_0 \frac{dz_0}{dt} \ , \tag{6-159}$$

and z_0 is defined by Equation 6-156. To summarize the outer boundary conditions, an observer at z looking back towards the source region sees the inductance of the line between z and z_0 and a resistance at the edge of the source region given by Equation 6-158.

A couple of useful cases for which the time integrals of $1/f$ can be analytically evaluated are when f behaves as an exponential function or as a power of t. If

$$G = G_0 e^{-\alpha z - \beta t} , \tag{6-160}$$

then

$$\int_{t_0}^{t} \frac{dt'}{f(t')} = \frac{1}{G_0 \beta} \left(e^{\beta t} - e^{\beta t_0}\right)$$

$$\rightarrow \frac{e^{\beta t}}{G_0 \beta} \qquad t >> t_0 , \tag{6-161}$$

If we define $z = 0$ as the point where

$$\left[\int_{-\infty}^{0} \frac{dt}{L_0 G(z,t)}\right]^{1/2} = \frac{1}{\alpha} , \tag{6-162}$$

so that at $t = 0$, $z = 0$ is the edge of the source region then

$$G_0 = \frac{\alpha^2}{L_0 \beta} . \tag{6-163}$$

The Green's function has a simple limit when $z_0 << 0$, $t_0 < 0$, $z >> 0$, $t >> t_0$

$$\mathcal{G} \sim \frac{\alpha}{L_0} e^{-\alpha(z+z_0)-2\beta t} \exp\left\{- e^{-\alpha z_0 - \beta t}\right\} , \tag{6-164}$$

which peaks at

$$\beta t = - \alpha z_0 - \ell n 2 . \tag{6-165}$$

The voltage associated with $\mathcal{G}$ is, in the same limit

$$V \sim e^{-\alpha z_0 - \beta t} \exp\left\{- e^{-\alpha z_0 - \beta t}\right\} , \tag{6-166}$$

which peaks at

$$\beta t = - \alpha z_0 \ , \tag{6-167}$$

which is the time that the edge of the source region defined by Equation 6-162 passes z_0. The edge of the source region moves in the - z direction at a uniform velocity

$$v = \frac{\beta}{\alpha} \ , \tag{6-168}$$

and the late-time resistance looking into the source region defined by Equation 6-158 is

$$R = \frac{\beta L_0}{\alpha} \ . \tag{6-169}$$

The second case is where the conductivity decreases as a power of t

$$G = G_0 t^{-n} e^{-\alpha z} \ , \tag{6-170}$$

so that

$$\int_{t_0}^{t} \frac{dt'}{f(t')} = \frac{1}{(n+1)G_0} \left(t^{n+1} - t_0^{n+1}\right)$$
$$\Rightarrow \frac{t^{n+1}}{(n+1)G_0} \qquad t >> t_0 \ . \tag{6-171}$$

The edge of the source region, defined by

$$\left[\int_0^t \frac{dt}{L_0 G(z,t)}\right]^{1/2} = \frac{1}{\alpha} \ , \tag{6-172}$$

is

$$z = - \frac{1}{\alpha} \ln \left(\frac{\alpha^2 t^{n+1}}{(n+1)L_0 G_0}\right) \ . \tag{6-173}$$

The limit of the Green's function for $z >> z_0$, $t >> t_0$ and (z_0,t_0) deep within the source region is

$$\mathcal{G} \sim \frac{(n+1)^2 L_0 G_0^2}{\alpha^3 t^{2n+2}} e^{-\alpha(z_0+z)} \exp\left\{ - \frac{(n+1) G_0 L_0 e^{-\alpha z_0}}{\alpha^2 t^{n+1}} \right\} , \qquad (6\text{-}174)$$

which peaks when

$$t = \left(\frac{(n+1) L_0 G_0 e^{-\alpha z_0}}{2\alpha^2} \right)^{\frac{1}{n+1}} . \qquad (6\text{-}175)$$

The voltage associated with $\mathcal{G}$ is

$$V \sim \frac{(n+1)^2 L_0 G_0}{\alpha^2 t^{n+2}} e^{-\alpha z_0} \exp\left\{ - \frac{(n+1) G_0 L_0 e^{-\alpha z_0}}{\alpha^2 t^{n+1}} \right\} , \qquad (6\text{-}176)$$

which peaks at

$$t = \left(\frac{(n+1)^2 L_0 G_0 e^{-\alpha z_0}}{(n+2)\alpha^2} \right)^{\frac{1}{n+1}} . \qquad (6\text{-}177)$$

The edge of the source region moves in the - z direction at a decreasing velocity

$$v = \frac{n+1}{\alpha t} , \qquad (6\text{-}178)$$

and, consequently, the resistance represented by the source region is decreasing

$$R = \frac{(n+1) L_0}{\alpha t} . \qquad (6\text{-}179)$$

The results of this section and Section 6.3 can be summarized in the circuit model shown in Figure 6-7. The edge of the source region is defined by the point z_s where the local skin depth equals the conductivity attenuation

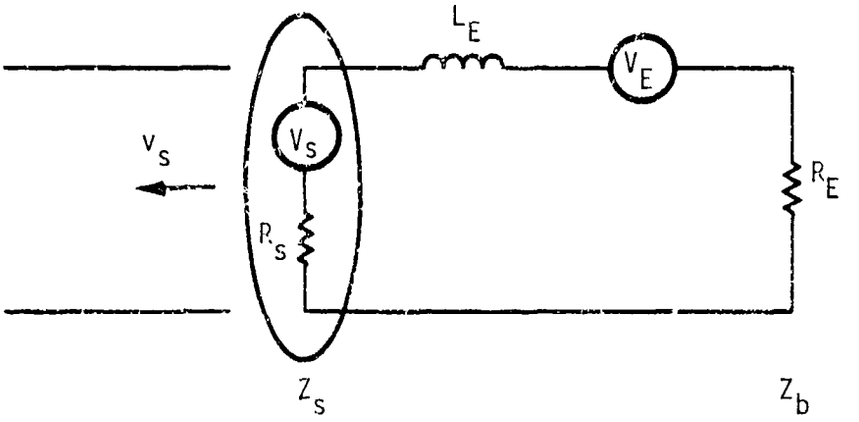

$$V_s = v_s L_0 I_s(Z_s,t) ,$$

$$R_s = v_s L_0 ,$$

$$L_E = L_0(Z_b - Z_s) ,$$

$$V_E = \int_{Z_s}^{Z_b} E_{inc} dz ,$$

$$Z_s = -\frac{1}{\alpha} \ell n\left(\frac{\alpha^2}{L_0} \int_{t_{pk}}^{t} \frac{dt'}{f(t')}\right)$$

$$v_s = \frac{1}{\alpha f(t) \int_{t_{pk}}^{t} \frac{dt'}{f(t')}}$$

$$I_s(z,t) = \frac{1}{L_s(z,t)} \int_{t_{diff}}^{t} E_{inc}(z,t')dt' + I_{wave}(z,t)$$

Figure 6-7. Circuit model of source region power line coupling.

length. To the left of this point, the current on the line is proportional to the time integral of the electric field in the diffusion phase (plus the wave phase current). The external circuit shown is composed of the voltage source (V_s) determined from the Green's function, the resistance (R_s) determined from the solution looking back into the source region, and the external circuit parameters L_E, V_E and R_E. L_E is the line inductance between z_s and the termination, V_E is the applied electric field integrated over the same region and R_E is the line termination resistance.

The assumption that the local current deep within the source region is determined solely by the time integral of the electric field is modified slightly by the expansion of the fireball. As the fireball grows, it pushes most of the magnetic field on its powerline ahead of it. The practical effect of this is small because the magnetic relaxation distance in the ionized air ahead of the fireball is substantially larger than the fireball radius.

6.5 APPLICATION OF FORMULAE TO EXAMPLE

In this section we apply the approximate theory of Section 6.4 to determine the late-time currents at a shelter. The parameters of the example are the same as that of Section 5.10 except that the line is at a height of 10 meters above the surface of the earth. The small line resistance (0.3 milliohms/m) is ignored. The air conductivity as a function of range at various times is shown in Figure 6-8. This conductivity was calculated with gamma fluxes of Chapter 3 scaled up to represent a 3 MT burst—the conductivity resulting from device X rays and ionization caused by the elastic scattering of neutrons off air nuclei was ignored. The first step in the calculation was to determine the point where

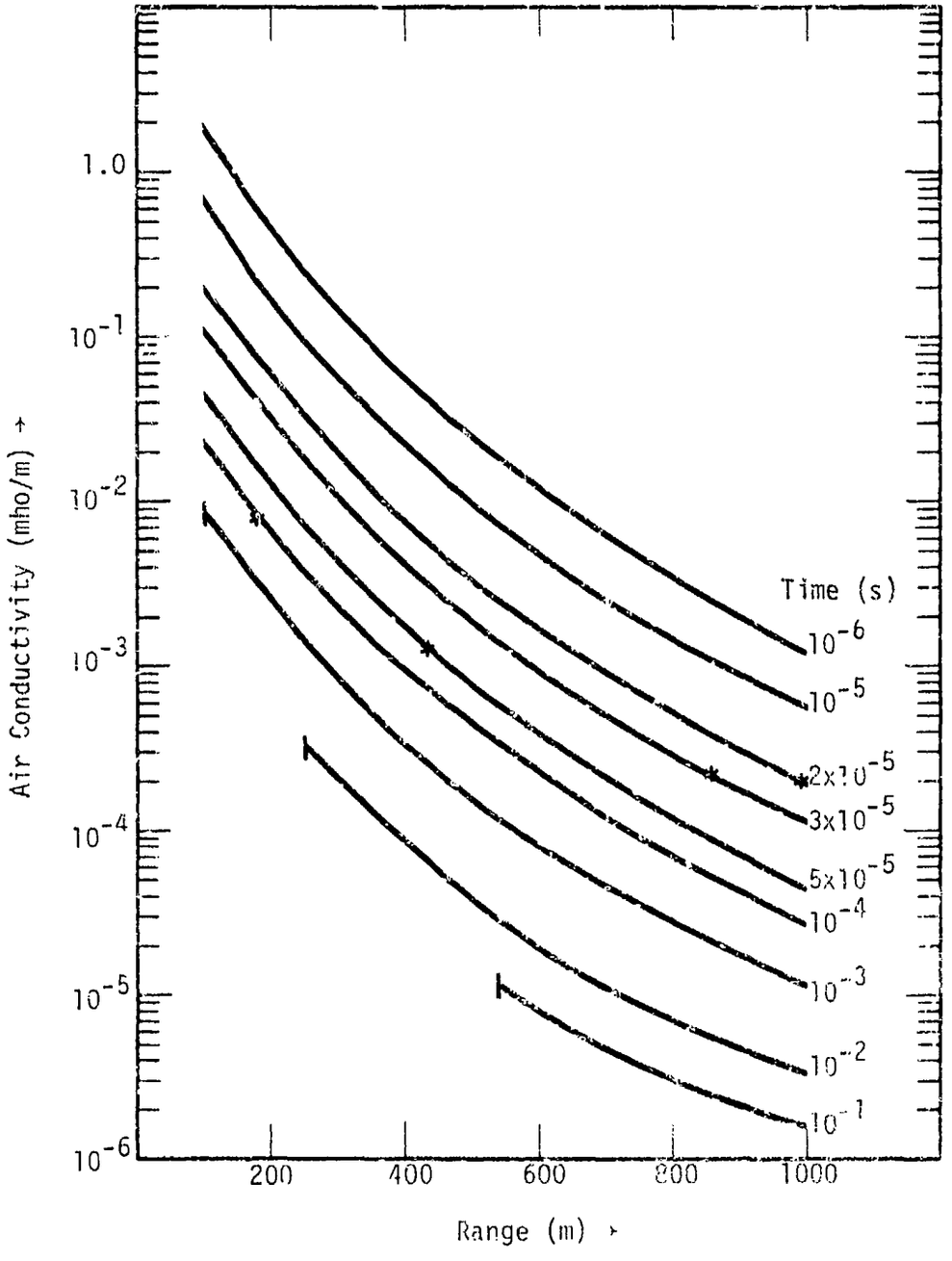

Figure 6-8. Air conductivity as a function of range and time. The asterisks indicate the edge of the source region and the vertical bars indicate the fireball radius.

$$\int_0^t \frac{dt}{\mu_0 \sigma(z,t)} = \frac{1}{\alpha^2} , \tag{6-180}$$

which is (6-172) with the fact that

$$L_0 G(z,t) = \mu_0 \sigma(z,t) . \tag{6-181}$$

To do this we assume that σ varies locally as

$$\sigma = t^{-n} e^{-\alpha z} , \tag{6-182}$$

n is evaluated as a function of time from Figure 6-8, and we first assume $\alpha \sim 200$ meters^{-1}. $\sigma(z,t)$ is then evaluated from

$$\sigma(z,t) = \frac{\alpha^2 t}{(n+1)\mu_0} . \tag{6-183}$$

Since α is a function of distance this formula is iterated until we find the point where (6-183) is satisfied. One iteration suffices as α is a weak function of distance, if we use the α from the last time step as the initial value in (6-183). The velocity of the edge of the source region is evaluated from (6-178). After the edge of the source region reaches the fireball radius, V_s is zero and R_s is the sum of R_s or R_{fb} and the 10 ohm termination resistance. The time integral of the incident electric field is evaluated from the curves at the appropriate ranges in Figure 6-9, and

$$V_s = v_s \int_0^t E dt' . \tag{6-184}$$

V_E is the spatial integral of the electric field outside the source region and V_I is the sum of V_s and V_E. L_E is the inductance outside the source region; we have included the effects of this inductance in the cal-

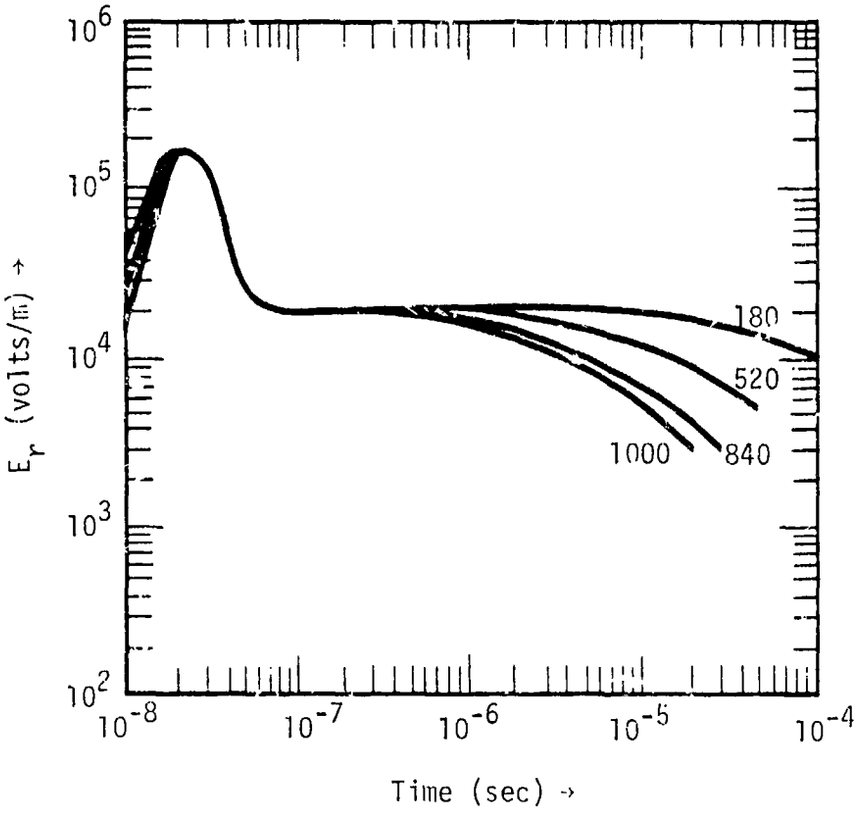

Figure 6-9. Early time radial electric fields at various ranges.

culation of the current in an iterative manner. An initial guess at the shelter current is made by

$$I_1 = V_t/R \ . \tag{6-185}$$

The resistance associated with L_E

$$\frac{L_E}{I_1}\frac{\partial I_1}{\partial t} \ , \tag{6-186}$$

(we have assumed that the overhead line extends sufficiently far into the fireball to result in a low resistance between the line and the fireball) is calculated and added to R_T and the current is recalculated as I_2. As the difference between I_1 and I_2 is always less than about 30 percent, it is not necessary to iterate further. These operations are summarized in Table 6-1 and the resulting current is plotted in Figure 6-10. The peak current occurs somewhat earlier and is larger than that shown in Figure 5-6. This results primarily from the air conductivity being smaller than the ground conductivity at most ranges so that the large electric fields near the source are seen at an earlier time.

REFERENCES FOR CHAPTER 6

6-1. Longmire, C. L., "EMP Induced High-Frequency Currents in Aerial Wires," MRC-R-164, DNA 3633T, Mission Research Corporation, Santa Barbara, California, August 1975.

6-2. Harberger, J. H., and C. L. Longmire, "Diffusion Approximation to Surface Currents in a Long Metal Cylinder Due to Excitation by a Longitudinal Electric Field," MRC-N-197, Mission Research Corporation, Santa Barbara, California, May 1975.

6-3. Sunde, E. D., Earth Conduction Effects in Transmission Systems, Dover Publications, New York, 1968.

6-4. Morse, P. M., and H. Feshbach, "Methods of Theoretical Physics," McGraw-Hill Book Company, New York, 1953. The discussion of bipolar coordinates is on page 1210 in Volume II.

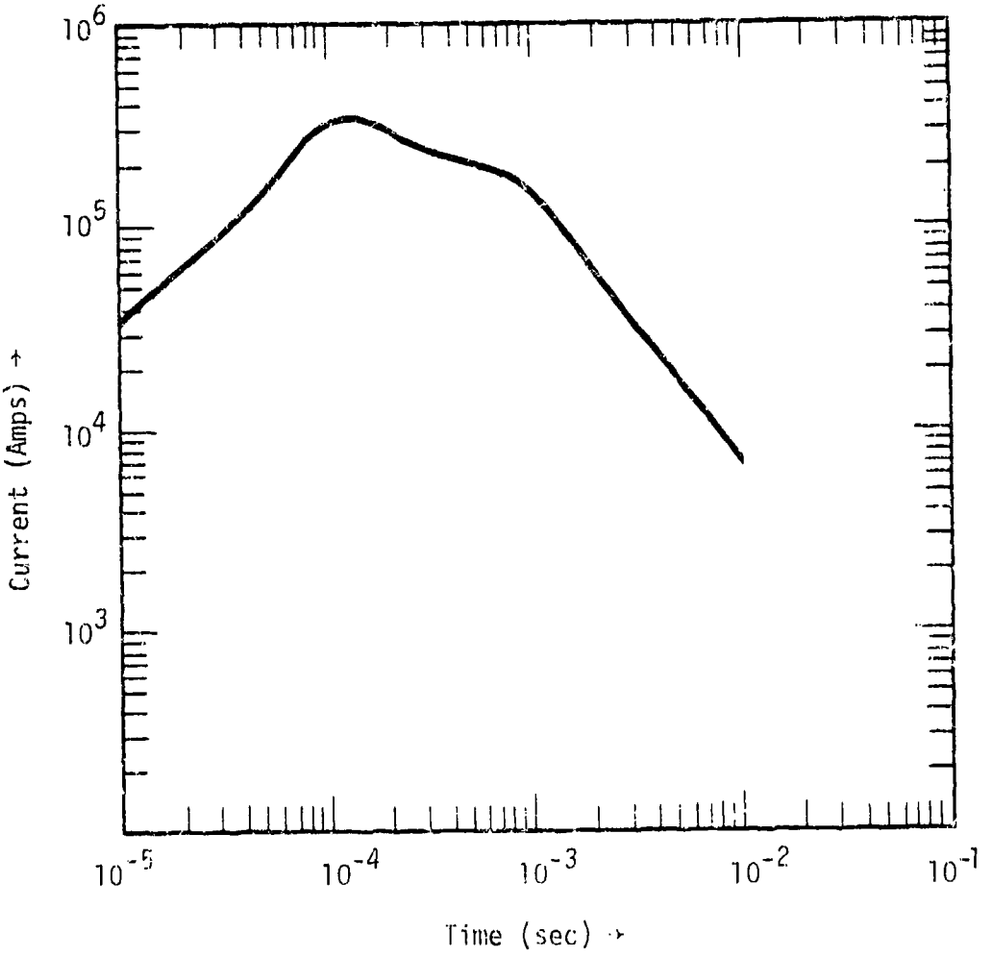

Figure 6-10. Current at shelter as a function of time.

Table 6-1. Computation of shelter current.

t	2×10^{-5}	3×10^{-5}	5×10^{-5}	10^{-4}	3×10^{-4}	10^{-3}	3×10^{-3}	10^{-2}	sec
n	3/2	2	2	1/2					
λ	200	200	150	90					m
σ	2×10^{-4}	2.5×10^{-4}	7×10^{-4}	8×10^{-3}					mho/m
r	1000	840	520	180					m
v_s	2.5×10^{7}	2.0×10^{7}	9.0×10^{6}	1.4×10^{6}					m/s
R_s	38	30	14	2					ohms
r_{sb}				40	62	100	157	253	m
R_{fb}				6.3	4.0	2.5	1.6	1.0	ohms
R_t	49	40	28	12	14.0	12.5	11.6	11.2	ohms
$\int E dt$	.12	.2	.6	1.5					volt-sec/m
V_s	3×10^{6}	4×10^{6}	5.4×10^{6}	2.1×10^{6}					volts
V_E	0	4.3×10^{5}	1.3×10^{6}	3.3×10^{6}	3.1×10^{6}	1.8×10^{6}	3.7×10^{5}	7.8×10^{4}	volts
V_t	3×10^{6}	4.4×10^{6}	6.7×10^{6}	5.4×10^{6}	3.1×10^{6}	1.8×10^{6}	3.7×10^{5}	7.8×10^{4}	volts
L_E	0	2.4×10^{-4}	7.2×10^{-4}	1.2×10^{-3}	1.4×10^{-3}	1.4×10^{-3}	1.3×10^{-3}	1.1×10^{-3}	henries
$I_1=\frac{V_t}{R_t}$	6.3×10^{4}	1.1×10^{5}	2.4×10^{5}	4.5×10^{5}	2.2×10^{5}	1.4×10^{5}	3.2×10^{4}	7.0×10^{3}	amps
$\frac{L_E}{I_1}\frac{\partial I_1}{\partial t}$	0	12	14	4	-1.3	-1.4	-.6	-.15	ohms
I_2	6.3×10^{4}	8.4×10^{4}	1.6×10^{5}	3.4×10^{5}	2.4×10^{5}	1.6×10^{5}	3.4×10^{4}	7.1×10^{3}	amps

6-5. Hildebrand, F. B., "Advanced Calculus for Applications," Prentice-Hall, Inc., Englewood Cliffs, New Jersey, 1962. The solution of equations of the form of (6-105) is on page 156.

6-6. Erdelyi, A., W. Magnus, F. Oberhettinger, and F. G. Tricomi, Tables of Integral Transforms, McGraw-Hill Book Company, New York, 1954.

CHAPTER 7
COUPLING TO SHORT VERTICAL CONDUCTORS

7.1 INTRODUCTION

Systems that are hardened to source-region EMP from surface or near-surface nuclear explosions, and to the accompanying blast effects, are unlikely to use above-ground vertical antennas for mission-critical functions. However, such antennas and other vertical conductors may be present as part of non-survivable subsystems that serve peacetime functions. Examples are communications antennas for maintenance and security operations, light poles, etc. It is necessary to know what currents will be collected by such structures under EMP conditions and whether these currents can get into the parts of the system that are required to survive.

It is likely that such structures will be no more than about 10 meters in height and no more than 0.3 meters in diameter. Thus the incident vertical electric field can be taken as uniform around the circumference. Usually, the conductor will be thin to gamma rays, but we shall include the case in which it is not. The conductor may or may not be grounded at its base, but since it is not likely to be hardened to EMP, an arc to ground may form anyway. For the purposes of this chapter we shall assume that the base of the structure is in electrical contact with soil; the impedance of this connection is included in the analysis. One would hope that a wire does not run from the structure into any shielded enclosure containing mission-critical electronic equipment. The current flowing into such wires could be calculated, usually as a perturbation, if the specifics of their connection were known.

7.2 DRIVING FIELD AND SKIN DEPTHS

We shall use the vertical field E_θ graphed in Figure 3-5 as an example in this chapter. That field is appropriate at the ground-air surface. We need to discuss how E_θ depends on height above the surface. This discussion uses ideas contained in Sections 3.8 and 3.9.

At the onset of α-saturation at the location of our conductor, E_θ extends into the air to a height (Equation 3-49)

$$\delta_E \approx c/\alpha \approx 1.5 \text{ meters (example)} . \tag{7-1}$$

This is the time when E_θ reaches its peak value. Previous to this time (in the period of λ-saturation) E_θ has been rising as $e^{\alpha t/2}$, and δ_E has been decreasing. The current in the conductor at ground level cannot be appreciably affected by the field at heights greater than $2c/\alpha$. Thus, for times before the peak of E_θ, it is a modest overestimate to assume that the driving field is independent of height up to δ_E.

After the onset of α-saturation, E_θ extends up to the conductivity-determined skin depth δ_a in the air. In this (diffusion) phase also, the conductor current at ground level cannot depend on the field at heights greater than δ_a. Thus again only a modest overestimate is made by regarding E_θ as independent of height up to δ_a. Eventually, the incident E_θ is indeed independent of height, at least up to 10 meters. We shall regard it as constant in height at all times over that range of heights which can affect the current at the base.

A composite formula for this height is

$$\begin{aligned} \delta_a &= c/\alpha \quad \text{when} \quad \sigma < \varepsilon_0\alpha , \\ &= 1/\sqrt{\mu_0\sigma\alpha} \quad \text{when} \quad \varepsilon_0\alpha < \sigma < \sigma_p , \\ &= \sqrt{\frac{t}{(n+1)\mu_0\sigma}}\left[1 - \frac{\sigma t_p}{\sigma_p t}\left(1 - \frac{n+1}{\alpha t_p}\right)\right]^{1/2} \text{after peak } \sigma . \end{aligned} \tag{7-2}$$

The first line here is appropriate up to the time of the peak in E_θ, the phase in which displacement current exceeds conduction current. The second line is appropriate from this time up to the time of the peak in σ. The third line is appropriate after σ has peaked, and is based on the assumption that σ falls as t^{-n}. The power n is determined by

$$n = [\ell n(\sigma_p/\sigma)]/[\ell n(t/t_p)] \ , \tag{7-3}$$

where $\sigma = \sigma(t)$ and $\sigma_p = \sigma(t_p)$. The value of n varies somewhat with t.

It can be seen that Equation 7-2 provides continuous values of δ_a. For the conductivity of Figure 3-3, the δ_a computed from Equation 7-2 is graphed in Figure 7-1. For this case, $\alpha = 2 \times 10^8$ sec^{-1}.

We see from Figure 7-1 that δ_a reaches 10 meters at $t = 2 \times 10^{-6}$ second. As will be seen, the coupling to a conductor of height h depends on whether δ_a is smaller or greater than h.

7.3 INDUCTIVELY LIMITED CURRENT

The current in the conductor is limited, in varying degrees at various times, by both inductive and capacitive reactance and by resistance in both air and ground. We shall first calculate the current based on inductive limitation alone. This calculation assumes that $h >> \delta_a$, that the ground is perfectly conducting, and that the driving field E_0 is independent of height. The current I in the conductor is determined by the equation

$$\frac{d}{dt}(LI) = E_0(t) \ . \tag{7-4}$$

The inductance L per unit length is

$$L = \frac{\mu_0}{2\pi} \ell n\left(1 + \frac{\delta_a}{a}\right) \frac{\text{henry}}{\text{meter}} \ , \ \left(\frac{\mu_0}{2\pi} = 2 \times 10^{-7}\right) \ . \tag{7-5}$$

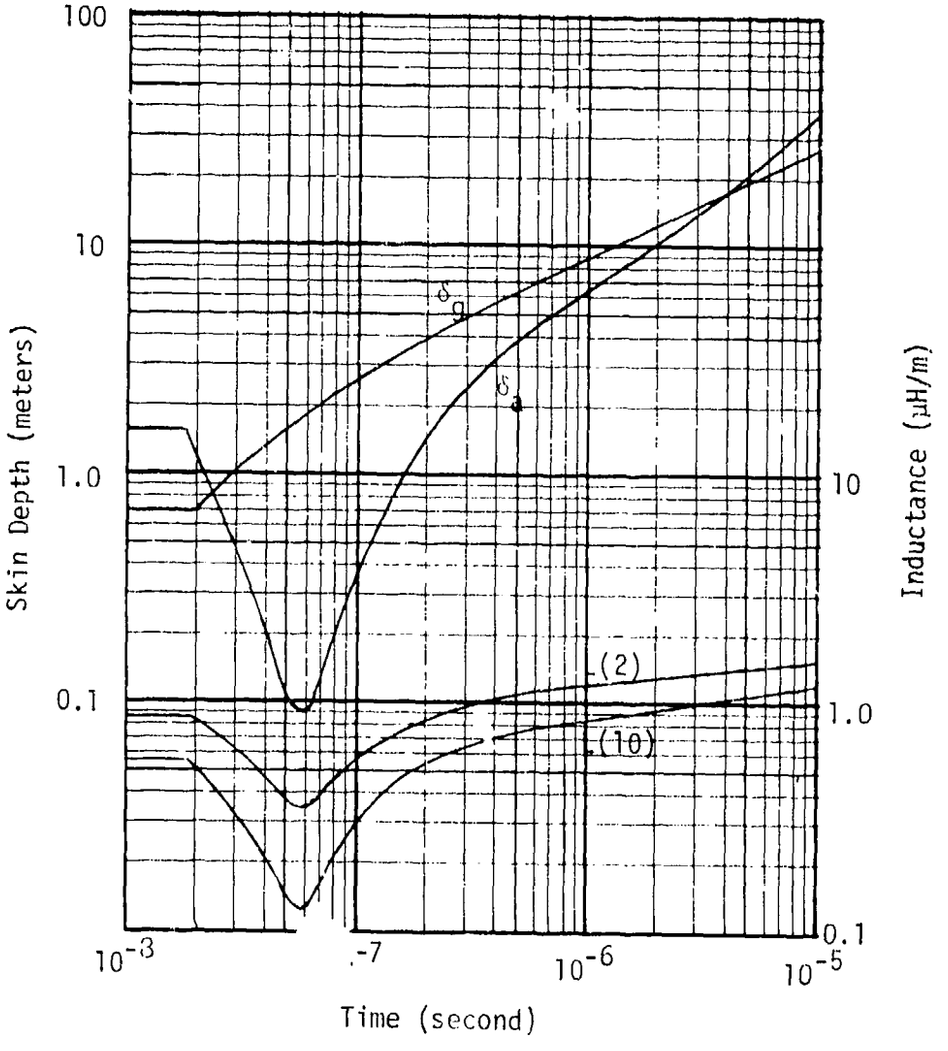

Figure 7-1. Skin depths δ_a in air and δ_g in ground. Inductances L(2) and L(10) of 2 and 10 cm radius conductors.

Here a is the radius of the conductor. The argument of the logarithm has been written so as to cover the possibility that δ_a may be less than a. We shall treat two examples, with $a = 2$ cm and 10 cm. The inductance for these two cases is graphed in Figure 7-1.

Before α-saturation, L is constant and E rises exponentially as $e^{\alpha t/2}$. In this phase,

$$I(t) = \frac{2}{\alpha L} E_\theta(t) \ . \tag{7-6}$$

For the two conductors chosen as examples,

$$\left.\begin{aligned} \frac{\alpha L}{2} &= 87 \text{ ohms/m} \quad , \quad a = 2 \text{ cm} \ , \\ &= 55 \text{ ohms/m} \quad , \quad a = 10 \text{ cm} \ . \end{aligned}\right\} \tag{7-7}$$

At the time of α-saturation, E_θ reaches its peak value and is no longer rising exponentially. Use of the peak value of E_θ from Figure 3-5 would give an underestimate of the current at this time. Use of the exponentially extrapolated value of E_0, i.e., $E_\theta = cB_\phi$, will give an overestimate. We choose the latter, setting

$$E_\theta(\text{peak}) = 2 \times 10^5 \text{ V/m} \ . \tag{7-8}$$

Thus the currents at this time are

$$\left.\begin{aligned} I(\alpha\text{-sat.}) &= 2.3 \times 10^3 \text{ Amp} \ , \ a = 2 \text{ cm} \ , \\ &= 3.6 \times 10^3 \text{ Amp} \ , \ a = 10 \text{ cm} \ . \end{aligned}\right\} \tag{7-9}$$

In Figure 3-5, α-saturation occurs at 1.8×10^{-8} second. According to Figure 3-3, σ continues to rise exponentially (as $e^{\alpha t}$) until about 5×10^{-8} second, then changes much more slowly. The increase in σ causes the decrease in inductance shown in Figure 7-1. During this period of decreasing inductance it is not correct to keep L inside the time derivative in Equation 7-4, as we shall now explain.

The magnetic flux Φ circling the conductor is determined by integrating the Maxwell equation

$$\frac{\partial B}{\partial t} = \frac{\partial E}{\partial r} \tag{7-10}$$

over r from the radius a of the conductor to large distances. (In this equation E is the electric field parallel to the conductor and B is the magnetic field circling the conductor). Integration over r yields

$$\frac{\partial \Phi}{\partial t} = \frac{\partial}{\partial t}\int B dr = E_\infty - E(a) = E_\theta \ , \tag{7-11}$$

where E_∞ is the electric field at large distances and $E(a) = 0$ is the field at the conductor surface (resistance of conductor neglected). E_∞ is the E_θ of the burst coordinate system. Equation 7-11 would be the same as Equation 7-4 if we define the inductance by the Equation $\Phi = LI$. The inductance defined by Equation 7-5 assumes that $B \sim I/r$ out to $r = a + \delta_a$ and then falls rapidly. That assumption is not correct when the conductivity increases rapidly with time. In this case, magnetic flux produced in a given time interval $1/\alpha$ is frozen in place shortly afterward by the increasing conductivity. The additional flux produced in the next time interval is distributed only over the decreased skin depth given by the second line of Equation 7-2. Thus the inductance defined using this skin depth applies only to the increment in current in the next time interval, and all previously established current is frozen in, i.e., does not change appreciably. Therefore, in the time period from α-saturation to the time 5×10^{-8} second when σ stops increasing exponentially, Equation 7-4 should be replaced by

$$\frac{dI}{dt} = \frac{E_0}{L} \ . \tag{7-12}$$

In the time period indicated here, the ratio E_0/L does not change much for either of our example conductors. Average values are

$$E_\theta/L = 1.5 \times 10^{11} \text{ Amp/sec} , \quad a = 2 \text{ cm} ,$$
$$= 2.9 \times 10^{11} \text{ Amp/sec} , \quad a = 10 \text{ cm} . \tag{7-13}$$

The increase in current in this time period is therefore

$$\Delta I = 4.8 \times 10^3 \text{ Amp} , \quad a = 2 \text{ cm} ,$$
$$= 9.3 \times 10^3 \text{ Amp} , \quad a = 10 \text{ cm} . \tag{7-14}$$

Equation 7-4 would have given a larger increase in current in this time period, since that equation can be written as

$$\frac{dI}{dt} = \frac{E_0}{L} - \frac{I}{L}\frac{dL}{dt} . \tag{7-15}$$

During the period after θ peaks, in which L increases, this equation would yield smaller currents than Equation 7-12. Which equation should we use in this time period? We argue as follows. The flux going with the current at the time of α-saturation, Equation 7-9, is frozen in over radii up to $\delta_a = 1.5$ meters and will not diffuse appreciably until $t = 2 \times 10^{-7}$ second when δ again reaches that value; that part of the current will remain constant. We add to this constant current one half of ΔI, Equation 7-14. The other half of ΔI is associated (we say) with flux distributed only up to $\delta_a(\text{min}) = 0.09$ meters, and this flux diffuses immediately, together with additional flux produced by E_0 after $t = 5 \times 10^{-8}$ second. For this part of the current Equation 7-4 is appropriate. Thus the current has two parts, for which, until $t = 2 \times 10^{-7}$ second,

$$I_1 = \text{constant} = 4.7 \times 10^3 \text{ Amp} , \quad a = 2 \text{ cm} ,$$
$$= 8.2 \times 10^3 \text{ Amp} , \quad a = 10 \text{ cm} , \tag{7-16}$$

and

$$\frac{d}{dt}(LI_2) = E_0 , \tag{7-17}$$

where, at $t = 5 \times 10^{-8}$ second,

$$I_2 = \frac{\Delta I}{2} = 2.4 \times 10^3 \text{ Amp}, \; a = 2 \text{ cm}, \qquad = 4.6 \times 10^3 \text{ Amp}, \; a = 10 \text{ cm}. \tag{7-18}$$

Hand integration of Equation 7-17 in three steps yields for the total current:

$t = 5 \times 10^{-8}$	7×10^{-8}	1×10^{-7}	2×10^{-7} sec	(7-19)
I = 7.1	8.5	8.4	9.6 KA, a = 2 cm	
I = 12.8	15.9	14.3	15.3 KA, a = 10 cm	

The currents are graphed as a function of time in Figure 7-2.

After $t = 2 \times 10^{-7}$ second, all of the flux diffuses, and Equation 7-2 is appropriate. Since E_0 is approximately constant in this period, that equation yields

$$LI = (LI)_i + (t-t_i)E_0 . \tag{7-20}$$

where the subscript i indicates evaluation at $t = 2 \times 10^{-7}$ second. Currents calculated from this equation are used to extend the curves in Figure 7-2 out to 10^{-5} second.

7.4 EFFECT OF GROUND TERMINATION

In considering the effect of a finitely conducting ground termination of the vertical conductor, it is important to understand that the current carried by the conductor is exactly equal to the current (conduction and displacement) removed from the surrounding medium due to the presence of the conductor. This follows from the fact that the magnetic field at distances appreciably larger than the skin depth is unaffected by the presence of the conductor; hence the net change in current over an area comparable with $\pi\delta_a^2$ must vanish by Stokes' theorem.

The flow of (the change in) current in the ground must therefore be as sketched in Figures 7-3a and 7-3b for the cases in which the air

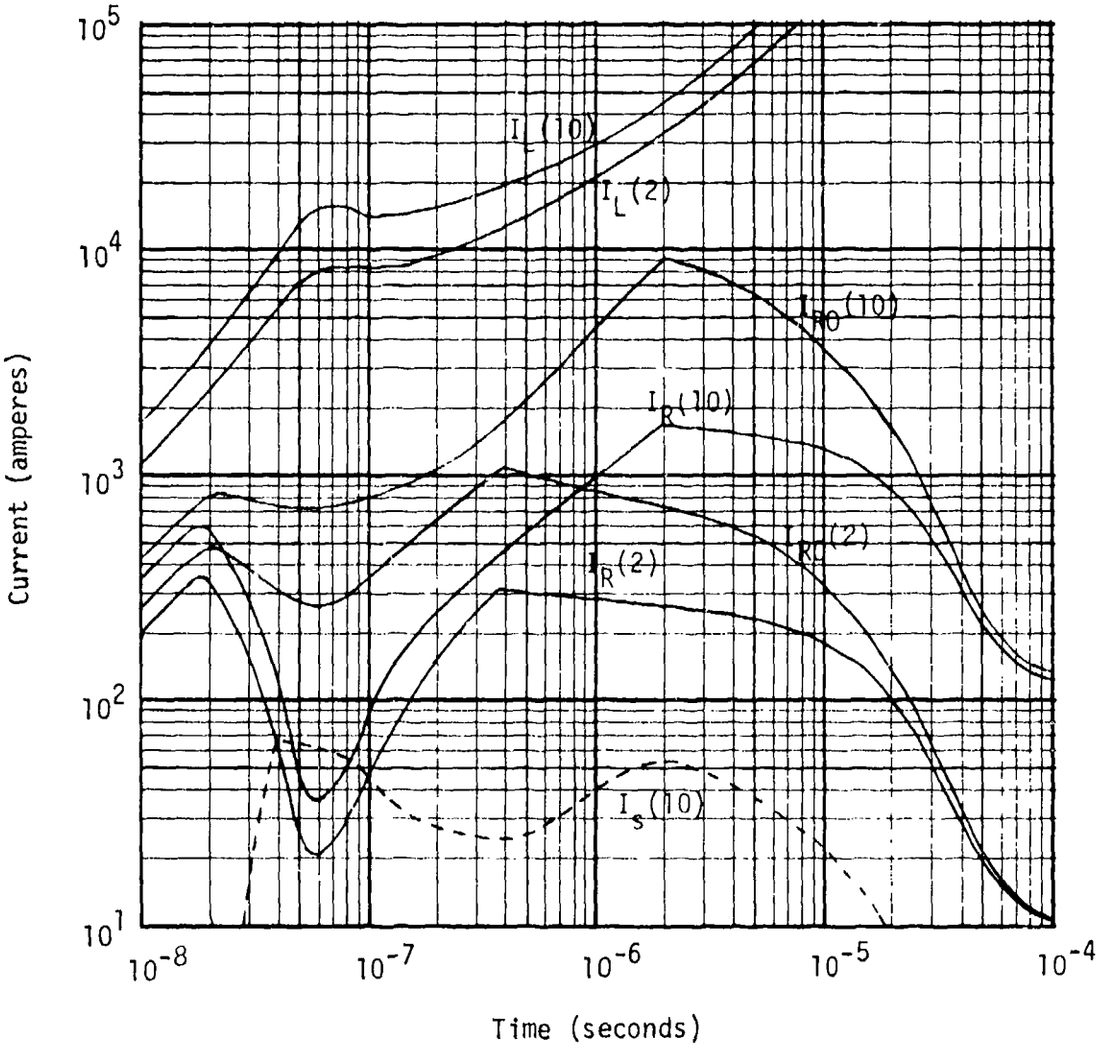

Figure 7-2. Currents at base of conductor. I_L, inductively limited current; I_R, resistively limited current; I_{R0}, resistively limited current with perfectly conducting ground; I_S, Compton current collected by aluminum pipe conductor. Number in parentheses is radius of conductor in cm. Conductor (2) is 3 m high, conductor (10) is 10 m high.

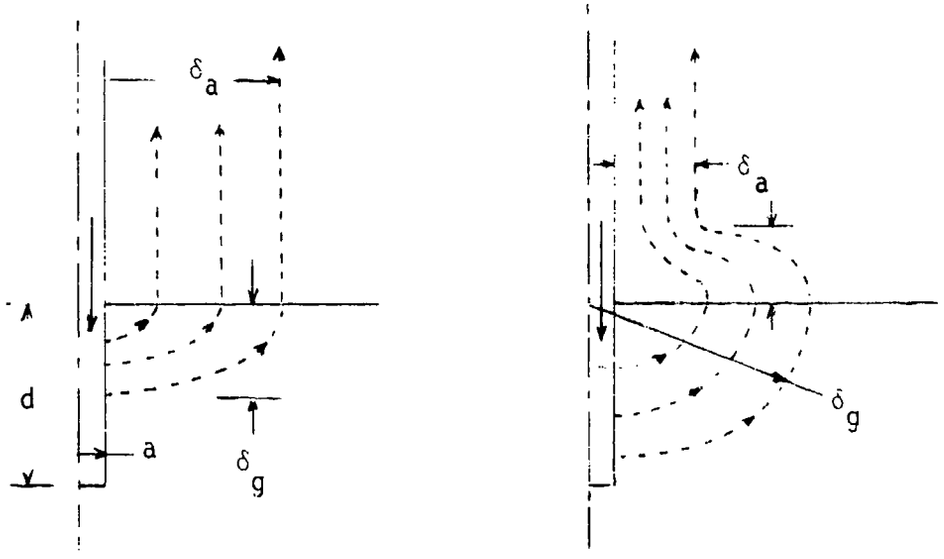

a. $\sigma_a < \sigma_g$, $\delta_a > \delta_g$ b. $\sigma_a > \sigma_g$, $\delta_a < \delta_g$

Figure 7-3. Current flow patterns in air and ground near conductor.

conductivity σ_a is less or greater than the ground conductivity σ_g. This figure has been drawn for the case in which the conductor extends to a depth $d > \delta_g$ into the ground. The resistances in the ground termination are estimated as

$$R_t = \frac{1}{2\pi\sigma_g \delta_g} \ln\left(1 + \frac{\delta_a}{a}\right) , \quad (\delta_a > \delta_g < d) , \tag{7-21}$$

$$R_t = \frac{1}{2\pi\sigma_g \delta_g} \ln\left(1 + \frac{\delta_g}{a}\right) , \quad (\delta_a < \delta_g < d) . \tag{7-22}$$

At late times, the condition $\delta_a > \delta_g > d > a$ is likely to hold. In this case an estimate of R_t is

$$R_t = \frac{1}{2\pi\sigma_g d} \left[\ln\left(\frac{d}{a}\right) + 1 - \frac{d}{\delta_g}\right] + \frac{1}{2\pi\sigma_g \delta_g} \ln \frac{\delta_a}{\delta_g} . \tag{7-23}$$

In the time period before α-saturation, the conductor current rises exponentially as $e^{\alpha t/2}$. In this period,

$$\delta_a = c/\alpha \quad , \quad \delta_g = \sqrt{\frac{2}{\mu_0 \sigma_g \alpha}} \quad . \tag{7-24}$$

With $\alpha = 2 \times 10^8$ sec^{-1} and $\sigma_g = 1.6 \times 10^{-3}$ mho/m (10 percent water soil at frequency 1.6×10^7 Hz, see Chapter 2) we obtain

$$\delta_a = 1.5 \text{ m} \ , \ \delta_g = 0.7 \text{ m} \ . \tag{7-25}$$

Equation 7-21 gives

$$\left.\begin{aligned} R_t &= 61 \text{ ohms} \ , \ a = 2 \text{ cm} \ , \\ &= 39 \text{ ohms} \ , \ a = 10 \text{ cm} \ . \end{aligned}\right\} \tag{7-26}$$

Now according to Equation 7-7, the inductive reactance of a length $\delta_a = 1.5$ meters of the conductor is 130 and 82 ohms in the two cases. Thus the current before α-saturation will be reduced by a factor of about

$$\frac{130}{130 + 61} = 0.68 \sim \frac{82}{82 + 39} \ , \tag{7-27}$$

in both cases because of the termination resistance.

By $t = 5 \times 10^{-8}$ second, the rise time τ (e-folding time) of the conductor current has increased to about

$$\tau \sim 2.6 \times 10^{-8} \text{ second} \ . \tag{7-28}$$

At frequency $1/2\pi\tau \sim 6 \times 10^6$ Hz, Chapter 2 gives $\sigma_g = 1.3 \times 10^{-2}$ mho/m, and

$$\delta_g = \sqrt{\frac{t}{\mu_0 \sigma_g}} \sim 1.3 \text{ m} \ . \tag{7-29}$$

As described in Section 7.3, the magnetic flux in the air is distributed over a range of radii (δ_a's) from 0.09 to 1.5 meters. The geometric mean gives $\delta_a = 0.37$ meter. Equation 7-22 then gives the termination resistance

$$R_t = 39 \text{ ohms} , \; a = 2 \text{ cm} ,$$
$$= 24 \text{ ohms} , \; a = 10 \text{ cm} . \qquad (7\text{-}30)$$

At $\delta_a = 0.37$ meter, the inductance of a length δ_a of the conductor is

$$\left.\begin{aligned} L\delta_a &= 0.22 \; \mu\text{H} , \; a = 2 \text{ cm} , \\ &= 0.11 \; \mu\text{H} , \; a = 10 \text{ cm} . \end{aligned}\right\} \qquad (7\text{-}31)$$

The relaxation time of the current into the ground is

$$\frac{L\delta_a}{R_t} = 0.56 \times 10^{-8} \text{ sec} , \; a = 2 \text{ cm} ,$$
$$= 0.46 \times 10^{-8} \text{ sec} , \; a = 10 \text{ cm} . \qquad (7\text{-}32)$$

because this relaxation time is short compared with the rise time τ of the conductor current, most of the conductor current indicated in Figure 7-2 will flow in the air just above the ground rather than in the ground. The fraction of the current flowing in the ground is about

$$\frac{\sigma_g \delta_g}{\sigma_g \delta_g + \sigma_a \delta_a} = \frac{(0.013)(1.3)}{0.0169 + (0.4)(0.37)} = 0.10 . \qquad (7\text{-}33)$$

Thus the ground termination resistance substantially reduces the current in the base of the conductor at times in the neighborhood of 5×10^{-8} second. If the ground surface is covered by a conducting sheet or counter poise, the current in Figure 7-2 is correct.

7.5 RESISTIVELY LIMITED CURRENT

Section 7.4 has shown that resistance of the ground termination affects the current at the base of the conductor at quite early times. As the air conductivity falls (Figure 3-3), resistance in the air will also limit the current. In this section, we shall ignore inductive effects and calculate the current as in a static problem. It is helpful to distinguish

between two phases, according to whether the skin depth δ_a in the air is less or larger than the height h of the conductor.

First Phase: $\delta_a < h$.

The vertical electric field E_θ is not just a static field; the curl of $\vec{E}$ does not vanish at early times since, as shown by Figure 3-5, B_ϕ changes rapidly with time before $t = 10^{-7}$ second. However, that does not matter for the conductor response, which depends only on the vertical electric field. The same E_θ at the position of the (thin) conductor, even if it were derivable from a potential, would produce the same current in the conductor. We can therefore, for the convenience of familiarity, think in terms of a voltage $V(z)$,

$$V(z) = \int_0^z E_0(z')dz' \ , \qquad (7\text{-}34)$$

where z is the distance above the ground surface.

In the diffusion phase (which begins at α-saturation), E_θ extends only up to the skin depth δ_a above the ground; above that height the electric field is approximately radial from the burst point. Thus $V(z)$ has the z-dependence indicated in Figure 7-4a. The maximum voltage V_m is about

$$V_m \approx E_0\delta_a \ , \qquad (7\text{-}35)$$

where E_θ is the field just above the ground.

If we imagine the conductor to be opened just above the ground, as in Figure 7-4b, to what voltage will the conductor come? Remember that the conductor is in a conducting medium. Because currents in the conductor are limited by diffusion in this medium, the lower end of the opened conductor cannot be affected by conditions existing at heights much greater

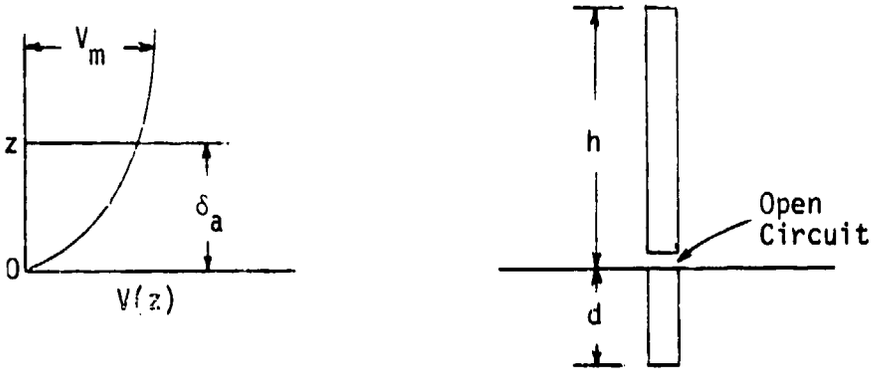

Figure 7-4. Potential function and open circuited conductor.

than δ_a. We conclude therefore that the open-circuit voltage of the conductor is about

$$V_0 \approx V_m/2 \approx E_0\delta_a/2 \ . \tag{7-36}$$

If we now reconnect the conductor to its ground end, a current will flow across the junction. The magnitude of this current will be

$$I = V_0/(R_i+R_t) \ , \tag{7-37}$$

where R_i is the "internal" resistance of the source of V_0 and R_t is the ground termination resistance. R_t has been estimated by Equations 7-21, 22 and 23. An estimate of R_i is

$$R_i = \frac{1}{2\pi\sigma_a\delta_a} \ln\left(1 + \frac{\delta_a}{a}\right) \ . \tag{7-38}$$

This is the resistance between a conductor of radius a, length δ_a and distant points in a medium of conductivity σ_a.

Second Phase: $\delta_a > h$.

In this phase the open-circuit voltage is about

$$V_0 \approx E_0 h/2 \ , \tag{7-39}$$

and the reconnected current is

$$I = V_0/(R_i'+R_t') \ . \tag{7-40}$$

The internal resistance here is modified by replacing δ_a with h, i.e.,

$$R_i' = \frac{1}{2\pi\sigma_a h} \ln(\frac{h}{a}) \ , \tag{7-41}$$

and the termination resistance is

$$R_t' = \frac{1}{2\pi\sigma_g \delta_g} \ln(\frac{h}{a}) \quad , \quad (h > d > \delta_g) \ , \tag{7-42}$$

$$= \frac{1}{2\pi\sigma_g d} [\ln(\frac{d}{a}) + 1 - \frac{d}{\delta_g}] + \frac{1}{2\pi\sigma_g \delta_g} \ln(\frac{h}{\delta_g}) \ , \ (h > \delta_g > d) \ , \tag{7-43}$$

$$= \frac{1}{2\pi\sigma_g d} [\ln \frac{d}{a} + 1 - \frac{d}{h}] \quad , \quad (\delta_g > h > d) \ . \tag{7-44}$$

The estimates given here are continuous between the three regimes of δ_g.

Let us calculate the resistively limited current for our two examples, choosing the heights and depths

$$\begin{aligned} h &= 3 \text{ m} \ , \ d = 1 \text{ m} \quad \text{for} \quad a = 2 \text{ cm} \ , \\ &= 10 \text{ m} \ , \ d = 1 \text{ m} \quad \text{for} \quad a = 10 \text{ cm} \ . \end{aligned} \tag{7-45}$$

The skin depth δ_a in the air has been graphed in Figures 7-1. For the soil we take $\sigma_g = 0.01$ mho/meter and

$$\sigma_g = \sqrt{(0.7 \text{ m})^2 + \frac{t'}{\mu_0 \sigma_g}} \ , \tag{7-46}$$

where

$$t' = t - 2 \times 10^{-8} \text{ sec} \ . \tag{7-47}$$

This estimate of δ_g is continuous with the value in the exponential phase given by Equation 7-25. δ_g is also graphed in Figure 7-1.

The first phase, $\delta_a < h$, ends at

$$\left.\begin{aligned} t_1 &= 3.7 \times 10^{-7} \text{ sec} \quad \text{for} \quad a = 2 \text{ cm} , \\ &= 2.0 \times 10^{-6} \text{ sec} \quad \text{for} \quad a = 10 \text{ cm} . \end{aligned}\right\} \tag{7-48}$$

In this phase V_0 is given by Equation 7-36 and R_i by Equation 7-38. These quantities are graphed in Figure 7-5, where they are also extended into the second phase, $\delta_a > h$, by use of Equations 7-39 and 7-41.

For the termination resistance, we see that δ_g is greater than the assumed d at almost all times of interest, and that $\delta_g > \delta_a$ in most of the first phase (when $\delta_a < h$). Since Equations 7-21, 22, 23 do not apply in this case, we need another estimate of R_t for the case $h > \delta_a$, $\delta_g > \delta_a$, $\delta_g > d$. This is

$$R_t = \frac{1}{2\pi\sigma_g d} \ln\left(\frac{d}{a}\right) \quad , \quad (\delta_a < d) , \tag{7-49}$$

$$= \frac{1}{2\pi\sigma_g d} \left[\ln\left(\frac{d}{a}\right) + 1 - \frac{d}{\delta_a}\right] \quad , \quad (\delta_a > d) . \tag{7-50}$$

From Figure 7-1 we see that δ_a exceeds d after $t = 1.6 \times 10^{-7}$ second. Before this time, Equation 7-49 gives R_t. From this time until t_1 (Equation 7-48), R_t is given by Equation 7-50. After t_1, R_t is given by Equation 7-44. R_t is also graphed in Figure 7-5 for the two conductors.

In computing R_i at times before α-saturation in Figure 7-5, we have replaced σ_a by $\varepsilon_0\alpha$ in Equations 7-38 and 7-41, since the displacement current is larger than the conduction current in that phase. Hence the current is limited by capacitive reactance rather than by air resistance in that phase. Note that the capacitive reactance is real for exponentially rising field, and is approximately constant.

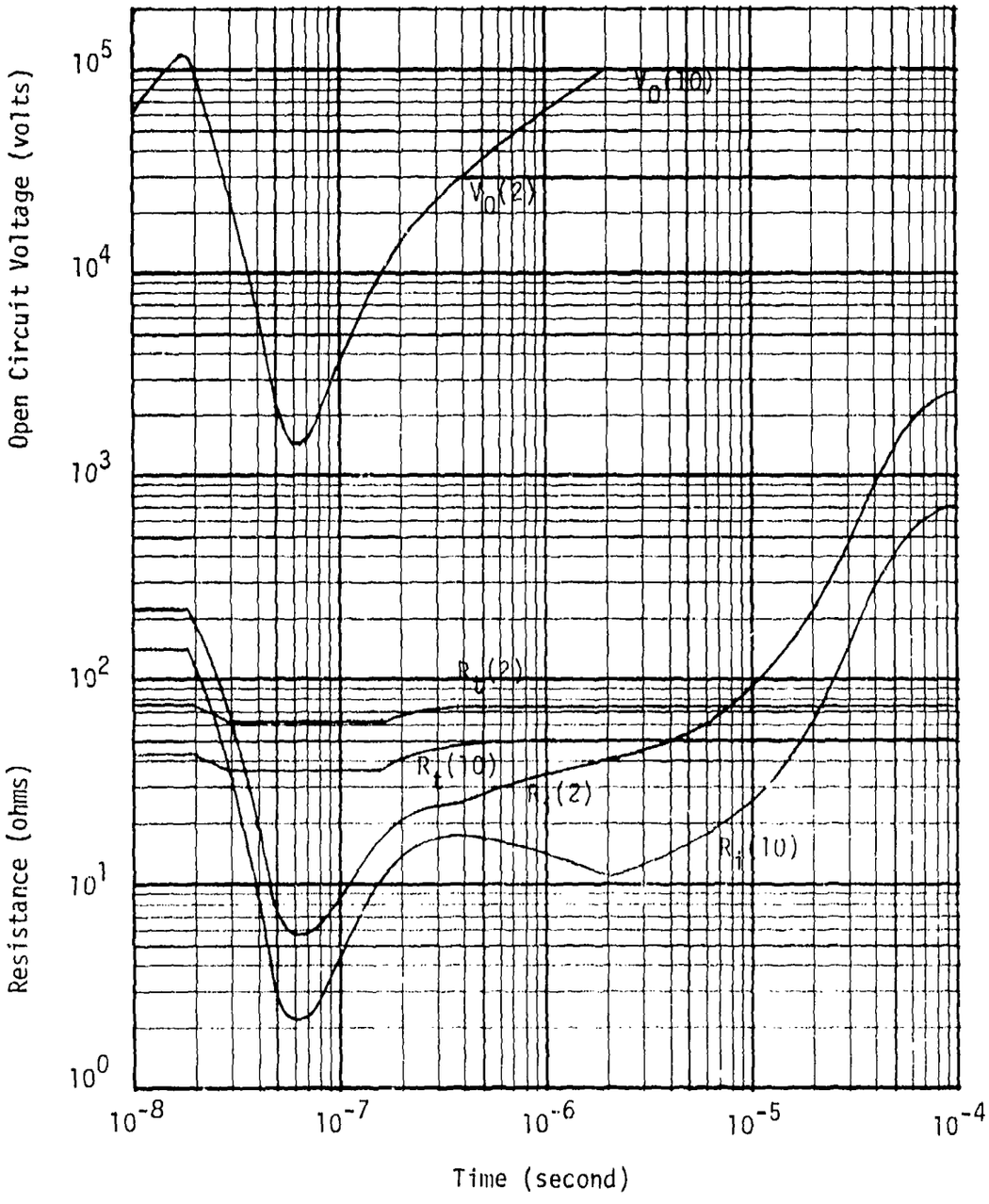

Figure 7-5. Open circuit voltage V_0 of two vertical conductors: (2) 2 cm radius, 3 m high; (10) 10 cm radius, 10 m high. Source resistance R_i and termination resistance R_t for the two conductors.

The resistively (and capacitvely) limited currents calculated from Equations 7-37 and 7-40 are graphed in Figure 7-2, for the two conductor radii and for both perfectly and imperfectly conducting ground. It is seen that these currents are substantially smaller at all times than the inductively limited current. For the examples considered, inductive reactance is small at all times compared with resistance or capacitive reactance. The correct current I can be estimated from the equation

$$I \approx I_R I_L/(I_R+I_L) \ , \qquad (7\text{-}51)$$

where I_R and I_L are the resistively and inductively limited currents. I is only a little less than I_R in our examples. The sign of the current is such that electrons flow down the conductor into the ground.

7.6 COMPTON CURRENT COLLECTION

If the conductor provides appreciable attenuation of the gamma rays, the Compton current emerging from its back side will be less than that entering its front side. Thus the conductor collects negative charge due to gamma attenuation. Gamma attenuation lengths are of the order of 30 grams/cm^2.

If the conductor is made of high-atomic-number material, then the ratio of Compton electron flux to gamma flux coming out of the conductor is smaller than the ratio going in, provided the conductor is an electron range in thickness. Compton electron ranges are of the order of 0.3 grams/cm^2 in air and aluminum, but are smaller (due to nuclear scattering) in high Z materials. Most conductors will be thicker than an electron range. An iron conductor collects about 30 percent of the Compton current striking it, even without the gamma attenuation effect.

Let us assume that our 10 cm radius conductor is an aluminum pipe (density ρ = 2.7 gram/cm^3) with wall thickness D = 1/4 inch $\approx$ 0.6 cm. Its average projected thickness in grams/cm^2 is then

$$m = \frac{2\pi a D \rho}{2a} = \pi D \rho = 5.1 \text{ gram/cm}^2 \ . \qquad (7\text{-}52)$$

The fraction of Compton current collected, due to gamma attenuation, is

$$f = 1 - \exp(-m/30) \approx 0.16 \ . \qquad (7\text{-}53)$$

The total Compton current collected in a height of the pipe equal to the smaller (δ_a, h) of δ_a and h is

$$I_s = 2fJ_s a(\delta_a, h) \ , \qquad (7\text{-}54)$$

where J_s is the Compton current density, which we take from Figure 3-2. The current computed from Equation 7-54 is also graphed in Figure 7-2. Note that it is small compared with the other currents, except for a short period of time for the resistvely limited currents into imperfectly conducting ground. Actually, the current I_s affects the resistvely limited current. Since the impedance of the Compton current source is very large, the current into the ground is given by

$$\begin{aligned} I &= \frac{V_0}{R_i + R_t} + \frac{I_s R_i}{R_i + R_t} \\ &= I_R + I_s \frac{R_i}{R_i + R_t} \ , \end{aligned} \qquad (7\text{-}55)$$

where I_R is the resistively limited current calculated in Section 7.5 We see from Figure 7-5 that the ratio $R_i/(R_i+R_t)$ is small (≈ 0.1) in the time period in which I_s exceeds I_R. Thus the collected Compton current makes little difference for our aluminum conductor. If the pipe were made of iron, f and I_s would be about four times larger than for aluminum.

7.7 NUCLEAR LIGHTNING

It is likely that a discharge would form in the air at the upper end of the conductors in our examples, and grow upwards. Such discharges were

observed in several large yield nuclear tests. The theory of this "nuclear lightning" is currently under development at MRC (by J. Gilbert, R. Gardner, M. Frese, and C. Longmire). It is believed that the currents in these discharges reach peak values of several times 10^4 amperes, much larger than the resistively limited currents of Figure 7-2 because of the increased height of the discharges. These heights were observed to reach several hundred meters in the millisecond time frame. The authors hope to add a chapter on nuclear lightning to this report when the theory is firmly established.

DISTRIBUTION LIST

DEPARTMENT OF DEFENSE

Assistant to the Secretary of Defense
Atomic Energy
ATTN: Executive Assistant

Defense Communications Agency
ATTN: Code 312
ATTN: Code C313

Defense Communications Engineer Center
ATTN: Code R400
ATTN: Code R123
ATTN: Code R720, C. Stansberry

Defense Intelligence Agency
ATTN: DB 4C2, D. Spohn
ATTN: RDS-3A

Defense Nuclear Agency
2 cy ATTN: RAEV
2 cy ATTN: RAEE
4 cy ATTN: TITL

Defense Technical Information Center
12 cy ATTN: DD

Field Command
Defense Nuclear Agency
ATTN: FCP
ATTN: FCLMC

Field Command
Defense Nuclear Agency
Livermore Branch
ATTN: FCPRL

Interservice Nuclear Weapons School
ATTN: TTV

Joint Strat Tgt Planning Staff
ATTN: NRI STINFO, Library

Under Secretary of Defense for Rsch & Engrg
Department of Defense
ATTN: Strategic & Space Sys (OS)

DEPARTMENT OF THE ARMY

BMD Systems Command
Department of the Army
ATTN: BMDSC-HLE, R. Webb
ATTN: BMDSC-AOLIB
ATTN: BMDSC-HW, R. DeKalb

U.S. Army Engineer Div, Huntsville
ATTN: T. Bolt

U.S. Army Intelligence & Sec Cmd
ATTN: Technical Library
ATTN: Tech Info Fac

DEPARTMENT OF THE ARMY (Continued)

Harry Diamond Laboratories
Department of the Army
ATTN: DELHD-N-EMD
ATTN: DELHD-N EM
ATTN: DELHD-N-RCC
ATTN: DELHD-N-RB
ATTN: NWPO
ATTN: DELHD-I-TL
ATTN: DELHD-N-TD
ATTN: DELHD-N-TF
ATTN: DELHD-N-EMC
ATTN: DELHD-N-EMA
ATTN: DELHD-N EMB
ATTN: DELHD-N-EME
2 cy ATTN: DELHD-N-RBC

DEPARTMENT OF THE NAVY

Naval Ocean Systems Center
ATTN: Code 54, C. Fletcher
ATTN: Code 08, J. Rockway
ATTN: Code 7309, R. Greenwell
ATTN: Code 8123, S. Lichtman

Naval Postgraduate School
ATTN: Code 1424, Library

Naval Research Laboratory
ATTN: Code 1434, E. Brancato
ATTN: Code 2627, D. Folen
ATTN: Code 6624
ATTN: Code 6623, R. Statler

Naval Surface Weapons Center
ATTN: Code F32, E. Rathbun
ATTN: Code F30

Naval Surface Weapons Center
ATTN: Code F-56

Strategic Systems Project Office
Department of the Navy
ATTN: NSP-43

DEPARTMENT OF THE AIR FORCE

Air Force Weapons Laboratory
Air Force Systems Command
ATTN: CA
ATTN: NTYE, J. Castillo
ATTN: NT
ATTN: NTYEE, C. Baum
ATTN: NTYEP, W. Page

Air University Library
Department of the Air Force
ATTN: AUL-LSE

Ballistic Missile Office
Air Force Systems Command
ATTN: ENSN, J. Allen

DEPARTMENT OF THE AIR FORCE (Continued)

Foreign Technology Division
Air Force Systems Command
ATTN: TQTD, B. Ballard
ATTN: NIIS, Library

Strategic Air Command
Department of the Air Force
ATTN: NRI STINFO, Library
ATTN: NRI, G. Matzke
ATTN: DLL
ATTN: XPFS, F. Tedesco

DEPARTMENT OF ENERGY

Department of Energy
Albuquerque Operations Office
ATTN: WSSC
ATTN: CTID

Department of Energy
Economic Regulatory Administration
ATTN: Office of Utility Systems, L. O'Neill

OTHER GOVERNMENT AGENCY

Central Intelligence Agency
ATTN: OSWR/NED

DEPARTMENT OF ENERGY CONTRACTORS

Lawrence Livermore National Lab
ATTN: L-10, H. Kruger
ATTN: L-156, L. Miller
ATTN: L-156, M. Cabayan
ATTN: L-96, T. Donich
ATTN: Technical Info Dept, Library

Los Alamos National Laboratory
ATTN: C. Benton
ATTN: MS 670, J. Hopkins
ATTN: B. Noel

Sandia National Lab
ATTN: L. Hartman
ATTN: C. Vittitoe
ATTN: R. Parker

DEPARTMENT OF DEFENSE CONTRACTORS

BDM Corp
ATTN: Corporate Library

BDM Corp
ATTN: Library

Computer Sciences Corp
ATTN: A. Schiff

Dikewood Corporation
ATTN: Technical Library
ATTN: L. Davis
ATTN: C. Jones

Dikewood Corporation
ATTN: K. Lee

Electro-Magnetic Applications, Inc
ATTN: D. Merewether

DEPARTMENT OF DEFENSE CONTRACTORS (Continued)

Georgia Institute of Technology
ATTN: R. Curry

Georgia Institute of Technology
ATTN: M. Denny

IIT Research Institute
ATTN: I. Mindel
ATTN: J. Bridges

IRT Corp
ATTN: N. Rudie
ATTN: B. Williams

JAYCOR
ATTN: W. Radasky

JAYCOR
ATTN: R. Stahl
ATTN: L. Wenaas

JAYCOR
ATTN: Library

Kaman Sciences Corp
ATTN: W. Rich
ATTN: N. Beauchamp
ATTN: F. Shelton
ATTN: A. Bridges

Kaman Tempo
ATTN: DASIAC

Kaman Tempo
ATTN: DASIAC

Lutech, Inc
ATTN: F. Tesche

McDonnell Douglas Corp
ATTN: S. Schneider

Mission Research Corp
ATTN: LMP Group
ATTN: W. Crevier
4 cy ATTN: C. Longmire
4 cy ATTN: J. Gilbert
15 cy ATTN: Document Control

Mission Research Corp
ATTN: A. Chodorow
ATTN: L. McCormick

Mission Research Corp, San Diego
ATTN: V. Van Lint

Mission Research Corporation
ATTN: J. Lubell
ATTN: W. Stark
ATTN: W. Ware

Pacific-Sierra Research Corp
ATTN: H. Brode
ATTN: L. Schlessinger

Physics International Co
ATTN: Document Control

DEPARTMENT OF DEFENSE CONTRACTORS (Continued)

R & D Associates
ATTN: C. Mo
ATTN: M. Grover
ATTN: Document Control
ATTN: P. Haas

R & D Assoociates
ATTN: J. Bombardt

Science Applications, Inc
ATTN: R. Parkinson

DEPARTMENT OF DEFENSE CONTRACTORS (Continued)

Science Applications, Inc
ATTN: W. Chadsey

SRI International
ATTN: E. Vance
ATTN: A. Whitson

TRW Defense & Space Sys Group
ATTN: W. Gargaro